

# Suppression of convection during protein crystal growth

Paul Poodt

Poodt, Paul

Suppression of convection during protein crystal growth

Ph.D. thesis, Radboud University Nijmegen, the Netherlands

With summary in Dutch

ISBN 978-90-9022807-5

Printed by Print Partners Ipskamp

Front cover: A schlieren image of a growing potassium dihydrogen phosphate crystal.

Back cover: Shadowgraphy images of growing lysozyme crystals with  $G_{eff} = 1$  (top),  $G_{eff} = 0$  (centre) and  $G_{eff} = -0.15$  (bottom)

Images and design by the author.

This work is part of the research programs of the Stichting voor Fundamenteel Onderzoek der Materie (FOM); and the Council for the Chemical Sciences (CW), financially supported by the Netherlands Organisation for Scientific Research (NWO).

# Suppression of convection during protein crystal growth

Een wetenschappelijke proeve op het gebied van de  
Natuurwetenschappen, Wiskunde en Informatica

Proefschrift

ter verkrijging van de graad van doctor  
aan de Radboud Universiteit Nijmegen  
op gezag van rector magnificus  
prof. mr. S.C.J.J. Kortmann  
volgens besluit van het College van Decanen  
in het openbaar te verdedigen op  
maandag 21 April 2008  
om 13.30 uur precies

door

Paulus Willibrordus George Poodt

geboren op 17 November 1979  
te Zevenaar

Promotores:

Prof. dr. E. Vlieg

Prof. dr. ir. J.C. Maan

Copromotores:

Dr. W.J.P. van Enkevort

Dr. P.C.M. Christianen

Manuscriptcommissie:

Prof. dr. W. J. de Grip

Prof. dr. P. Gros (Universiteit Utrecht)

Prof. dr. K. Tsukamoto (Tohoku University, Sendai, Japan)

*A poet once said "The whole universe is in a glass of wine." We will probably never know in what sense he meant that, for poets do not write to be understood. But it is true that if we look at a glass closely enough we see the entire universe. There are the things of physics: the twisting liquid which evaporates depending on the wind and weather, the reflections in the glass, and our imaginations adds the atoms. The glass is a distillation of the Earth's rocks, and in its composition we see the secret of the universe's age, and the evolution of the stars. What strange array of chemicals are there in the wine? How did they come to be? There are the ferments, the enzymes, the substrates, and the products. There in wine is found the great generalization: all life is fermentation. Nobody can discover the chemistry of wine without discovering, as did Louis Pasteur, the cause of much disease. How vivid is the claret, pressing its existence into the consciousness that watches it! If our small minds, for some convenience, divide this glass of wine, this universe, into parts — physics, biology, geology, astronomy, psychology, and so on — remember that Nature does not know it! So let us put it all back together, not forgetting ultimately what it is for. Let it give us one more final pleasure: drink it and forget it all!*

Richard P. Feynman



## Beste lezer

Voor u ligt het resultaat van ruim vier jaar promotieonderzoek. Vier jaar lijkt een lange tijd, maar voor je het weet is het voorbij. Terwijl ik al schrijvend aan dit voorwoord terugdenk aan alle dingen die ik heb geleerd, alle mensen met wie ik heb samengewerkt en aan alle hoogte- en dieptepunten die we hebben meegemaakt, kan ik niets anders denken dan dat vier jaar veel te kort was. Er valt nog zo veel te leren, zoveel werk te doen en nog zoveel mee te maken. Dit is een compliment voor alle mensen die, direct of indirect, een rol hebben gespeeld in het tot stand komen van dit proefschrift en mijn promotie, maar ook in de fijne tijd die ik in Nijmegen heb doorgebracht.

Dit proefschrift is onderdeel van een samenwerkingsproject tussen verschillende afdelingen en er waren veel personen bij betrokken. Er waren natuurkundigen, chemici en biochemici, experimentelen en theoreten. Dat is een type omgeving waar ik mij prettig in voel; het delen van kennis en kunde door mensen met verschillende achtergronden. Dit heb ik altijd proberen op te zoeken, zowel tijdens mijn stages en promotie als in mijn huidige werk. Dit maakt mijn positie soms wat ambivalent voor anderen; ben ik nu een chemicus, een fysicus, een fysisch chemicus of een chemisch fysicus? Voor een fysicus ben ik een chemicus, voor een chemicus een fysicus. Soms is het nodig en ook handig om een dergelijk stempel op te drukken, maar eigenlijk is het irrelevant, net zo als het verbinden van een waarde-oordeel aan een dergelijk stempel. We zijn onderzoekers, we streven hetzelfde doel na en gebruiken dezelfde methoden. En waar onderzoekers met verschillende achtergronden bij elkaar komen kunnen mooie, leuke en interessante dingen kunnen ontstaan. De trekkers van dit project hebben een dergelijk omgeving gecreëerd. Een omgeving waarin ik mij, zoals gezegd, bijzonder heb thuis gevoeld. Hiervoor mijn dank en wat mij betreft veel lof.

Er zijn veel mensen betrokken geweest in dit project. Ik wil iedereen bedanken die direct of indirect een rol hebben gespeeld in het gehele project. Een aantal wil ik graag bij naam noemen.

Maurits, het was even spannend aan het begin; twee volslagen vreemden die vier jaar lang zeer nauw zouden gaan samenwerken. Maar vanaf het eerste moment klikte het tussen ons en ging het samenwerken als vanzelf. Hoewel afzonderlijk verschillend van stijl, complementeerden wij elkaar daar waar nodig. Dit proefschrift zie ik dan ook niet als mijn werk, maar als ons werk en daar ben ik erg trots op. We zijn toch een

beetje collega's gebleven nu we beiden "iets met zonnecellen" doen, ook al werken en wonen we een flink aantal kilometers van elkaar. Maar we zijn bovenal ook vrienden geworden. Ik wens jou en Saskia veel succes en plezier in de toekomst. Bedankt voor alles.

Elias, bedankt voor de mogelijkheden die je mij geboden hebt, zowel tijdens mijn afstudeerstage als tijdens mijn promotietijd. Je oprechte betrokkenheid, aanstekelijk enthousiasme en scherp inzicht zijn altijd inspirerend voor mij geweest.

Willem, je bent een bijzonder persoon in de positieve zin van het woord. Ik heb veel van je geleerd en prettig samengewerkt tijdens de (werk)colleges en computerpractica, hiervoor mijn dank. Ik hoop dat je gezondheid je niet teveel in de weg zal staan om ook toekomstige studenten en promovendi enthousiast te maken voor het vak.

Jan Kees, een groot en uniek laboratorium van de grond krijgen en draaiend houden terwijl er dan ook nog eens van die "zweverige" kristalgroeiers langs komen, verdient veel respect. Bedankt voor de begeleiding, met name het blijven wijzen op het scherp en duidelijk formuleren van het werk, zowel in presentaties als publicaties.

Peter, je enthousiaste maar nuchtere, geduldige en altijd stimulerende inbreng tijdens mijn promotietijd waren van groot belang. Hiervoor mijn dank.

Wim, bedankt voor de niet te onderschatten bijdrage aan het project. Ook bedankt voor het zorgvuldig doorlezen van mijn manuscript.

Katsuo, thank you for your hospitality during our visit to Japan. Thank you for the fruitful coöperation and being part of the manuscript committee.

Hugo, hoewel niet direct betrokken in het project heb ook jij een belangrijke rol gespeeld. Je gevoel voor humor, je altijd open deur en je volkomen eigen stijl op de afdeling werden zeer gewaardeerd. Ook dank voor de prettige samenwerking tijdens het projectpracticum.

Jan van Kessel, bedankt voor alle hulp, maar ook voor de gezelligheid.

Jan Los, bedankt voor alle discussies en hulp.

Elisabeth, Martha en Ine, bedankt voor alle hulp, het regelwerk, administratieve zaken en de gezelligheid.

Mijn studenten: Saskia, Gerbe, Jordy en "snuffelaars" Maaïke, Daniel, Max en Tristan. Bedankt voor jullie bijdragen. Ik hoop dat ik jullie net zo veel heb kunnen leren als jullie mij. Veel succes met jullie toekomst.

Ramon, Jos en alle medewerkers van TZ, bedankt voor de technische bijstand en het maken van de microscopen.

Stef en Jos en Igor, bedankt voor de hulp, begeleiding en geduld voor het leren werken en aan de gang houden van de magneten.



Hung, Lijnis. Henk, Harry, Wiesiek, bedankt voor alle hulp.

Alle leden en ex-leden van het HFML en de afdeling Vaste Stof Chemie: ik ga jullie niet allemaal bij naam noemen, want dan wordt de lijst te lang. Maar, een welgemeend bedankt voor de gezelligheid, steun en hulp door de jaren heen. Een prettige werkomgeving is het halve werk. Ook de leden en ex-leden van Applied Materials Science wil ik bedanken, ook al waren we nog niet zo lang “echte” collega’s.

Aan mijn kamergenootjes Edwin, Ismail en Maurits: bedankt dat jullie het met mij hebben kunnen uithouden.

Dank voor Prof. dr. Piet Gros voor het zorgvuldig doorlezen van mijn manuscript. Tevens bedankt voor de afdeling Crystal and Structural Chemistry van de Universiteit Utrecht voor de gastvrijheid tijdens het doen van metingen. Met name Arie Schouten bedankt voor het uitvoeren van de röntgen diffractie experimenten en analyses zoals beschreven in hoofdstuk 9.

Mijn ouders, bedankt voor de onvoorwaardelijke steun, ook al was het soms lastig te begrijpen wat ik allemaal heb gedaan tijdens mijn promotietijd. Ook de rest van mijn familie hiervoor bedankt.

De familie van Joke bedankt voor de steun, met name met en tijdens het klussen aan ons huis.

Mijn vrienden, oud studiegenoten en oud huisgenoten, met name Gang 83, wil ik bedanken voor de fijne tijd naast het werk.

Lieve Joke. Met name de laatste jaren van mijn promotietijd waren soms hectisch; het klussen aan ons huis, jouw studie en mijn promotie hebben ons veel energie gekost. Je moet niet onderschatten hoe belangrijk je was voor mij in deze tijd. Hoewel het niet altijd makkelijk was heb je altijd geprobeerd je in te leven in mijn frustraties en enthousiasme over mijn onderzoek en dat waardeer ik enorm. Toen we eindelijk in ons huis zaten en ik ’s avonds toch al laat thuis was, heb ik ook nog weer vele avonden aan mijn proefschrift zitten werken. Maar ook toen heb je me gesteund en geholpen en daar ben ik je erg dankbaar voor. Zonder jou was het niet gelukt...

Paul



# Contents

<b>1</b>	<b>Introduction</b>	<b>5</b>
1.1	Protein crystallization . . . . .	6
1.2	Protein crystal growth in microgravity . . . . .	9
1.3	Protein crystal growth in high magnetic fields . . . . .	10
1.3.1	Diamagnetic levitation . . . . .	10
1.3.2	Suppression of convection . . . . .	11
1.4	The BAD method . . . . .	13
1.5	This thesis . . . . .	15
<b>2</b>	<b>Experimental</b>	<b>19</b>
2.1	High Field Magnet Laboratory . . . . .	20
2.1.1	Cell 2 . . . . .	20
2.1.2	Cell 5 . . . . .	21
2.2	Optical techniques . . . . .	22
2.2.1	Schlieren microscopy . . . . .	22
2.2.2	Shadowgraphy . . . . .	25
<b>I</b>	<b>Gradient magnetic fields</b>	<b>31</b>
<b>3</b>	<b>Suppression of convection during crystal growth of <math>\text{NiSO}_4 \cdot 6\text{H}_2\text{O}</math></b>	<b>33</b>
3.1	Introduction . . . . .	34
3.2	Experimental . . . . .	36
3.3	Results and discussion . . . . .	37
<b>4</b>	<b>Crystal growth of <math>\text{NiSO}_4 \cdot 6\text{H}_2\text{O}</math> in gradient magnetic fields</b>	<b>43</b>
4.1	Introduction . . . . .	44
4.2	Experimental . . . . .	44

---

4.2.1	Setup . . . . .	44
4.2.2	The position in the magnet . . . . .	44
4.3	Results and discussion . . . . .	45
4.3.1	Suppression of convection . . . . .	45
4.3.2	The width of the depletion zone as function of $G_{\text{eff}}$ . . . . .	47
4.3.3	Expansion of depletion zone and crystal growth rate . . . . .	49
4.3.4	Homogeneity of $G_{\text{eff}}$ . . . . .	52
4.4	Conclusions . . . . .	53
<b>5</b>	<b>Magnetically controlled gravity for protein crystal growth</b>	<b>57</b>
<b>6</b>	<b>The critical Rayleigh number in low gravity crystal growth from solution</b>	<b>67</b>
6.1	Introduction . . . . .	68
6.2	The critical Rayleigh number . . . . .	69
6.3	The 3-term model . . . . .	70
6.4	Finite element simulations . . . . .	71
6.5	Results . . . . .	72
6.5.1	Uniform effective gravity and steady state . . . . .	72
6.5.2	Non-steady-state . . . . .	74
6.5.3	Inhomogeneous effective gravity . . . . .	76
6.5.4	Optimizing growth conditions for inhomogeneous $G_{\text{eff}}$ . . . . .	79
6.6	Discussion . . . . .	80
6.7	Conclusion . . . . .	81
<b>7</b>	<b>A comparison between simulations and experiments for microgravity crystal growth in gradient magnetic fields</b>	<b>85</b>
7.1	Introduction . . . . .	86
7.2	Finite element simulations . . . . .	86
7.3	Nickel sulfate hexahydrate experiments . . . . .	88
7.3.1	Results . . . . .	88
7.3.2	Optimization . . . . .	90
7.4	Lysozyme experiments . . . . .	93
7.5	Discussion and conclusions . . . . .	95
<b>II</b>	<b>The BAD method</b>	<b>99</b>

---

<b>8</b>	<b>Buoyancy assisted diffusion limited crystal growth: harnessing gravity to suppress convection</b>	<b>101</b>
8.1	Introduction . . . . .	102
8.2	Theory . . . . .	104
8.3	Experimental . . . . .	106
8.4	Results . . . . .	107
8.5	Discussion and conclusion . . . . .	113
8.6	Appendix. . . . .	114
<b>9</b>	<b>Buoyancy assisted diffusion limited growth of lysozyme crystals</b>	<b>119</b>
9.1	Introduction . . . . .	120
9.2	The nucleation substrate . . . . .	120
9.3	Substrate preparation and crystal growth . . . . .	121
9.4	Results . . . . .	122
9.5	Discussion and conclusion . . . . .	126
	<b>Summary and outlook</b>	<b>131</b>
	<b>Samenvatting</b>	<b>136</b>
	<b>List of publications</b>	<b>142</b>
	<b>Curriculum Vitae</b>	<b>144</b>



# Chapter 1

## Introduction

## 1.1 Protein crystallization

Proteins are a group of bio-macromolecules that play an important role in life. They act as building blocks, catalysts, transporters and regulators in all living organisms and even some non-living objects like viruses. Proteins are large, complicated molecules that come in a variety of sizes, shapes, structures and functions. However, proteins can be very specific; a small mutation in structure can cause the whole protein molecule to dysfunction, sometimes with lethal consequences. That is why understanding of the structure-function relationship of protein molecules is highly relevant to biology, biochemistry and medical and pharmaceutical science, from both an academic and an industrial point of view [1].

To understand the structure-function relation, the molecular structure of a protein molecule needs to be known. The most comprehensive method available for structure determination for both small and large proteins is x-ray crystallography [2], for which single crystals are required with adequate size and perfection. The step of obtaining biological information from diffraction data is by now almost automated, but the bottleneck of the whole process is to obtain crystals of sufficient quality and size [1].

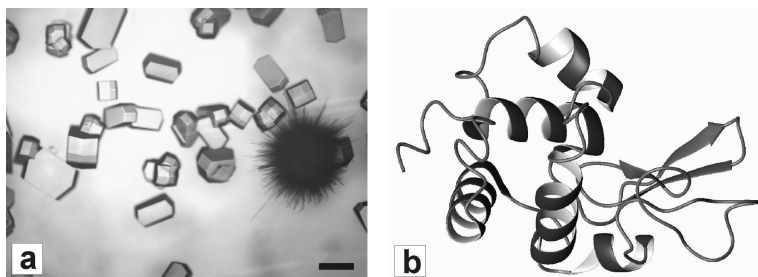


Figure 1.1: (a) Tetragonal hen egg-white lysozyme crystals and a spherulite. The scalebar corresponds to 0.25 mm. (b) The crystal structure of lysozyme determined by x-ray diffraction.

Protein crystals can be grown in many different appealing shapes [3] (Fig. 1.1). Unfortunately, esthetics are rarely an indication of the crystallographic quality. Although it has a history of over 165 years [4], protein crystal growth has largely remained a question of trial and error. Proteins are only stable in a narrow range



---

of biochemical conditions and crystallization involves many variables, including the solvent, buffer, precipitant, pH, temperature, concentrations and of course the protein itself. When a crystal is obtained, the high solvent content, the flexibility of the molecules and the presence of disorder, various defects and impurities cause a high background of diffuse scattering. Bragg peak intensities can be limited by small domain and crystal size, and peak spreading due to slight variations in unit cell parameters and crystallographic orientation can occur. The quality of the diffraction data, and thus the quality of the structure determination, is therefore limited by the crystal quality. This makes protein crystal growth very often the quality limiting step in the process of structure determination of proteins.

Protein crystals are grown from solution, a process that involves nucleation, transport of molecules and subsequent incorporation of these molecules into the growing crystal (see [1] and references therein). To facilitate nucleation, highly supersaturated solutions are required. As the crystal grows, it depletes the surrounding solution of protein molecules and protein molecules will diffuse to balance the variations in concentration. If, however, the diffusion of molecules cannot keep up with the rate of incorporation of molecules into the crystal, a concentration gradient near the crystal is formed. As the density of the solution varies with concentration, buoyancy pushes the depleted solution upwards, forming convective flows around the growing crystal, evening out the variations in concentration. At the crystal interface, however, the drag between the flowing solution and the crystal leads to a thin boundary layer where flows are very slow and a concentration gradient can persist. On top of the crystal, this so called depletion zone detaches from the crystal and follows the convective flow, as can be seen in Fig. 1.2a. This convection- or growth plume, together with the depletion zone, can be made visible with optical techniques like schlieren microscopy, shadowgraphy or interferometry [5].

As the depletion zone is very thin, the growing crystal remains in close contact with the highly supersaturated solution, which results in a relatively high growth rate. A first attempt to improve the quality of the growing protein crystal could be aimed at obtaining lower growth rates, hopefully decreasing the formation of defects and lowering mosaicity. This can for instance be done by replacing the nucleation solution with one having a lower supersaturation or by adapting the supersaturation by tuning the temperature. In practice, this can be problematic; protein crystals are often too fragile to handle, accurate knowledge of solubilities is absent and the amount of available material often limited.

Another factor that limits the quality of protein crystal is the presence of impurities

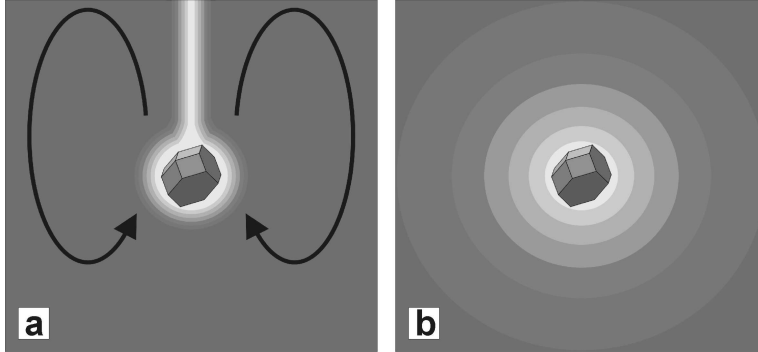


Figure 1.2: (a) Buoyancy driven convection during protein crystal growth. Rising depleted solution forms a convective flow, indicated by the arrows, and leads to a convection plume. (b) In the absence of gravity, convection is suppressed and mass transfer occurs by diffusion: an extended depletion zone is formed.

like dimers and denaturated molecules in the growth solution. If these impurities become incorporated into the crystal, they can act as a source of defects and sometimes even block growth [1]. Extensive purification of the solutions however, can lead to significant loss of material which is undesirable, while impurities can still be formed after purification.

Suppressing buoyancy driven convection would help to overcome these problems [6]. If convection is absent, molecules can only be transported to the crystal by diffusion, which is much slower than mass transport by convection. In the absence of convection, an extended depletion zone will form around the crystal and the growth rate will decrease (Fig. 1.2b). As impurities are often larger than the growth units, they will diffuse even slower, resulting in a decreasing impurity incorporation rate [7]. So, crystal growth under conditions where diffusion dominates mass transport instead of convection can lead to an improvement of crystal quality.

Mass transport by convection and diffusion depend on factors like the viscosity of the solution, the dimensions of the growth container, the density of the solution, the diffusion coefficient of the protein and the gravitational acceleration. This can be quantified by using the dimensionless Rayleigh number. The Rayleigh number  $Ra$  is

a measure of the ratio of convective to diffusive mass transport [8], and is given by

$$Ra \equiv \frac{\gamma L^3 g}{\nu D}, \quad (1.1)$$

with  $g$  the gravitational acceleration,  $\nu$  the kinematic viscosity,  $\gamma$  the dimensionless density difference,  $D$  the diffusion coefficient and  $L$  a characteristic length. If the Rayleigh number is high, transport of protein molecules is primarily in the form of convection while for low values, mass transport is limited by diffusion. To obtain a low Rayleigh number, one can change  $\nu$  by using highly viscous growth solution, like growing crystals in gels [9, 10]. Or one can decrease  $L$  by using very small growth volumes, as in microfluidics [11]. Another possibility that has received a lot of attention the past decades, is reducing the gravitational acceleration. In the absence of gravity, there is no driving force for buoyancy driven convection [6]. An added benefit of protein crystal growth in the absence of a gravitational acceleration is that sedimentation and subsequent incorporation of microcrystallites will not occur [6]. Growing crystals in the absence of gravity is thus expected to deliver better quality crystals than crystals grown under the same conditions, but under normal gravity. The scientific and pharmaceutical drive for better crystals has led to significant investments in both time and money to pursue zero gravity protein crystal growth in space.

## 1.2 Protein crystal growth in microgravity

To obtain a significant reduction of the gravitational acceleration, one is required to go far away from earth. For example, to reduce the gravitational acceleration to one millionth of that on earth, one has to travel about 40 earth-sun distances from earth [6]. Another method to achieve weightlessness is to bring the object in free fall. This can be done by parabolic flights, droptowers or sounding rockets, but the time scales are in the order of seconds to minutes, much too short to facilitate protein crystal growth, which takes hours to days. An object that is orbiting the earth, however, is experiencing free fall for as long as the object is in orbit, which can be days to many years. The amount of gravity an object in orbit experiences is measured in units of  $g$ , the gravitational acceleration on earth, being  $9.8 \text{ m}^2/\text{s}$ . The centre of mass of the orbiting object feels  $0g$ . Away from the centre of mass, residual accelerations occur up to  $10^{-3}g$ . NASA refers to this in terms of microgravity, where

micro' has the meaning of 'small' [12].

The first protein crystal growth experiment in microgravity was performed by Littke in 1981 [13], with a sounding rocket. The first growth experiments in orbit were performed in Space Shuttle mission STS-9 in 1983 [6]. Since then, many experiments have been performed on board Space Shuttle missions and space stations like Mir and ISS. The results have been classified as 'significant' [14] or 'marginal' [15], depending on one's point of view. Most growth experiments were aimed at obtaining crystals, but in recent years, there has been more focus on investigating what actually happens during microgravity crystal growth. Crystal growth was monitored by optical microscopy, schlieren microscopy and interferometry to see the effects of reduced gravity on the hydrodynamic conditions, growth rate and impurity incorporation (see for examples Refs. [16-18]). Unfortunately, the question whether protein crystal growth in space results in better crystals is still not conclusively answered, and more experiments are required.

There are a number of inherent drawbacks to growth experiments in space. There are for instance the huge launch costs (\$10.000-20.000 per kilo [19]), the low frequency of Space Shuttle flights (to date only 7 since the crash of the Colombia in 2003 [19]) and the fact that, while in space, the experiments are inaccessible to the experimenters. Another problem that recently has received much attention, are residual accelerations, and subsequent movements of crystals and distortions of depletion zones, referred to as *g*-jittering [6]. These are caused by e.g. exercising astronauts, course corrections, venting etc., which can ruin the beneficial effects of microgravity. It has been stated that *g*-jittering can be hold responsible for many negative results in microgravity protein crystal growth [6]. All these drawbacks have led protein crystal growers to look for an alternative method to suppress convection during crystal growth. In this thesis, two possible alternatives are investigated; the use of gradient magnetic fields and the BAD method.

## 1.3 Protein crystal growth in high magnetic fields

### 1.3.1 Diamagnetic levitation

In 1991, Beaugnon and Tournier reported levitating diamagnetic organic material in gradient magnetic fields [20]. They stated that: "Our technique can be used to provide a (...) microgravity environment for the elaboration of a wide range of materials." Most organic materials, like proteins, are diamagnetic, meaning a relatively small

and negative magnetic susceptibility. If introduced into a gradient magnetic field, a diamagnetic material experiences a force that repels it from a higher field. If this force is equal in size but opposite in direction to the gravitational force, there is a balance of forces and the object levitates. In equations:

$$F_{net} = F_m + F_g = \frac{\chi}{\mu_0} B_z B'_z - \rho g = 0, \quad (1.2)$$

with  $F_{net}$ ,  $F_m$ , and  $F_g$  the net, magnetic and gravitational force per unit volume respectively, in the  $z$ -direction,  $\chi$  the volume magnetic susceptibility,  $\mu_0$  the magnetic permeability of the vacuum and  $B_z B'_z$  the product of magnetic field and magnetic field gradient in the  $z$ -direction [21]. Note that it is not just the magnetic field that is important, but its product with the field gradient. Eqn. 1.2 can be satisfied if

$$B_z B'_z = \frac{\rho}{\chi} \mu_0 g, \quad (1.3)$$

which is known as the levitation condition. If this condition is fulfilled, objects can levitate, just like in microgravity. A famous example is the levitating frog, at the High Field Magnet Laboratory at the Radboud University Nijmegen [21] (Fig. 1.3). Until recently it was thought that levitating the growth solution using gradient magnetic fields was sufficient to create a microgravity-like condition and to suppress convection. A number of crystallization experiments have been performed under levitation conditions, some claiming improved crystal quality, e.g. [22-26]. However, the assumption that magnetic levitation creates a microgravity-like condition for convection, is not correct. Although it was already shown before that thermal convection can be suppressed for both dia- and paramagnetic fluids [27, 28], the proper method to suppress convection during crystal growth was only recently described by Ramachandran and Leslie [29]. They showed that instead of the bulk magnetic susceptibility and solutal density it is necessary to exploit the concentration dependence of the magnetic susceptibility and of the solutal density.

### 1.3.2 Suppression of convection

The net force per unit volume along the  $z$ -direction on an object in a gradient magnetic field is given by Eqn. 1.2. For convection, not the absolute force but the difference in force between different volumes of solution is important. This effective force is given



Figure 1.3: A frog levitating in a gradient magnetic field at the HFML, seen from the top.

by:

$$F_{eff} = \frac{\Delta\chi}{\mu_0} B_z B'_z - \Delta\rho g, \quad (1.4)$$

with  $\Delta\rho$  and  $\Delta\chi$  the difference in the density and the volume magnetic susceptibility, respectively, between different solutal volume elements. For small variations in concentration, the density and susceptibility can be written as  $\rho(c) = \alpha c + \rho_0$  and  $\chi(c) = \beta c + \chi_0$ , with  $\alpha$  and  $\beta$  the coefficients of the linear concentration dependence of  $\rho$  and  $\chi$ , respectively. Eqn. 1.4 now reduces to

$$F_{eff} = \frac{\beta\Delta c}{\mu_0} B_z B'_z - \alpha\Delta c g. \quad (1.5)$$

To achieve damping of convection, the force acting on different volume elements of the growth solution should be equal, i.e.  $F_{eff} = 0$ , leading to the following condition for suppression of convection:

$$B_z B'_z = \frac{\alpha}{\beta} \mu_0 g. \quad (1.6)$$

The net effective acceleration the solution experiences is given by

$$g_{eff} = -\frac{F_{eff}}{\Delta\rho} = \frac{F_{eff}}{\alpha\Delta c} = g \left[ 1 - \frac{\beta}{\alpha} \frac{B_z B'_z}{\mu_0 g} \right]. \quad (1.7)$$

Now we can define a dimensionless effective gravity as a measure of the net force difference acting on the growth solution:

$$G_{eff} = \frac{g_{eff}}{g} = \left[ 1 - \frac{\beta}{\alpha} \frac{B_z B'_z}{\mu_0 g} \right], \quad (1.8)$$

and the Rayleigh number becomes

$$Ra = \frac{G_{eff} \gamma L^3 g}{\nu D}. \quad (1.9)$$

Eqns. 1.8 and 1.9 offer means to tune the effective gravity and Rayleigh number by changing  $B_z B'_z$ . This makes this technique unique with respect to others, because the amount of convection can be tuned. Not only is it possible to completely suppress convection, but one can also allow for some convection, if desired. It is even possible to increase the amount of convection ( $G_{eff} > 1$ ) or use a negative effective gravity. None of this is possible in space, gels, microfluidics or using other techniques.

## 1.4 The BAD method

The BAD method is introduced in this thesis as another method to suppress convection during protein crystal growth. Where gradient magnetic fields are used to compensate for the effects of gravity, the BAD method makes use of gravity in an upside-down geometry, to achieve the same. In Fig. 1.4, a growing crystal is located at the top of a closed growth cell filled with supersaturated solution. During growth of the crystal, the solution near the crystal becomes depleted of solute. As the density of the depleted solution decreases, it feels an upward buoyant force. For a freely suspended crystal buoyancy driven convection would set in, but for the upside down geometry there is no room for a convective flow to develop. The depleted solution is forced to accumulate at the top of the cell and fresh material has to be supplied from below the crystal. Under the influence of buoyant forces, the depleted solution forms a horizontally stratified depletion zone, expanding downwards, while convective flows

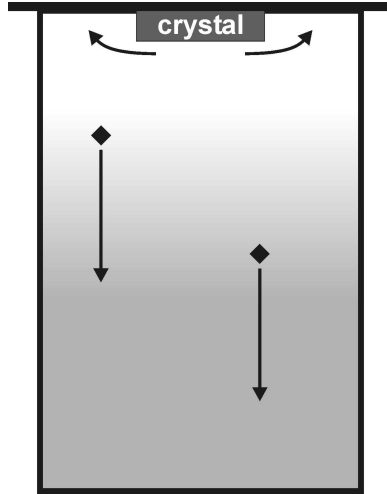


Figure 1.4: Crystal growth in the upside-down geometry. A growing crystal is attached to the top of a growth cell. Depleted solution is forced to accumulate at the top because of buoyancy, leading to diffusion limited growth. Also, sedimenting microcrystals will not be incorporated into the growing crystal.

cannot form. We will call this a Buoyancy Assisted Depletion (BAD) zone. During the BAD zone formation, mass transport towards the crystal becomes increasingly more difficult, and the growth of the crystal becomes diffusion limited. On top of that, due to diffusional purification, impurity incorporation rates are reduced and, for obvious reasons, sedimenting microcrystals will not be incorporated. Whereas conventionally it requires suppression of gravity to achieve these conditions, using the upside down geometry it is possible to harness gravity to achieve the same.

In terms of the Rayleigh number, the BAD method is described by the characteristic length  $L$ . For a given crystal growth geometry, the characteristic length is a measure of the most relevant length scale, for which in most cases the size of the crystal is taken. If, however, the dimensions of the growth container are very small, as in microfluidics [11], drag becomes significant and the amount of convection is reduced. In that case, the size of the growth container has to be taken for  $L$ . A drawback of this method is the small volume of growth solution, resulting in very small crystals. For



---

the BAD method, a normal sized container can be used, but  $d$ , the distance between the crystal and the nucleation substrate becomes very small, and buoyancy driven convection can not develop. Now, the Rayleigh number can be defined as

$$Ra = \frac{\gamma g d^3}{\nu D}. \quad (1.10)$$

If  $d$  becomes small, the Rayleigh number will be small, convection will be suppressed and mass transport limited by diffusion, just as would occur in microgravity.

## 1.5 This thesis

In this thesis, the possibilities of protein crystal growth using gradient magnetic fields or the BAD method as alternatives for crystal growth in microgravity are explored. This is done using a combination of experiments, theory and simulations, investigating crystal growth, fluid dynamics and mass transport, while focussing on applicability as well as the fundamentals.

After discussing some experimental details in chapter 2, part 1 of this thesis covers the use of gradient magnetic fields during crystal growth from solution. In chapter 3, a proof of principle of suppression of convection using gradient magnetic fields is demonstrated, using nickel sulfate as a model system. In chapter 4, the fluid dynamics, mass transport and growth rate behavior in gradient magnetic fields are studied in detail. In chapter 5 it is shown that, though experimentally challenging, convection can also be suppressed for growth of the diamagnetic protein lysozyme. In chapter 6, a closer look is taken at the behavior of the Rayleigh number at low values of the effective gravity, both theoretically and by using simulations. Simulations are also used in chapter 7 to get a more complete understanding of the observations in chapter 3 to 5. In part 2, the BAD method is introduced. In chapter 8, the formation of a buoyancy assisted depletion zone and its effect on the growth of sodium chlorate crystals is investigated. In chapter 9, the BAD method is applied to hen egg-white lysozyme crystal growth.



# Bibliography

- [1] A. McPherson, *Crystallization of biological macromolecules* (Cold Spring Harbor Laboratory Press, Cold Spring Harbor, 1999)
- [2] J. Drenth, *Principles of protein X-ray crystallography* (Springer-Verlag, New York, 1994)
- [3] See for instance <http://www.hamptonresearch.com/stuff/Gallery.aspx>
- [4] F. L. Hunefeld, *Der Chemismus in der tierischen Organisation* (Leipzig, 1840)
- [5] P. J. Schlichta, *Journal of Crystal Growth* **76**, 656 (1986)
- [6] E. H. Snell, J. R. Helliwell, *Reports on Progress in Physics* **68**, 799-853 (2005)
- [7] C.P. Lee, A.A. Chernov, *Journal of Crystal Growth* **240**, 531 (2002)
- [8] V. G. Levich, *Physicochemical Hydrodynamics* (Prentice-Hall international series in the physical and chemical engineering sciences, Englewood Cliffs, 1962)
- [9] M. C. Robert, K. Provost and F. Lefauchaux, *Crystallization of nucleic acids and proteins: a practical approach*, edited by A. Ducruix and R. Giegé (IRL Press, Oxford, 1999)
- [10] J. M. García-Ruiz, J. Drenth, M. Riés-Kautt and A. Tardieu, *A world without gravity - research in space for health and industrial processes*, edited by S. Seibert et al. (ESA, Noordwijk, 2001)
- [11] D. C. Carter, P. Rhodes, D. E. McRee, L. W. Tari, D. R. Dougan, G. Snell, E. Abola and R. Stevens, *Journal of Applied Crystallography* **38**, 87 (2005)
- [12] NASA educational brief EB-1997-02-119-HQ, *The mathematics of microgravity*
- [13] W. Littke and C. John, *Science* **225**, 203 (1984)
- [14] C. E. Kundrot, R. A. Judge, M. K. Pusey and E. H. Snell, *Crystal Growth & Design* **1**, 87 (2001)
- [15] T. Reichhardt, *Nature* **404**, 114 (2000)

- 
- [16] T. J. Boggon, N. E. Chayen, E. H. Snell, J. Dong, P. Lautenschlager, L. Potthast, D. P. Siddons, V. Stojanoff, E. Gordon, A. W. Thompson, P. F. Zagalsy, R. C. Bi and J. R. Helliwell, *Philosophical Transactions of the Royal Society of London A* **356**, 1045 (1998)
- [17] Otálora F., Garcia-Ruiz J.M., Carotenuto L., Castagnolo D., Novella M.L., Chernov A.A., *Acta Crystallographica D* **58**, 1681 (2002)
- [18] M. Pusey and R. Naumann, *Journal of Crystal Growth* **90**, 105 (1988)
- [19] [http://:www.nasa.gov](http://www.nasa.gov)
- [20] E. Beaugnon and R. Tournier *Nature* **349**, 470 (1991)
- [21] M. V. Berry and A. K. Geim, *European Journal of Physics* **18**, 307 (1997)
- [22] N. I. Wakayama, *Crystal Growth & Design* **3**, 17 (2003)
- [23] M. Motokawa, M. Hamai, T. Sato, I. Mogi, S. Awaji, K. Watanabe, N. Kitamura and M. Makihara, *Physica B* **294**, 729 (2001)
- [24] M. Hamai, I. Mogi, M. Tagami, S. Awaji, K. Watanabe and M. Motokawa, *Journal of Crystal Growth* **209**, 1013 (2001)
- [25] M. Tagami, M. Hamai, I. Mogi, K. Watanabe and M. Motokawa, *Journal of Crystal Growth* **203**, 549 (1999)
- [26] D. C. Yin, N. I. Wakayama, K. Harata, M. Fujiwara, T. Kiyoshi, H. Wada, N. Niimura, S. Arai, W. D. Huang and Y. Tanimoto, *Journal of Crystal Growth* **270**, 184 (2004)
- [27] Braithwaite D., Beaugnon E., Tournier R., *Nature* **354**, 134 (1991)
- [28] I. Mogi, C. Umeki, K. Takahashi, S. Awaji, K. Watanabe and M. Motokawa, *Japanese Journal of Applied Physics* **42**, L715 (2003)
- [29] N. Ramachandran and F. W. Leslie, *Journal of Crystal Growth* **274**, 297 (2005)

## Chapter 2

# Experimental

## 2.1 High Field Magnet Laboratory

The manipulation of diamagnetic materials requires high values for the product of magnetic field and magnetic field gradient because of their small magnetic susceptibility. As for most organic materials the ratio  $\frac{\rho}{\chi}$  is constant and the required  $B_z B'_z$  for levitation is around  $\sim 1500 \text{ T}^2\text{m}^{-1}$  [1]. For suppression of convection, even higher gradients are needed. Achieving these high gradients is not trivial, but possible at high magnetic field laboratories like the High Field Magnet Laboratory (HFML) at the Radboud University Nijmegen [2], where all the magnet experiments described in this work have been performed. Two types of magnets at the HFML can be used for levitation and microgravity crystal growth; a 20 T Bitter type magnet with a maximum  $|B_z B'_z|$  of  $2300 \text{ T}^2\text{m}^{-1}$ , referred to as Cell 2, and a 33 T Bitter type magnet with a maximum  $|B_z B'_z|$  of  $6660 \text{ T}^2\text{m}^{-1}$ , referred to as Cell 5.

In a perfect microgravity growth experiment,  $G_{eff}$  is zero throughout the entire growth cell volume. If this is not the case, residual convection may limit the possible beneficial effects of microgravity crystal growth. The optimum position for the growth cell in the magnet therefore corresponds with the  $z$ -value where the variation in the magnetic force is minimal, thus where the derivative of  $B_z B'_z$  equals 0. For diamagnetic materials, the magnetic susceptibility  $\chi$  is negative, leading to a negative  $B_z B'_z$  to fulfill Eqn. 1.6 and experiments are performed in the upper part of the magnet. For paramagnetic materials, both  $\chi$  and  $B_z B'_z$  are positive, and experiments are performed in the lower part of the magnet.

### 2.1.1 Cell 2

Cell 2 is a water-cooled Bitter type, 5.8 MW magnet with a maximum field of 20 Tesla and a room temperature bore of 32 mm. A double walled tube connected to a thermostatic waterbath can be inserted into the bore to control temperature. This reduces the bore diameter to 28 mm. Fig. 2.1a show the field profile and field gradient, Fig. 2.1b the product of both. The field profile is symmetric around the field center.  $B_z B'_z$  has extrema at 63.6 mm from the field center. At these positions,  $B_z = 0.75B_0$  and  $B'_z = \pm 10.24B'_z$ .  $B_z B'_z$ , and thus the effective gravity, can be tuned by varying  $B_0$  with  $|B_z B'_z|$  having a maximum value of  $2300 \text{ T}^2\text{m}^{-1}$ . These are the optimum positions for suppression of convection. From Fig. 2.1b it can be seen that  $B_z B'_z$  varies more or less parabolically around the optimum position.

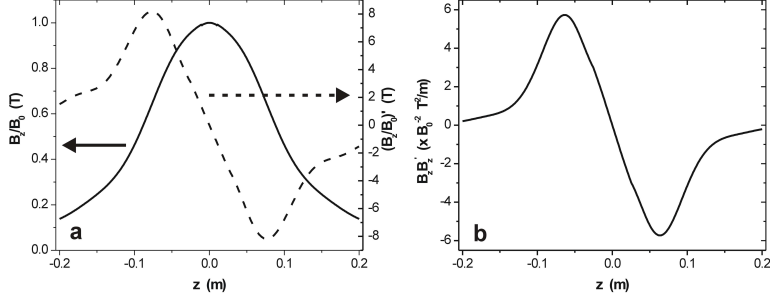


Figure 2.1: (a)  $B_z$ ,  $B'_z$  and (b)  $B_z B'_z$  for Cell 2.

### 2.1.2 Cell 5

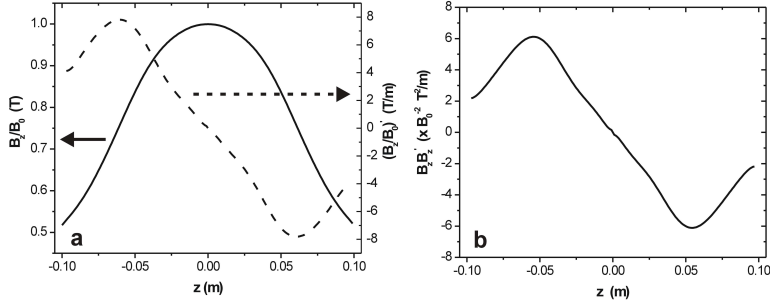


Figure 2.2: (a)  $B_z$ ,  $B'_z$  and (b)  $B_z B'_z$  for Cell 5.

To obtain higher values of  $B_z B'_z$ , Cell 5 was used. Cell 5 is a Bitter type, 17 MW magnet with a field maximum of 33 Tesla and a room temperature bore of 32 mm. A similar thermostatic tube as for Cell 2 can be inserted in the bore. The field profile, gradient and product of both are given in Fig. 2.2. The optimum position is at 54.3 mm from the field center, where  $B_z = 0.805B_0$ ,  $B'_z = \pm 9.44B_z$  and the maximum  $|B_z B'_z|$  is  $6660 \text{ T}^2\text{m}^{-1}$ . From Fig. 2.2b, it can again be seen that  $B_z B'_z$  varies more or less parabolically around the optimum position.

## 2.2 Optical techniques

The concentration gradients in the depletion zone and convection plume are invisible to the naked eye. However, they are accompanied by variations in the refractive index that can be visualized by phase-sensitive optical techniques. Such techniques can be used to *in-situ* observe the development of the depletion zone and growth plume as well as the transitions that occur if convection is suppressed. The two techniques used in the work described in this thesis are schlieren microscopy and shadowgraphy. As commercially available microscopes could not be used because of size limitations, custom microscopes were constructed for use in Cells 2 and 5. In the following sections, the schlieren and shadowgraphy techniques will be discussed.

### 2.2.1 Schlieren microscopy

Schlieren microscopy is an optical technique that visualizes gradients in refractive index, and can thus be used to observe gradients in concentration [3]. According to a design by Toepler [4], a slit light source combined with a condenser lens is used to pass a collimated beam through the sample. In the back focal plane of the objective lens, the Fourier transform of the object convolutes with the projection of the slit. There, a knife edge is placed, parallel to the slit, filtering out half of the Fourier components in the  $x$ -direction, including part of the 0<sup>th</sup> order peak. After inverse transformation by the projective lens, gradients in refractive index are transformed in intensity variations on the projection screen, according to [3]

$$I(x, y) \propto \int_0^d \frac{\partial n(x, y, z)}{\partial x} dz \propto \int_0^d \frac{\partial c(x, y, z)}{\partial x} dz, \quad (2.1)$$

with  $I(x, y)$  the intensity in the  $(x, y)$ -plane, and  $\frac{\partial n(x, y, z)}{\partial x}$  and  $\frac{\partial c(x, y, z)}{\partial x}$  the gradient in refractive index and concentration respectively, perpendicular to the knife edge, integrated along the  $z$ -direction over a distance  $d$ . Schlieren microscopy is a relatively easy, sensitive and robust technique, by which concentration gradients in the depletion zone and convection plume can be readily visualized. Fig.2.3 shows an example of a schlieren image of a growing  $\text{KH}_2\text{PO}_4$  crystal. On the left of the crystal, the concentration gradient is negative and the image is darker than the background, while on the right, the gradient is positive and the image is lighter than the background. Above the crystal, the convection plume is visible.



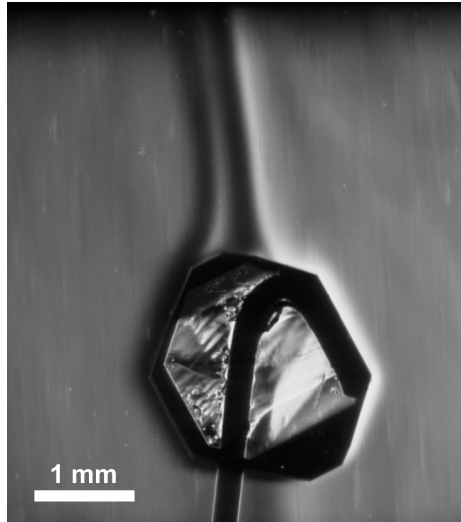


Figure 2.3: A schlieren image of a growing  $\text{KH}_2\text{PO}_4$  crystal. The depletion zone and growth plume can be clearly seen. The black line at the bottom of the crystal is a copper wire to which the crystal is glued for support,

A long working distance schlieren microscope was specially designed and constructed for Cell 2 to fit our demands as well as the geometrical restrictions imposed by the magnet. A schematic drawing is given in Fig. 2.4a. In order to observe the transition from convection dominated to diffusion dominated crystal growth in the magnet, the microscope should give a side view of the crystal, with a large enough field of view to see the crystal as well as the depletion zone and the convection plume. On the other hand, because it is not possible to place a CCD-camera inside the magnet, the distance between sample and camera will be relatively large. Also, the bore of the magnet limits the size of the optical components inside the magnet. All the optics, except the light source, the projective zoomlens and the CCD-camera, are mounted on an insert and placed inside the magnet bore (Fig. 2.4b). All components inside the bore are mounted on anodized aluminium flanges connected by two stainless steel rods, which are attached to a height adjustable head (A), directly fixed to the thermostatic tube for mechanical stability. The light source is a Schott KL1500

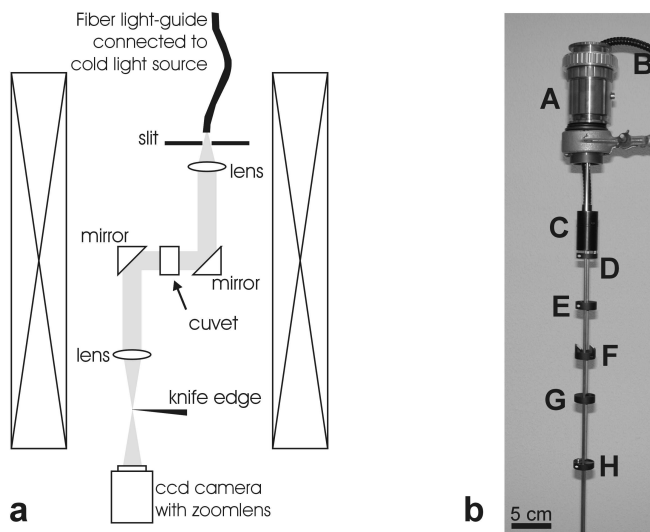


Figure 2.4: (a) A schematic drawing of the schlieren microscope inside the magnet. (b) A photograph of the schlieren microscope insert.

cold light source. Using a fiber light-guide (B), the light is projected on a 1 mm slit (D), via a condenser lens and a diffuser (C). A collimated beam was obtained by placing the slit in the focal plane of a 12.5 mm diameter achromatic lens (E) with a focal distance of 80 mm. Using two mirrors (F), the beam is guided through a 7.5 x 7.5 x 14 mm inner diameter, 10 x 10 x 15 mm outer diameter glass cuvette from Hellma, containing the sample. The objective lens (achromat with diameter 12.5 mm, focal distance 80 mm) has a numerical aperture of 0.078 (G). The knife edge (H) is a thin copper plate that has to be aligned beforehand. The projective zoomlens is a 70-200 mm F2.8 photographic zoomlens from Sigma. The images are recorded using a Nikon DS-5M-L1 CCD camera system. To overcome vignetting of the light beam, all components, except the sample cell, were placed under a small angle of about  $2^\circ$  with respect to the bore central axis, to assure that the optical axis would exit through the middle of the bore. For experiments with diamagnetic materials, negative field gradients are required, i.e. above the field centre, while for paramagnetic materials, positive gradients are required, i.e. below the field centre. The schlieren microscope

can be used in both cases, by swapping and rotating the components above and below the sample holder. The microscope can also be used in a bright field mode, by removing the knife edge, and in a dark field mode, by blocking the entire 0<sup>th</sup> order peak or more. In addition to visualizing the depletion zone and the growth plume, also the size of the crystal can be recorded to determine the growth rate and test particles can be observed to visualize convective flows.

## 2.2.2 Shadowgraphy

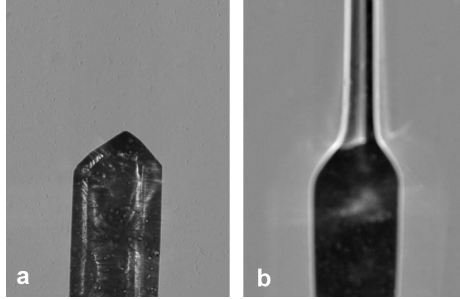


Figure 2.5: (a) focussed image of a growing KDP crystal. No plume is visible. (b) If the crystal is imaged out of focus (shadowgraphy), the growth plume becomes clearly visible, although the crystal becomes blurred.

A light ray passing through a transparent object with a gradient in refractive index, like for instance a convection plume, is deflected according to [3]

$$\varepsilon_x = \frac{1}{n_0} \int \frac{\partial n(x, y, z)}{\partial x} dz, \quad \varepsilon_y = \frac{1}{n_0} \int \frac{\partial n(x, y, z)}{\partial y} dz, \quad (2.2)$$

with  $\varepsilon_x$  and  $\varepsilon_y$  the deflection angles in the  $x$  and  $y$ -direction,  $n_0$  the refractive index of the surrounding medium and  $\frac{\partial n(x, y, z)}{\partial x}$  and  $\frac{\partial n(x, y, z)}{\partial y}$  the gradient in refractive index. If we place such an object between a light source and a projection screen, the shadow of the object will show variations in intensity. This is because the deflected ray reaches the projection screen displaced from its original position. There, it contributes extra intensity, while its previous position suffers an intensity deficit. The total intensity reflects the second order derivative of the refractive index, though this only holds for

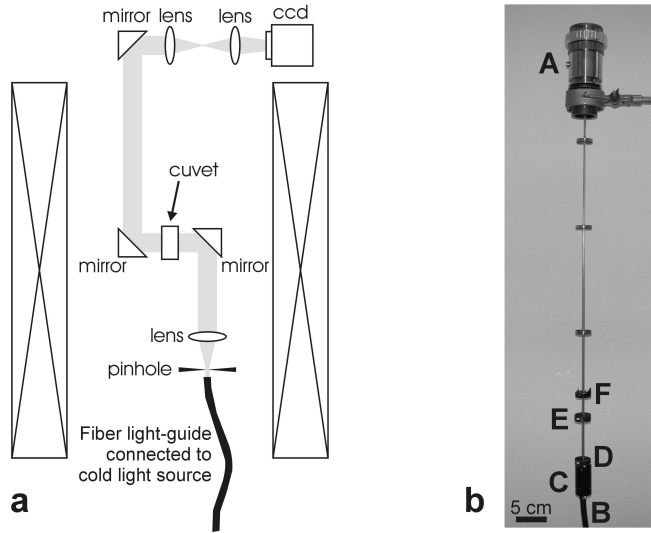


Figure 2.6: (a) A schematic drawing of the shadowgraphy microscope inside the magnet. (b) A photograph of the shadowgraphy insert.

simple cases. A nice example is the shadow of the hot air rising above a candle cast upon a white table cloth.

If this concept is combined with microscopy, it can be used to observe convection plumes during crystal growth. This can be done by looking at the shadow of plume, instead of the plume itself, i.e. placing the growing crystal out of focus. If the crystal is placed in focus, there will be a sharp image of the crystal, but the plume and depletion zones cannot be seen. If the crystal is placed out of focus, the crystal will become blurred, but the plume will become visible (Fig. 2.5). If the cell is placed more out of focus, intensity variations caused by smaller angles will come up, thus increasing sensitivity. However, the crystal will become more blurred and the contrast will decrease. Possible intensity variations caused by the depletion zone will be overwhelmed by the blurring of the crystal, but convection plumes can be made clearly visible. Shadowgraphy can be done in the "real mode", where the shadow of the crystal is placed in the focal plane of the objective lens, or in the "virtual mode", where the focal plane is placed behind the crystal, thus imaging the virtual

---

shadow [3]. Virtual shadowgraphy often gives the best results for small refractive index gradients. Although shadowgraphy does not deliver the nice and sharp images schlieren microscopy does, its simplicity and sensitivity make it a perfect tool to qualitatively observe the transition from convection-dominated to diffusion-dominated crystal growth.

A shadowgraphy microscope insert with a very long working distance was designed and constructed for use in Cell 5, given schematically in Fig. 2.6a. Again, all components inside the bore are mounted on anodized aluminium flanges connected by two stainless steel rods (Fig. 2.6b), which are attached to a height adjustable head (A), directly fixed to the thermostatic tube for mechanical stability. Using a fiber light-guide (B), the light of a Schott KL1500 cold light source is projected on a  $75\ \mu\text{m}$  pinhole (D) via a condenser lens and a diffuser (C). A collimated beam was obtained by placing the pinhole in the focal plane of a 12.5 mm diameter achromatic lens (E) with a focal distance of 80 mm. Using two mirrors (F), the beam is guided through a glass cuvette containing the sample. The beam is guided out of the bore and towards the objective lens, an achromat with a diameter of 30 mm, a focal distance of 80 mm and a numerical aperture of 0.18. The projective zoomlens is a 70-200 mm F2.8 photographic zoomlens from Sigma. The images are recorded using a Nikon DS-5M-L1 CCD camera system.



# Bibliography

- [1] J. F. Schenk, *Annals of the New York Academy of Sciences* **649** (1992) 258
- [2] [www.hfml.ru.nl](http://www.hfml.ru.nl)
- [3] G.S. Settles, *Schlieren and Shadowgraph Techniques* (Springer, Berlin, 2001)
- [4] A. Toepler, *Beobachtungen nach einer neuen optischen Methode* (Maximilian Cohen und Sohn, Bonn, 1864).





## Part I

# Gradient magnetic fields



## Chapter 3

# Suppression of convection during crystal growth of $\text{NiSO}_4 \cdot 6\text{H}_2\text{O}$

A magnetic field was successfully used to suppress buoyancy driven convection during solution growth of a  $\text{NiSO}_4 \cdot 6\text{H}_2\text{O}$  crystal. The disappearance of the convection plume and the expansion of the depletion zones, typical for crystal growth in the absence of gravity, were observed with schlieren microscopy when the product of magnetic field and field gradient corresponds to the condition that for all relevant concentrations buoyancy is compensated by paramagnetic counterforces. We show both theoretically and experimentally, that levitation of the growth solution is not the correct condition to suppress convection\*.

---

\*Adapted from: P. W. G. Poodt, M. C. R. Heijna, K. Tsukamoto, W. J. de Grip, P. C. M. Christianen, W. J. P. van Enkevort, J. C. Maan, E. Vlieg, *Applied Physics Letters* **87**, 214105 (2005)

### 3.1 Introduction

During crystal growth from solution, the solution near the crystal gets depleted of solute, resulting in a lower concentration and density. Under the influence of gravity, the solution with lower density rises, resulting in convective flows around the crystal. This leads to a convection plume and a boundary layer with a large concentration gradient at the crystal interface. In systems where mass transport plays an important role in crystal growth, a large concentration gradient leads to a high growth rate, often negatively affecting crystal quality, because defects are readily formed. Impurities are easily incorporated, because the thin boundary layer only forms a small barrier for fresh supplies of impurities from the bulk. Furthermore, gravity leads to sedimentation of microcrystals beyond a certain size, and can become incorporated into larger crystals, increasing mosaïcity due to misorientation.

In crystal growth experiments under conditions where gravity is absent or very small, buoyancy driven convection will no longer take place [1]. The convection plume will disappear, the depletion zone surrounding the crystal will expand continuously and growth is slowed down because of slower mass transport [2,3]. Under such conditions, impurities are less likely to incorporate [4,5], and sedimentation will be dramatically reduced [6]. All of this can have beneficial effects on crystal quality. This is of particular interest to protein crystal growers, because defects, impurities and mosaïcity are detrimental for a structure determination using X-ray diffraction. Experiments in space are an option and many protein crystal growth experiments have been performed on board space shuttle missions or space stations. The question if growing protein crystals in microgravity actually leads to better crystal quality is still open. Problems with space based experiments are that they suffer from g-jittering [7], are rare, very expensive, have a low accessibility and low controllability. That is why efforts have been made to look for an alternative for space based experiments. One of the more promising approaches is the suppression of convection by means of gradient magnetic fields. Until recently it was thought that levitating the growth solution using gradient magnetic fields was sufficient to create a microgravity-like condition and to suppress convection. A number of crystallization experiments have been performed under levitation conditions, some claiming improved crystal quality e.g. Refs. [8-12]. However, the assumption that magnetic levitation creates a microgravity-like condition for convection, is not correct. Although it was already shown before that thermal convection can be suppressed for both dia- and paramagnetic fluids [13,14], the proper method to suppress convection during crystal growth was only recently described by

Ramachandran and Leslie [15]. They show that it is necessary to exploit the concentration dependence of the magnetic susceptibility as compared to the concentration dependence of the solutal density. Schieber [16] already reported the effects of high magnetic fields on the growth rate of paramagnetic  $\text{Fe}(\text{NH}_4)_2(\text{SO}_4)_2 \cdot 6\text{H}_2\text{O}$  crystals in 1967, although he was unaware of the likely cause of these effects, which rely on suppression of convection by a magnetic gradient.

Following a recent analysis of Ramachandran and Leslie [15] we first briefly discuss the forces acting on a body in a magnetic field. The net force  $F_z$  per unit volume along the  $z$ -direction on an object in a gradient magnetic field in vacuum or air is the sum of the magnetic force and the gravitational force given by [15,17]

$$F_z = F_{\text{magnetic}} + F_{\text{gravity}} = \frac{\chi}{\mu_0} B_z B'_z - \rho g, \quad (3.1)$$

with  $B'_z = dB_z/dz$ ,  $\chi$  the volume magnetic susceptibility,  $\rho$  the density,  $\mu_0$  the magnetic permeability of the vacuum,  $g$  the gravitational acceleration in the  $-z$  direction and  $B_z$  the magnetic field along the  $z$ -direction. To achieve levitation, the magnetic and gravitational force should cancel each other so that  $F_z = 0$ , from which the levitation condition directly follows and which is demonstrated in levitating diamagnetic materials like bismuth [18], droplets of ionic solution [9], glass [9] and even frogs [17]. However, to obtain a microgravity-like condition for crystal growth where buoyancy driven convection is suppressed, levitation is not the correct condition. During crystal growth from solution, local variations in concentration occur, and thus also local variations in density and magnetic susceptibility. To achieve suppression of convection the force acting on different volume elements of the growth solution should be equal, leading to the following condition:

$$B_z B'_z = \frac{\Delta\rho}{\Delta\chi} \mu_0 g, \quad (3.2)$$

with  $\Delta\rho$  and  $\Delta\chi$  the difference in the density and the volume magnetic susceptibility respectively between different solutal volume elements. For small variations in the concentration the density and susceptibility can be written as  $\rho(c) = \alpha c + \rho_0$  and  $\chi(c) = \beta c + \chi_0$ , with  $\alpha$  and  $\beta$  the coefficients of the linear concentration dependence of  $\rho$  and  $\chi$  respectively. Eqn. 3.2 then becomes

$$B_z B'_z = \frac{\alpha}{\beta} \mu_0 g. \quad (3.3)$$

$\alpha$  is usually positive, while for diamagnetic materials  $\chi$  is negative and of the order of  $10^{-6}$ , with  $\beta$  usually also negative and small. Therefore,  $B_z B'_z$  has to have a large and negative value, mostly beyond the reach of conventional magnets. For paramagnetic solutions,  $\beta$  is positive and much larger, which makes suppression of convection more easy. Note that Eqn. 3.2 and 3.3 show that if  $\beta = 0$  it is impossible to suppress buoyancy driven convection, although it is possible to levitate the solution [12, 19]. The net effective acceleration the solution experiences is given by

$$g_{eff} = \frac{F_{eff}}{\Delta\rho} = -\frac{F_{eff}}{\alpha\Delta c} = g \left[ 1 - \frac{\beta B_z B'_z}{\alpha \mu_0 g} \right]. \quad (3.4)$$

Now we can define a dimensionless effective gravity as a measure of the net force difference acting on the growth solution:

$$G_{eff} = \frac{g_{eff}}{g} = \left[ 1 - \frac{\beta B_z B'_z}{\alpha \mu_0 g} \right]. \quad (3.5)$$

We thus have a simple way to vary  $G_{eff}$  over a wide range, by tuning the applied magnetic field.

A consequence of the previous analysis is that the criteria for levitation, to reduce sedimentation and to suppress convection are different. So, unlike in real microgravity, suppression of convection, reducing sedimentation or levitation cannot be done simultaneously using gradient magnetic fields.

## 3.2 Experimental

For an experimental validation of this method for convection suppression during growth, we investigated the growth of  $\text{NiSO}_4 \cdot 6\text{H}_2\text{O}$  crystals from solution in a gradient magnetic field. Nickel sulfate crystals and their solution are paramagnetic. In order to calculate the conditions for convection suppression we measured the density and volume susceptibility as function of concentration range near the equilibrium concentration of 48.88 wt% at 25°C [20]. The density measurements were performed by weighing a precisely determined volume of solution. The volume susceptibility measurements were performed using a MSB-Auto magnetic susceptibility balance from Sherwood Scientific Ltd. Results for these measurements are shown in Fig. 3.1. We determined the following values:  $\alpha = 12.1 \pm 0.5 \text{ kgm}^{-3} \text{ wt}\%^{-1}$  and

$$\beta = (3.8 \pm 0.2) \times 10^{-6} \text{wt}\%^{-1}.$$

With all parameter values known, we can calculate the required  $B_z B'_z$  to suppress convection, stop sedimentation or to levitate the solution. We have estimated  $\chi_{crystal}$  to be  $3.2 \times 10^{-4}$  by extrapolation of the data in figure 3.1. The values are shown in Table 3.1, which also shows the predicted effective  $g$  value for convection.

Our experiments were performed using a 20 Tesla 32 mm bore resistive magnet with a calibrated field profile at the High Field Magnet Laboratory at the Radboud University Nijmegen. The position in the magnet we chose to perform our experiment has values of  $B_z = 0.434 B_0$  and  $B'_z = 14.555 B_z$ , where  $B_0$  is the maximum field at the center of the magnet. The samples were prepared by glueing small single crystal fragments to a thin copper wire using superglue. These crystals were submerged in a slightly supersaturated solution so that they grew to a size of about 1 mm. The crystals were mounted in a glass cuvette with an inner volume of  $7.5 \times 7.5 \times 15 \text{ mm}^3$ . A long distance schlieren-type microscope was built to fit inside the magnet bore. With schlieren microscopy it is possible to visualize concentration gradients in-situ because the intensity is proportional to the gradient in concentration along the  $x$ -direction, i.e.  $I \propto \partial n / \partial x \propto \partial c / \partial x$  [21-23]. The temperature inside the bore was set to  $25^\circ \text{C}$  and controlled by a double-walled tube connected to a thermostatic waterbath. As growth solution, a 10.5% supersaturated nickel sulfate hexahydrate solution was used.

### 3.3 Results and discussion

Fig. 3.2 shows the main result of our experiment. At  $B_z = 0T$ , under normal gravity conditions, a growth plume can be seen rising from the crystal (Fig. 3.2a). At the sides of the crystal, zones of low and high intensities are visible. These are the

Table 3.1: The conditions to achieve suppression of convection, no sedimentation, or levitation.

Condition	$B_z B'_z$ ( $\text{T}^2 \text{m}^{-1}$ )	$B_z B'_z$ ( $\text{T}^2 \text{m}^{-1}$ )	$G_{eff}$ ( $\text{m s}^{-1}$ )
	Predicted	Experimental	
No field	0		1
Suppression of convection	$39 \pm 3$	$37.5 \pm 0.5$	0
No sedimentation	$45 \pm 5$		-0.1
Levitation	$123 \pm 3$		-2

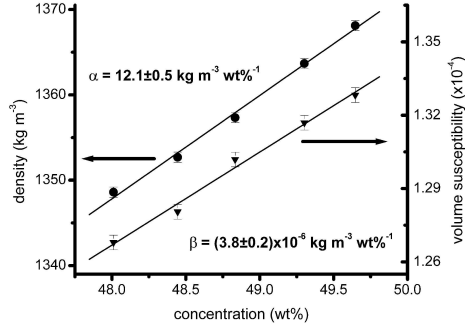


Figure 3.1: Density and susceptibility as function of concentration of an aqueous  $\text{NiSO}_4 \cdot 6\text{H}_2\text{O}$  solution.

depletion zones surrounding the crystal. The concentration gradient on the left side of the crystal is positive and on the right side of the crystal negative, leading to higher and lower intensities because of the schlieren principle. The average width of this depletion zone in the  $x$ -direction is 0.25 mm, which is a normal value. When slowly sweeping the field, we found that the growth plume disappeared for  $B_z = 1.6T$ . At this point, an effective microgravity condition was obtained with complete suppression of convection. After a transient of a few seconds due to the disappearance of the plume, the expansion of the depletion zones around the crystal took several minutes until the depleted zone reached a more or less fixed width of about 1 mm, 4 times as wide as at normal gravity conditions (Fig. 3.2b). Table 3.1 shows that the experimental value for  $B_z B'_z$  as calculated from the field profile, agrees well with the predicted one from  $\alpha$  and  $\beta$ . From this we can conclude that linearization of  $\rho(c)$  and  $\chi(c)$  is a valid approximation

Increasing  $B_z B'_z$  creates an inverse effective gravity. In Fig. 3.2c, a schlieren image is shown of the same growing crystal, but now with the growth plume directed downwards. The applied field was  $B_z = 3.5T$ . The width of the depletion zones decreased to approximately 0.25 mm again. We observed a similar situation for all values of  $B_z B'_z$  well above the convection suppression. Thus for the condition of magnetic levitation, convection is strong, and even enhanced as compared to normal gravity (see Table 3.1).

In summary, we have reported for the first time that solutal convection during



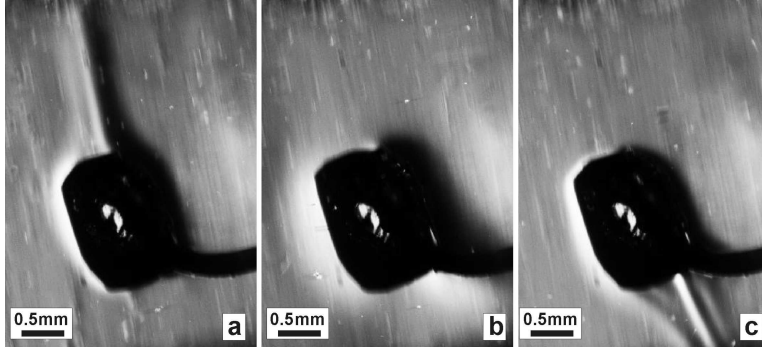


Figure 3.2: Schlieren images of growing nickel sulfate crystals. (a)  $B_z = 0T$  (normal gravity). The crystal is black and the black stripe on the bottom-right is the copper wire on which the crystal is fixed. The plume is vertical, but the camera was slightly tilted. (b) After 5 minutes at  $B_z = 1.6T$  (suppression of convection) with an expanded depletion zone. (c)  $B_z = 3.5T$  (inverse effective gravity). The grayscale indicates the concentration gradient, with white a large negative and black a large positive gradient.

crystal growth can be suppressed by gradient magnetic fields, mimicking microgravity. We have found that the balance between magnetic and gravitational forces can be made sufficiently precise that the depletion zone expands, as expected in the absence of gravity. This leads to a strong reduction in the effective supersaturation, and thus holds promise to yield better crystals. We have proven theoretically as well as experimentally by in-situ schlieren microscopy that levitating the solution is not the right condition to achieve this situation. Some earlier experiments performed under levitation conditions can thus not have achieved convection suppression [12, 19]. Using gradient magnetic fields combined with in-situ optical techniques like schlieren microscopy offers a great opportunity to study the effects of microgravity-like conditions on crystal growth in general and protein crystal growth in particular. Although, unlike in real microgravity, suppression of convection and reducing sedimentation cannot occur simultaneously, the use of gradient magnetic fields can offer a good alternative for microgravity experiments in crystal growth.



# Bibliography

- [1] A. McPherson, A.J. Malkin, Y.G. Kuznetsov, S. Koszelak, M. Wells, G. Jenkins, J. Howard, G. Lawson, *Journal of Crystal Growth* **196**, 572 (1999)
- [2] F. Otálora, J.M. García-Ruiz, L. Carotenuto, D. Castagnolo, M.L. Novella, A.A. Chernov, *Acta Crystallographica D* **58**, 1681 (2002)
- [3] H. Lin, F. Rosenberger, J.I.D. Alexander, A. Nadaraja, *Journal of Crystal Growth* **151**, 153 (1995)
- [4] C.P. Lee, A.A. Chernov, *Journal of Crystal Growth* **240**, 531 (2002)
- [5] H. Lin, D.N. Petsev, S.T. Yau, B.R. Thomas, P.G. Vekilov, *Crystal Growth & Design* **1**, 73 (2001)
- [6] E. H. Snell, J. R. Helliwell, *Reports on Progress in Physics* **68**, 799-853 (2005)
- [7] T. J. Boggon, N. E. Chayen, E. H. Snell, J. Dong, P. Lautenschlager, L. Potthast, D. P. Siddons, V. Stojanoff, E. Gordon, A. W. Thompson, P. F. Zagalsy, R. C. Bi and J. R. Helliwell, *Philosophical Transactions of the Royal Society of London A* **356**, 1045 (1998)
- [8] N.I. Wakayama, *Crystal Growth & Design* **3**, 17 (2003)
- [9] M. Motokawa, M. Hamai, T. Sato, I. Mogi, S. Awaji, K. Watanabe, N. Kitamura and M. Makihara, *Physica B* **294**, 729 (2001)
- [10] M. Hamai, I. Mogi, M. Tagami, S. Awaji, K. Watanabe and M. Motokawa, *Journal of Crystal Growth* **209**, 1013 (2001)
- [11] M. Tagami, M. Hamai, I. Mogi, K. Watanabe and M. Motokawa, *Journal of Crystal Growth* **203**, 549 (1999)
- [12] D. C. Yin, N. I. Wakayama, K. Harata, M. Fujiwara, T. Kiyoshi, H. Wada, N. Niimura, S. Arai, W. D. Huang and Y. Tanimoto, *Journal of Crystal Growth* **270**, 184 (2004)
- [13] Braithwaite D., Beaugnon E., Tournier R., *Nature* **354**, 134 (1991)

- 
- [14] I. Mogi, C. Umeki, K. Takahashi, S. Awaji, K. Watanabe and M. Motokawa, *Japanese Journal of Applied Physics* **42**, L715 (2003)
  - [15] N. Ramachandran and F. W. Leslie, *Journal of Crystal Growth* **274**, 297 (2005)
  - [16] M.J. Schieber, *Journal of Crystal Growth* **1**, 131 (1967)
  - [17] M. V. Berry and A. K. Geim, *European Journal of Physics* **18**, 307 (1997)
  - [18] M. Hamai, I. Mogi, K. Awaji, K. Watanabe, M. Motokawa, *Japanese Journal of Applied Physics Part 2* **40**, L1336 (2001)
  - [19] N.I. Wakayama, *Japanese Journal of Applied Physics Part 2* **44**, L833 (2005)
  - [20] R. Rohmer, *Anneles de Chemie* **11**, 611 (1939)
  - [21] S. Kleine, W.J.P. van Enkevort, J. Derix, *Journal of Crystal Growth* **179**, 240 (1997)
  - [22] G.S. Settles, *Schlieren and Shadowgraph Techniques* (Springer, Berlin, 2001)
  - [23] F.J. Weinberg, *Optics of Flames* (Butterworths, London, 1963)

## Chapter 4

# Crystal growth of $\text{NiSO}_4 \cdot 6\text{H}_2\text{O}$ in gradient magnetic fields

Using in-situ schlieren microscopy, we have studied the growth process of nickel sulfate hexahydrate crystals in a gradient magnetic field under conditions where convection is suppressed, in order to investigate if the same features occur as during microgravity crystal growth. An expansion of the depletion zone with decreasing effective gravity was observed. If convection is suppressed, the depletion zone keeps expanding and the crystal growth rate decreases significantly, reaching a constant value. Although there remains some residual flow, it is very slow and does not affect the depletion zone. We find that homogeneity of the effective gravity in the milligravity range is sufficient to suppress convection. The results show that crystal growth in gradient magnetic fields is a good alternative for microgravity crystal growth in space\*.

---

\*Adapted from: P.W.G. Poodt, M.C.R. Heijna, P.C.M. Christianen, W.J.P. van Enkevort, W.J. de Grip, K. Tsukamoto, J.C. Maan, E. Vlieg, *Crystal Growth & Design* **6** (2006) 2275

## 4.1 Introduction

In this chapter we present the results of more detailed experiments on growing nickel sulfate hexahydrate (NSH) crystals in a gradient magnetic field under conditions where convection is suppressed. Also, the possibility of tuning the magnetic gradient is explored as a new tool to control the crystallization process by varying the effective gravity and the corresponding convection flow.

## 4.2 Experimental

### 4.2.1 Setup

The magnet used for these experiments is a 32 mm bore 20 T resistive magnet at the High Field Magnet Laboratory at the Radboud University Nijmegen. A double walled tube connected to a thermostatic water bath was inserted to control the temperature between 30 and 35°C, reducing the effective bore diameter to 28 mm. NSH crystals were grown from a supersaturated solution, cleaved along the (001) planes and cut into small pieces of approximately 2 x 2 mm wide and 1 mm thick. They were glued onto a copper wire for support using superglue, mounted in the sample cell and submerged in a supersaturated solution, ranging from 5% to 7% for the experiments described here. The cell was sealed off using Parafilm.

### 4.2.2 The position in the magnet

In a perfect microgravity growth experiment,  $G_{eff}$  is zero throughout the entire growth cell volume. If this is not the case, residual convection may limit the possible beneficial effects of microgravity crystal growth. The optimum position for the growth cell in the magnet corresponds with the  $z$ -value where the variation in the magnetic force is minimal, thus where the derivative of  $B_z B'_z$  equals 0. Figure 4.1a shows the field profile and its corresponding field gradient of the magnet we used in our experiment, where  $z = 0$  corresponds to the center of the magnet. From this profile, the product of field and field gradient as function of  $z$ ,  $B_z B'_z$ , was calculated, which is given in figure 4.1b. Because for paramagnetic compounds, a positive gradient is required, only the values for negative  $z$ , i.e. below the magnet center, are plotted. The derivative of  $B_z B'_z$  is zero for  $z = -63.6$  mm and at this optimum position we

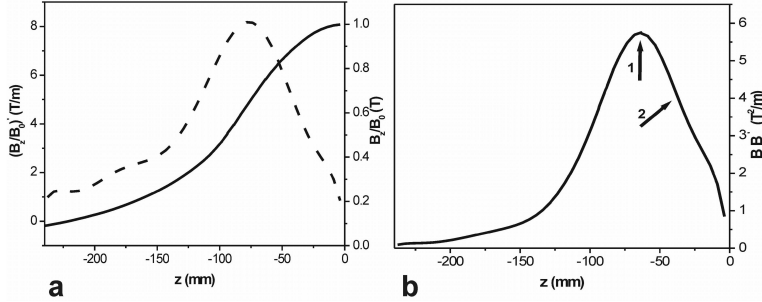


Figure 4.1: (a) Field profile (solid line) and field gradient (dashed line) of the 20 T magnet used in the experiments. (b) The product of field and gradient  $B_z B'_z$ . Arrow 1 shows the  $z$ -value of the optimum position where most experiments were performed and arrow 2 the position where the effect of inhomogeneity was studied.

have performed most of our experiments. The values for  $B_z$  and  $B'_z$  for this position are given by  $B_z = 0.75B_0$  T and  $B'_z = 10.24B'_0$  T/m, where  $B_0$  is the magnetic field at the center of the magnet.

## 4.3 Results and discussion

### 4.3.1 Suppression of convection

Figure 4.2a shows a false color schlieren image of a growing NSH crystal at 0T, thus at  $G_{eff} = 1$ . The boundary layer with the depletion zone and the convection plume are clearly visible.  $G_{eff}$  can now be varied by sweeping the field. Figure 4.2b shows the same crystal, but now for a  $B_z B'_z$  where  $G_{eff} = 0$ , after 1.5 hrs. The convection plume has disappeared and the depletion zone has expanded almost up to the wall of the growth cell and is approximately 12 times as wide as for  $G_{eff} = 1$ .

To calculate the value of  $B_z B'_z$  where  $G_{eff} = 0$ , an accurate value for the ratio between  $\alpha$  and  $\beta$  is needed. Therefore, the solutal density and volume magnetic susceptibility were measured as function of concentration. The density was measured by weighing a precisely determined volume of solution. The volume magnetic susceptibility was measured using a MSB-Auto magnetic susceptibility balance from Sherwood

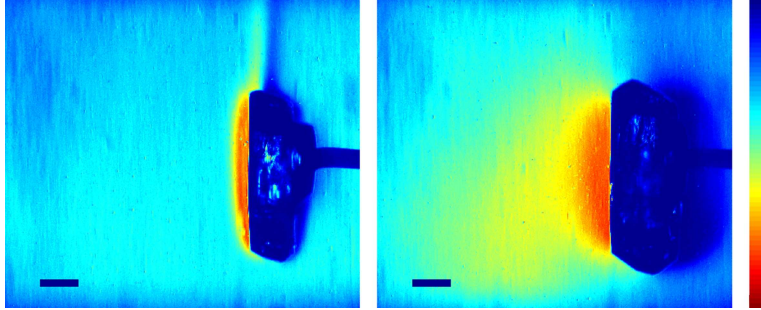


Figure 4.2: (a) False color schlieren image of a growing NSH crystal for  $G_{eff} = 1$ . The blue stripe on the right side is the copper wire on which the crystal is fixed. The convection plume and thin depletion zone are visible. (b) False color schlieren image of a growing NSH crystal for  $G_{eff} = 0$ . The convection plume has disappeared and the depletion zone has expanded. The color indicates the concentration gradient, with red a large negative and blue a large positive gradient, according to the color bar on the right. The scale bar corresponds to 0.5 mm.

Scientific Ltd. The measurements were performed for a limited concentration range near the equilibrium concentration. For higher concentrations, measurements become difficult due to crystallization. The values determined in this way are  $\alpha = 10.2 \pm 0.1 \text{ kg m}^{-3} \text{ wt}\%^{-1}$  and  $\beta = (4.0 \pm 0.2) \times 10^{-6} \text{ wt}\%^{-1}$ . The corresponding value for  $B_z B'_z$  then becomes  $31 \pm 2 \text{ T}^2/\text{m}$ . Note that levitation of the solution is expected to occur around  $123 \text{ T}^2/\text{m}$  [1]. Figure 4.3 shows the experimentally determined values for  $B_z B'_z$  to suppress convection for different concentrations, together with the value calculated from  $\alpha$  and  $\beta$ . We find that  $B_z B'_z$  varies slightly with concentration, ranging from 30.8 to 31.6  $\text{T}^2/\text{m}$ . For all concentrations in figure 4.3, the temperature was set in such a way that the supersaturation was 7%. As we could not find a temperature dependency for  $B_z B'_z$ , the variation in  $B_z B'_z$  must be completely caused by variations in concentration. This implies that  $\alpha$  and/or  $\beta$  vary slightly with concentration, but the concentration dependence is too weak to be visible in the measurements of the density and magnetic susceptibility within the investigated concentration range. Although the differences between the calculated value of  $B_z B'_z$  and the experimentally determined ones are small, they show the importance of either accurately determining  $\alpha$  and  $\beta$  for the domain of concentrations used in the experiments, or observing the



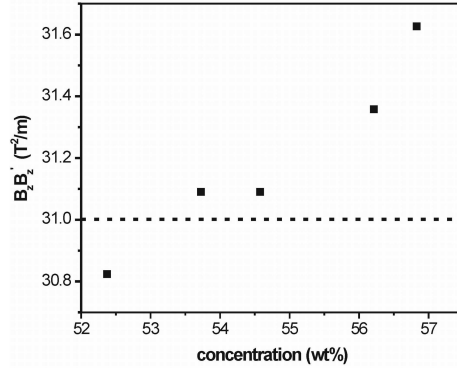


Figure 4.3: The experimentally determined values for  $B_z B'_z$  to suppress convection (squares) and the theoretical value, calculated from  $\alpha$  and  $\beta$  (dashed line).

system in-situ to be certain that convection is suppressed.

In our first report [1] we determined the values of  $\alpha$  and  $\beta$  to be  $\alpha = 12.1 \pm 0.5$   $\text{kg m}^3 \text{wt}\%^{-1}$  and  $\beta = (3.8 \pm 0.2) \times 10^{-6} \text{wt}\%^{-1}$ . The corresponding  $B_z B'_z$ , is  $39 \pm 3$   $\text{T}^2/\text{m}$ , which was in good agreement with our previous experimentally determined value of  $37.5 \pm 0.5$   $\text{T}^2/\text{m}$ , but which deviates from the values described in this chapter. Using UV-Vis spectroscopy, we found that the difference is most likely caused by the use of slightly dehydrated NSH, meaning more paramagnetic nickel ions per gram NSH, in the earlier experiment.

### 4.3.2 The width of the depletion zone as function of $G_{\text{eff}}$

According to Eqn. 3.5, it is possible to tune  $G_{\text{eff}}$  by simply changing  $B_z B'_z$ . To investigate how the width of the depletion zone,  $\delta$ , varies with  $G_{\text{eff}}$ , a growth experiment was performed for various levels of  $G_{\text{eff}}$ . A NSH crystal was submerged in a solution with a supersaturation of 5.8% at 35°C. After  $B_z B'_z$  was set, a schlieren image was recorded after the width of the depletion zone did not change with time anymore, and from these images  $\delta$  was determined. From the schlieren images it is possible to determine  $\delta$ , either from integrating the data, which is the most accurate method, or from direct measurement of the width of the concentration gradient profile from the

original image, which is easier. The systematic error introduced in the latter method is within the error bars of the first approach, so this was the method we used. The width of the depletion zone was measured for  $G_{eff}$  ranging from 1 to -2. The results are plotted in figure 4.4a. From  $G_{eff} = 1$  to 0.5, there is no dramatic change, but for lower values of  $G_{eff}$ ,  $\delta$  increases sharply to a maximum at  $G_{eff} = 0$ . The behavior of  $\delta$  is symmetric around  $G_{eff} = 0$ . It should be noted that the divergence near  $G_{eff} = 0$  is limited due to the finite size of the growth cell. Figure 4.4a shows that, by using gradient magnetic fields,  $G_{eff}$  can be used as an experimental parameter to control convection and  $\delta$ , which is not possible for space experiments.

The results have been analyzed using dimensionless numbers from fluid dy-

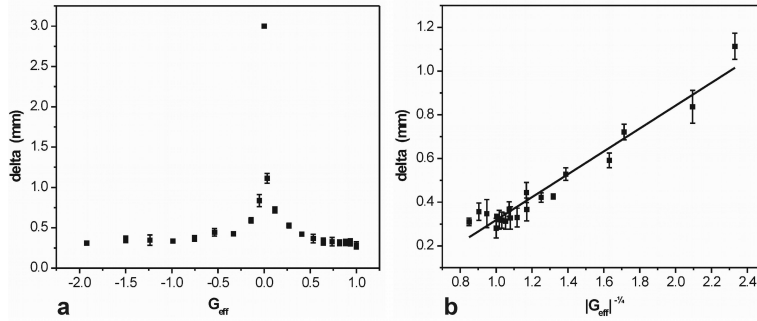


Figure 4.4: Width of the depletion zone (delta) (a) as function of  $G_{eff}$ . (b) as function of  $|G_{eff}|^{-\frac{1}{4}}$ .

namics. The relation between the thickness of the boundary layer and  $G_{eff}$  is given by the Sherwood ( $Sh$ ) number and the Rayleigh number ( $Ra$ ). The Sherwood number is a dimensionless number used in mass-transfer analysis. It represents the ratio of length scale to the diffusive boundary layer thickness and is represented by [2]

$$Sh \equiv \frac{L}{\delta}, \quad (4.1)$$

with  $L$  a characteristic length. The Rayleigh number is the ratio of natural convective to diffusive mass transport, given by [2]

$$Ra \equiv \frac{L^3 \beta_{\text{exp}} \Delta c g}{\mu D} G_{\text{eff}}, \quad (4.2)$$

with  $\beta_{\text{exp}}$  the bulk expansion coefficient,  $\mu$  the absolute viscosity and  $D$  the diffusion coefficient. The shape of the crystal used was more or less cube-like. The empirical relation between  $Sh$  and  $Ra$  for cubes for free convection is given by [2]

$$Sh = 0.55 Ra^{1/4}. \quad (4.3)$$

Considering that all parameters, except  $\delta$  and  $G_{\text{eff}}$ , are constant, Eqn. 4.3 reduces to

$$\delta \propto Ra^{-1/4}. \quad (4.4)$$

So if  $\delta$  is plotted vs.  $|G_{\text{eff}}|^{-1/4}$  and Eqn. 4.4 is valid, it should result in a straight line. Figure 4.4b shows such a plot. The data is in excellent agreement with Eqn. 4.4, so  $\delta$  indeed scales with  $|G_{\text{eff}}|^{-1/4}$ . For very large values of  $G_{\text{eff}}$ , within the turbulence regime, and thus very small values of  $|G_{\text{eff}}|^{-1/4}$ , Eqn. 10 is not valid, explaining the offset for low values of  $|G_{\text{eff}}|^{-1/4}$ .

### 4.3.3 Expansion of depletion zone and crystal growth rate

In microgravity crystal growth, it is expected that the depletion zone expands in time and the crystal growth rate decreases. To investigate if this also happens in a gradient magnetic field, a NSH crystal was submerged in a solution with a supersaturation of 5.3% at 30°C. The value of  $G_{\text{eff}}$  was set to 0 by tuning  $B_z B'_z$  until convection was suppressed. The expansion of the depletion zone for  $G_{\text{eff}} = 0$  was investigated by measuring the width of the depletion zone,  $\delta$ , at the (001) face as function of time. As can be seen in figure 4.5,  $\delta$  keeps expanding during the time of the experiment. After about 100 minutes, the depletion zone reaches the wall of the growth cell, where it has expanded to approximately 3 mm, 12 times as wide as at  $G_{\text{eff}} = 1$ . The insert shows the log-log plot of the data. The slope of the linear fit has a value of 0.31, indicating that the depletion zone expands according to  $\delta \propto t^{0.31}$ . In addition, the growth rate was measured by recording the displacement of the crystal's (001) face during growth. The results are shown in figure 4.6. The growth rate decreases dramatically in the first 10 minutes, after which it reaches an apparently constant value of about  $2 \times 10^{-5}$

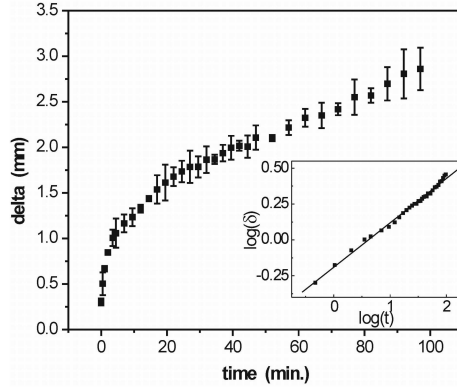


Figure 4.5: Width of the depletion zone as function of time for  $G_{eff} = 0$ . The insert shows the log-log plot of the data, which has a slope of 0.31.

mm/s, which is approximately 15% of the growth rate at  $G_{eff} = 1$ . It is somewhat surprising that the growth rate reaches a constant value in 10 minutes, while the depletion zone keeps expanding over 100 minutes.

If  $G_{eff}$  is reduced completely and diffusion is the only means of mass transport, the mass transfer can be described by Fick's second law, taking into account a moving boundary and interface kinetics. Otálora *et al.* [3] observed a more or less constant growth rate for lysozyme crystals growing under microgravity conditions on board a space shuttle. They analyzed their results by using a quasi steady state diffusion equation coupled with linear interface kinetics. This predicts a constant growth rate, because, as a boundary condition, a constant interface concentration is assumed. Although this approximation is widely used, in reality, neither the interface concentration nor the interface position is likely to remain constant during the experiment. Solving the diffusion equation in the proper way, shows that the depletion zone should expand according to  $\delta \propto t^{0.5}$ , the growth rate  $v_g$  should decrease, going towards zero according to  $v_g \propto t^{-0.5}$  for large  $t$  and no stationary growth rate is obtained. This does not correspond to the experimental data.

The difference between the diffusion model and the experimental results can be explained by assuming that  $G_{eff}$  is not reduced completely and some residual flow is present, as has been observed by monitoring moving dust particles and crystallites,

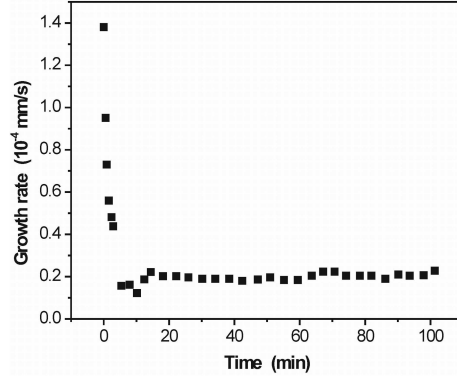


Figure 4.6: Crystal growth rate as function of time for  $G_{eff} = 0$ .

which were always present during the experiments. Because these particles are very small, they will not sediment, but act as tracers of the solution flow. The particle flow velocity for  $G_{eff} = 0$  was  $(0.5 - 2.5) \times 10^{-3}$  mm/s. The flow velocity for  $G_{eff} = 1$  could not be measured accurately, because particles moved out of the field of view within the time span of two consecutive images. A lower limit was determined to be 0.25 mm/s for  $G_{eff} = 1$ , but the actual velocity is likely to be higher. Therefore, the flow velocity at  $G_{eff} = 0$  is reduced to less than 1% of the value at  $G_{eff} = 1$ . The origin of the residual flow is difficult to determine, with some particles moving up and others moving down close to each other. Nevertheless, the flow does not seem to disturb the depletion zone.

If no growth cell wall was present, a new steady-state depletion zone would form because of the residual flow, with a width given by Eqn. 4.4 and a corresponding constant growth rate. The presence of the wall however, interferes with the solutal flow by slowing it down. According to Ramachandran et al. [4], below a certain  $G_{eff}$ , the flow velocity controlled by the wall effects begin to dominate over the velocity controlled by boundary layer thickness, thus decoupling the flow from the mass transport. If this occurs and the flow velocity becomes slower than the diffusion speed, the mass transfer due to convection becomes slower than mass transfer due to diffusion. Hence, the diffusion field expands, although there remains a small amount of solutal flow and mass transport due to this. Near the crystal, the stationary

concentration profile is reached quickly while further away it forms slower, as was observed in the schlieren images.

The relation between growth rate and  $G_{eff}$  can be estimated from the Rayleigh and Sherwood numbers. The latter can be rewritten as [5]

$$Sh = \frac{v_g L}{\Omega \Delta c D} \quad (4.5)$$

with  $\Omega$  the volume of the unit cell and  $\Delta c$  the concentration difference between the bulk and the interface. From Eqns. 4.3 and 4.5 it can then be seen that  $v_g \propto Ra^{1/4}$ . If the growth rate is reduced to 15%, this means an average  $G_{eff}$  of approximately  $5 \times 10^{-4}$ , which can be caused by an inhomogeneity in  $G_{eff}$  throughout the growth cell.

#### 4.3.4 Homogeneity of $G_{eff}$

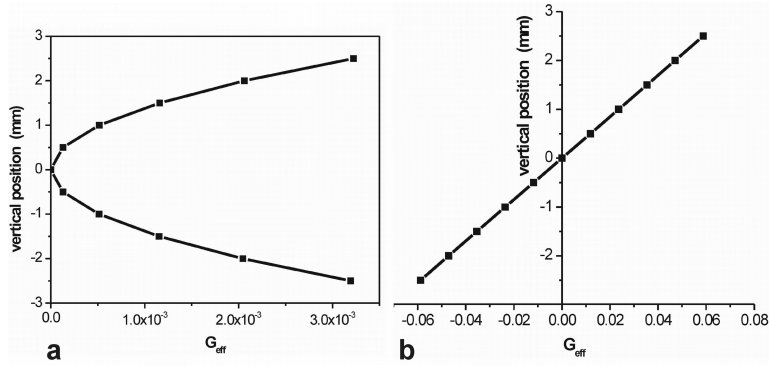


Figure 4.7: (a) The homogeneity of  $G_{eff}$  along the growth cell at the optimum position (position 1 in Fig. 4.1b), and (b) at a location with strong variation in the derivative of  $B_z B'_z$  (position 2 in Fig. 1b).

To investigate the homogeneity of  $G_{eff}$  in our experiments, the homogeneity of  $B_z B'_z$  along the  $z$ -axis of the magnet needs to be analyzed. Figure 4.7a shows  $G_{eff}$  vs. vertical position, calculated from the field profile, ranging from 2.5 mm above to

2.5 mm below the optimum position of  $z = -63.6$  mm. This covers the microscope's field of view, which is 4.5 mm in height. Although this is the position where we get a maximum expansion of the depletion zone (see figure 4.2a),  $G_{eff}$  varies from 0 to  $\sim 3.2 \times 10^{-3}$ , which agrees with the estimate of the average  $G_{eff}$  from the growth rate.

If the growth cell is placed at a position where  $d(B_z B'_z)/dz$  is not zero, the inhomogeneity of  $G_{eff}$  is much larger. As a test we positioned our sample at  $z = -38.4$  mm. Figure 4.7b shows  $G_{eff}$  vs.  $z$  for this position when  $B_z B'_z$  was adjusted so as to realize  $G_{eff} = 0$  in the center. The value of  $G_{eff}$  now varies from  $-5.8 \times 10^{-2}$  to  $4.7 \times 10^{-2}$ . Not only is there a significant inhomogeneity along the  $z$ -axis, the residual  $G_{eff}$  also changes sign; negative below  $z = 0$ , meaning a net downward force, and positive above  $z = 0$ , meaning a net upward force. Figure 4.8 shows a schlieren image of a growing NSH crystal at this position, for which  $B_z B'_z$  is adjusted to fulfill Eqn. 3.3. Even here, the depletion zone is clearly expanded by a factor 2.3, but two plumes are visible: one downwards and one upwards, demonstrating the opposite residual forces. The inhomogeneities in the  $G_{eff} = 10^{-2}$  range heavily influence solutal flow. From this it can be concluded that the position of the growth cell in the magnet has to be accurately chosen after careful analysis of the field profile. It is however possible to construct a magnet with a specially designed gradient to obtain a homogeneous  $B_z B'_z$  over a relatively large volume, overcoming problems caused by inhomogeneities [6].

## 4.4 Conclusions

Growing a NSH crystal in a gradient magnetic field under the right conditions, shows that all the features associated with suppression of convection that are expected to occur during microgravity crystal growth, also occur in a gradient magnetic field. Although we did not reach effective fields in the  $G_{eff} = 10^{-6}$  range (i.e. genuine microgravity), the extreme suppression of buoyancy driven convection, the expansion of the depletion zone and the significant decrease in growth rate are all observed. Also, the relation between  $\delta$  and  $G_{eff}$  shows that  $\delta$  varies with  $G_{eff}^{-1/4}$ , as expected from an analysis using the dimensionless Sherwood and Rayleigh numbers. We have also shown that it is important to have detailed knowledge of the field profile of the magnet as well as the concentration dependencies of the magnetic susceptibility and density of the growth solution. The question whether growth under conditions where convection is suppressed yields better crystals is not addressed in this chapter. The quality of NSH crystal grown under  $G_{eff} = 1$  is already quite good, so any improvements in

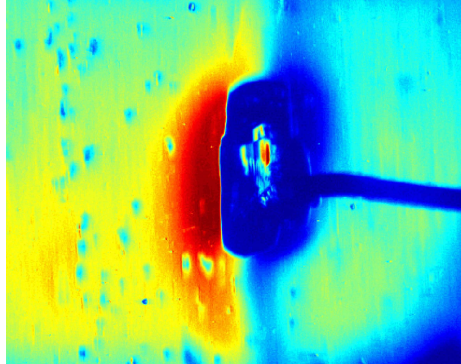


Figure 4.8: False color schlieren image of a growing NSH crystal for  $G_{eff} = 0$  at the position of Fig. 4.7b. In addition to an expanded depletion zone, two convection plumes are visible, one upwards and one downwards. The blue spots are small crystals grown on the wall of the growth cell.

crystal quality would be difficult to observe. Experiments in which protein crystals are grown in a gradient magnetic field are underway. These experiments will show the effect of suppressed convection on crystal quality. In this study, we have shown that all the aspects that are held responsible for crystal quality improvement for crystals grown in microgravity are also present for growth in gradient magnetic fields. On top of that, the use of gradient magnetic fields allows varying  $G_{eff}$ , in order to tune the solutal flow, the width of the depletion zone and growth rate. This, combined with the relative experimental ease of growing crystals in magnetic fields as compared to space based efforts, shows that the use of gradient magnetic fields offers a good alternative to protein crystal growth in space.



# Bibliography

- [1] P.W.G. Poodt, M.C.R. Heijna, P.C.M. Christianen, W.J.P. van Enckevort, W.J. de Grip, K. Tsukamoto, J.C. Maan, E. Vlieg, *Applied Physics Letters* **87**, 214105 (2005)
- [2] F.M. White, *Heat and mass transfer* (Addison-Wesley, Boston, 1991)
- [3] F. Otálora, J.M. García-Ruiz, L. Carotenuto, D. Castagnolo, M.L. Novella, A.A. Chernov, *Acta Crystallographica D* **58**, 1681 (2002)
- [4] N. Ramachandran, Ch.R. Baugher, R. Naumann, *Journal of Microgravity Science and Technology* **8**, 170 (1995)
- [5] J.M. Coulson, J.F. Richardson, *Chemical Engineering* (Pergamon Press, Oxford, 1964)
- [6] T. Kiyoshi, O. Ozaki, H. Morita, H. Nakayama, J. Hong-Beom, H. Wada, N.I. Wakayama, M. Ataka, *IEEE Transactions on Applied Superconductivity* **9**, 362 (1999)



## Chapter 5

# Magnetically controlled gravity for protein crystal growth

The occurrence of convective flows during crystal growth is believed to adversely affect crystal quality. Space-based crystal growth is therefore actively pursued, particularly for protein crystals, because buoyancy-driven convection is suppressed in microgravity. Here we demonstrate that magnetic fields can be used to tune the effective gravity from 1 to  $-0.15 g$  during the growth of diamagnetic lysozyme crystals and that convection can be damped, stopped, and even reversed. The growth velocity is strongly reduced in simulated microgravity. This method provides a versatile and accessible way to realize an earth-based tunable gravity environment for crystal growth in which protein crystal quality may be optimized\*.

---

\*Adapted from: M.C.R. Heijna, P.W.G. Poodt, J.L.A. Hendrix, K. Tsukamoto, P.C.M. Christiaenen, W.J.P. van Enkevort, W.J. de Grip, J.C. Maan, E. Vlieg, Applied Physics Letters **90** (2007) 264105

On earth, crystal growth from a supersaturated solution is accompanied by buoyancy-driven convection in the liquid, an effect often detrimental to crystal quality. For protein crystals a high quality is required for x-ray structure determination at high resolution [1, 2], which is of great biotechnological and pharmacological importance. In order to avoid the adverse effects of convection, much effort has been put in examining the virtues of space-based microgravity for protein crystal growth [1-3]. However, whether zero gravity is the ideal growth condition is still an open question.

It has been shown that gradient magnetic fields can influence convective flows in paramagnetic fluids [4-6], and to apply the same approach to seemingly nonmagnetic proteins is appealing, since in fact all diamagnetic materials can be magnetically levitated [7, 8]. A number of experiments have been performed on protein crystal growth under levitation conditions [9,10]. The criterion for damping convection during crystal growth is, however, quite different from that for levitation, because it relies on balancing buoyancy rather than gravitational force [5,6].

A growing crystal extracts solute from the solution and thus locally reduces the mass density of the solution. The diluted liquid close to the crystal surface will rise due to buoyancy, which leads to a convection pattern, comprising a thin (typically 0.1-0.3 mm) laminar flow boundary layer (depletion zone) and a so-called growth plume [11] on top of the crystal [Fig. 5.1a]. Without convection this plume disappears, diffusion remains the sole means of mass transport, and the depletion zone will expand to infinity [Fig. 5.1b]. To suppress convection the buoyancy forces caused by differences in mass density have to be opposed by magnetic buoyancy forces due to differences in magnetic susceptibility.

For small variations in concentration of the solute, both the density and the susceptibility depend linearly on concentration, i.e.,  $\rho(c) = \alpha c + \rho_0$  and  $\chi(c) = \beta c + \chi_0$ . The convection is then suppressed if

$$B_z B'_z = \frac{\alpha}{\beta} \mu_0 g, \quad (5.1)$$

where  $B_z$  is the vertical magnetic field,  $B'_z$  its gradient, and  $\mu_0$  the magnetic susceptibility. The suppression of buoyancy therefore depends on the concentration dependence of the mass density and susceptibility ( $\alpha$  and  $\beta$ ) and not on the mass density and susceptibility themselves, as for normal and magneto-Archimedes levitation [12, 13].

We demonstrate our method using the diamagnetic protein hen egg-white lysozyme (HEWL) for which crystallization conditions have been well established [14]. The

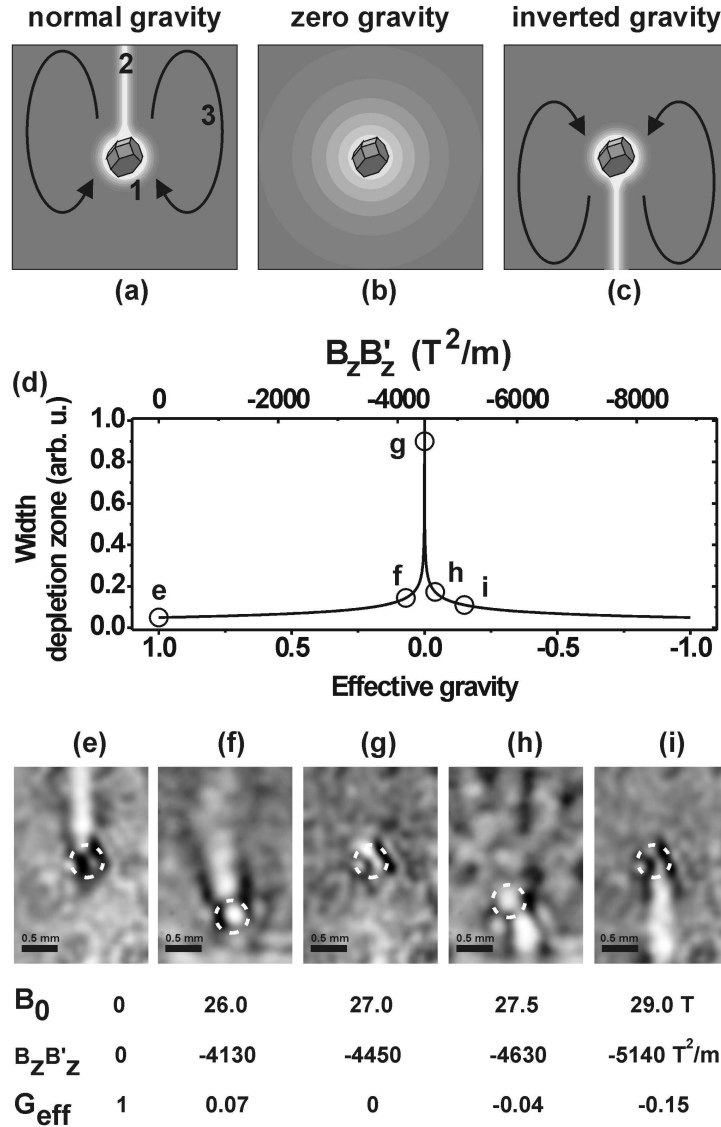


Figure 5.1: Magnetically tuned gravity during crystal growth. (a) A growing crystal depletes its surrounding solution (1), leading to a growth plume (2) and convective flows (3). (b) At zero effective gravity convection is cancelled and the diffusion field expands. (c) In inverted gravity the buoyancy-driven convection is reversed, and a downward growth plume is formed. (d) The width of the depletion zone as function of  $G_{eff}$ . (e)-(i) Experimental shadowgraphy images of a growing lysozyme crystal (indicated by the dashed white circles) in solution for  $G_{eff}$  ranging from -0.15 to 1.

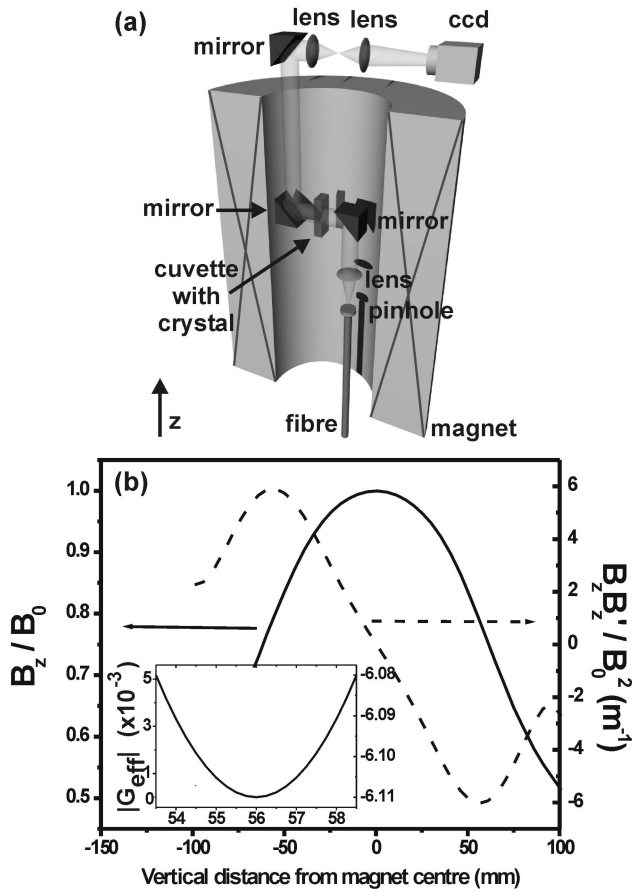


Figure 5.2: Experimental set-up for in-situ observation of convective fluid flows in a 33T magnet. (a) Schematic representation of the shadowgraphy insert used to visualise density variations in solutions. (b) Profiles of magnetic field and field times field gradient ( $B_z B'_z$ ) scaled to a  $B_0$  background field. The inset shows the  $B_z/B_0$  profile around the optimum position and the corresponding effective gravity.

experiments were performed in a 33 T water-cooled resistive magnet with a bore diameter of 32 mm at the High Field Magnet Laboratory at the Radboud University Nijmegen. The magnet, fitted with a double-walled tube for temperature control, contains a shadowgraphy [15] setup for imaging convection patterns around the growing crystal [Fig. 5.2a]. A glass cuvette (inner dimensions of 8 x 4 x 18 mm<sup>3</sup>) with crystal and solution was placed at the position of maximum field gradient [red curve in Fig. 5.2b]. The cuvette is illuminated from the side by a highly collimated beam of light from a halogen lamp, using an optical fiber in combination with a lens and a 75  $\mu\text{m}$  pinhole, leading to an image on a camera. Variations in the concentration of the fluid result in local differences in the refractive index, which appear as intensity variations in the image. The sensitivity to concentration differences scales with the degree of being out of focus [15].

We used HEWL from Sigma-Aldrich (Lot No. 094K1454), which was dissolved and dialyzed against a 0.05M NaOAc/HOAc buffer solution of pH 4.5 at room temperature before use. Tetragonal lysozyme crystals were grown from a solution of 30 mg/ml HEWL, 0.685M NaCl, and 0.05M NaOAc/HOAc at pH 4.5 and 18°C. Crystals were taken from the growth vessel and placed as a seed in the glass cuvette for the magnet experiments. The crystal was manipulated to be in the field of view of the insert, after which the solution was removed and the cuvette was placed in a refrigerator at 4°C for 20 min. As a result, the crystal is attached to the glass wall of the cuvette. Finally, the cuvette was refilled with the same solution as used during growth and placed in the insert for experiments.

The condition for convection damping is determined by  $\alpha$  and  $\beta$  in Eqn.5.1. For HEWL  $\alpha$  is 0.303kgm<sup>-3</sup>/mg ml<sup>-1</sup> [16], and we have determined  $\beta$  to be  $(-1.2 \pm 0.5) \times 10^{-9}$  ml/mg using a magnetic susceptibility balance. Inserting these values in Eqn. 5.1 we expect that convection is damped at  $B_z B'_z = -3100 \pm 1500 T^2/m$ , which is significantly larger than the -1500 T<sup>2</sup>/m needed for simple levitation of the bulk solution [9]. We determined the actual gradient field at which the growth plume disappears by using shadowgraphy. Figure 5.1e shows a growing HEWL crystal at zero field gradient, and the convection plume is clearly visible as a white streak rising upward from the crystal. In the picture the crystal itself is blurred because for shadowgraphy out-of-focus images have to be taken. The growth plume disappears, and thus convection is suppressed at a gradient magnetic field of  $-4450 \pm 30 T^2/m$  [Fig. 5.1g]. The value falls within our estimate using alpha and beta, but is much higher than previously expected [5, 9] and requires the largest magnets currently available. In fact, this value for the gradient field accurately determines beta as  $(-0.84 \pm 0.06) \times$

$10^{-9}ml/mg$ .

This result unambiguously shows that gradient magnetic fields can create conditions on earth that mimic those in space-based microgravity. Most importantly, however, is the fact that by changing the magnetic field strength the effective gravity for convection can be continuously varied. If we define [17]

$$G_{eff} = 1 - \frac{\beta}{\alpha\mu_0g}B_zB'_z, \quad (5.2)$$

$G_{eff}$  is expressed in terms of the earth's gravitational acceleration  $g$ . By varying the magnetic field we are able to change  $G_{eff}$  and as a result the convection is tuned from normal, with a growth plume upwards [Figs. 5.1e and f], via cancellation at  $G_{eff} = 0$  [Fig. 5.1g], to inverted with the growth plume downwards for negative values of  $G_{eff}$ [Figs. 5.1h and i].

The range of field gradients at which convection is stopped is quite small,  $\pm 30T^2/m$  centered around  $-4450T^2/m$ , which corresponds to  $B = 27$  T in the magnet we used. Decreasing (increasing) the magnetic field by only  $0.1T$  ( $G_{eff} \approx \pm 0.005$ ) already results in appreciable convection and thus in upward (downward) growth plumes. This strong effect is caused by the steep dependence of the balance between convective flow and mass diffusion on  $G_{eff}$ , which is reflected by the thickness of the depletion zone. For example, Fig. 5.1d shows the theoretically calculated, and for  $NiSO_4 \cdot 6H_2O$  experimentally demonstrated [17], dependence of the thickness of the depletion zone  $\delta$  on gravity. Since  $\delta \propto G_{eff}^{-1/4}$  it diverges near zero, which implies that the field gradient has to be set quite precisely. Such a strong dependence also puts constraints on the spatial variation of  $G_{eff}$  within a magnet. From Eqn. 5.2 we calculate  $G_{eff}$  as function of the position around the crystal using the experimental field profile [inset of Fig. 5.2b], which shows that changes of  $G_{eff}$  over the relevant region are within  $\pm 0.005$ . Despite the precise condition on the required field gradient, milligravity rather than microgravity [18] is sufficient to make convective transport slower than that due to diffusion and to dampen convection.

To show that the suppression of convection indeed affects crystal growth, we have measured the growth rate of two lysozyme crystals, one at  $G_{eff} = 1$  and one at 0, at otherwise identical conditions (Fig. 5.3). Here the same imaging setup was used, but now with the crystal in focus to determine the position of its surface. The growth rate drops a factor of 15 from  $30 \pm 2$  to  $2 \pm 2 \mu m/h$  when convection is stopped and the depletion zone is expanded, which is similar to results obtained under space-based microgravity [19].



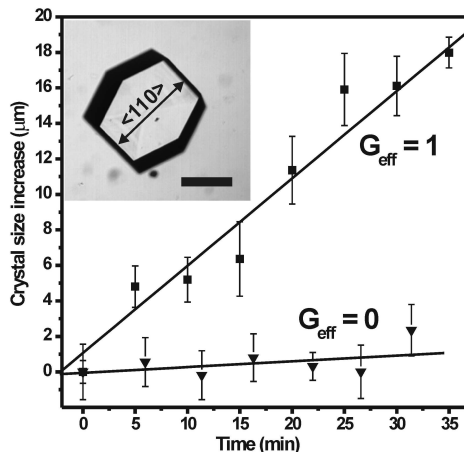


Figure 5.3: Growth rate of tetragonal HEWL crystals at normal and zero effective gravity,  $G_{eff}$ . The squares and triangles denote the increase in HEWL crystal size at a  $G_{eff} = 1$  and  $G_{eff} = 0$  respectively, obtained in the  $\langle 110 \rangle$  direction. The inset shows a tetragonal HEWL crystal similar to those used in the experiments, and the  $\langle 110 \rangle$  direction with respect to the morphology.

In contrast with other methods to suppress convection such as gel growth [20, 21] and microfluidics [22], gradient magnetic fields offer a powerful way to tune the effective gravity during crystal growth under earth-based conditions, with far easier access, availability, and including in situ observation. Especially for protein crystal growth this possibility is very attractive, since the tunability will allow the optimization of the crystal quality by finding the right balance between mass transport towards the crystal and the incorporation rate of molecules at the crystal surface. The required gradient magnetic fields for suppression of convection are found to be in the 4000–5000 T<sup>2</sup>/m range. Because density and susceptibility are closely related, we expect that this value is rather similar for most diamagnetic proteins. We foresee that our determination of the proper conditions for which convection is suppressed will trigger the design and construction of dedicated magnets that are capable of sustaining high field gradients for the several days that are needed to grow protein crystals.



# Bibliography

- [1] E. H. Snell, J. R. Helliwel, *Reports on Progress in Physics* **68**, 799 (2005)
- [2] A. Vergara, B. Lorber, C. Sauter, R. Giege, and A. Zagari, *Biophys. Chem.* **118**, 102 (2005)
- [3] W. Littke, C. John, *Science* **225**, 203 (1984)
- [4] D. Braithwaite, E. Beaunon, R. Tournier, *Nature* **354**, 134 (1991)
- [5] N. Ramachandran, F. W. Leslie, *Journal of Crystal Growth* **274**, 297 (2005)
- [6] P. W. G. Poodt, M. C. R. Heijna, K. Tsukamoto, W. J. de Grip, P. C. M. Christianen, J. C. Maan, W. J. P. van Enkevort, E. Vlieg, *Applied Physics Letters* **87**, 214105 (2005)
- [7] E. Beaunon, R. Tournier, *Nature* **349**, 470 (1991)
- [8] A. K. Geim, *Physics Today* **51**, 36 (1998)
- [9] N. I. Wakayama, *Crystal Growth & Design* **3**, 17 (2003)
- [10] N. I. Wakayama, *Japanese Journal of Applied Physics Part 2* **44**, L833 (2005)
- [11] P. J. Shlichta, *Journal of Crystal Growth* **76**, 656 (1986)
- [12] Y. Ikezoe, N. Hirota, J. Nakagawa, K. Kitazawa, *Nature* **393**, 749 (1998)
- [13] A. T. Catherall, L. Eaves, P. J. King, S. R. Booth, *Nature* **422**, 579 (2003)
- [14] A. McPherson, *Crystallization of Biological Macromolecules* (Cold Spring Harbor Laboratory, New York, 1999)
- [15] G. Settles, *Schlieren and Shadowgraphy Techniques* (Springer, Berlin, 2001)
- [16] W. J. Fredericks, M. C. Hammonds, S. B. Howard, F. Rosenberger, *Journal of Crystal Growth* **141**, 183 (1994)
- [17] P. W. G. Poodt, M. C. R. Heijna, K. Tsukamoto, W. J. de Grip, P. C. M. Christianen, J. C. Maan, W. J. P. van Enkevort, E. Vlieg, *Crystal Growth & Design* **6**, 2275 (2006)
- [18] N. Ramachandran, C. R. Baugher, R. J. Naumann, *Microgravity Science and Technology* **8**, 170 (1995)

- 
- [19] F. Otálora, J. M. García-Ruiz, L. Carotenuto, D. Castagnolo, M. L. Novella, A. A. Chernov, *Acta Crystallographica D* **58**, 1681 (2002)
- [20] M. C. Robert, K. Provost, F. Lefauchaux, *Crystallization of nucleic acids and proteins: a practical approach*, edited by A. Ducruix and R. Giegé (IRL, Oxford, 1999)
- [21] J. M. García-Ruiz, J. Drenth, M. Riés-Kautt A. Tardieu, *A World without Gravity: Research in Space for Health and Industrial Processes*, edited by G. Seibert, B. Titton, and B. Battrick (ESA, Noordwijk, The Netherlands, 2001)
- [22] D. C. Carter, P. Rhodes, D. E. McRee, L. W. Tari, D. R. Dougan, G. Snell, E. Abola, R. C. Stevens, *Journal of Applied Crystallography* **38**, 87 (2005)

## Chapter 6

# The critical Rayleigh number in low gravity crystal growth from solution

If crystal growth from solution takes place in a closed container, a critical Rayleigh number can be defined, below which buoyancy driven convection is suppressed and mass transport is completely determined by diffusion at gravitational accelerations higher than  $0g$ . Using finite element simulations and an analytical model, we show that it is possible to predict the critical value of the Rayleigh number. This result can be used to optimize growth conditions for microgravity protein crystal growth, if the gravitational acceleration cannot be cancelled completely, like in space, or is cancelled inhomogeneously, like in gradient magnetic fields\*.

---

\*Adapted from: P.W.G. Poodt, P.C.M. Christianen, W.J.P. van Enckevort, J.C. Maan, E. Vlieg, *submitted to Crystal Growth & Design*

## 6.1 Introduction

Crystal growth from solution in a reduced gravity environment has received a considerable amount of attention, because of its potential to improve the quality of protein crystals [1]. In the absence of gravity, buoyancy driven convection, induced by density gradients resulting from the depletion of the solution, is suppressed. As diffusion starts dominating over convective mass transport, a wide depletion zone develops and the growth rate reduces significantly, which is expected to lead to an improvement of protein crystal quality as compared to crystals grown under normal gravity. This is highly relevant, because for protein structure determination by X-ray diffraction, protein crystallization is often the quality limiting step. A considerable number of growth experiments have been performed in space, where gravity levels as low as  $10^{-6}g$  can be attained. However, the question whether this indeed leads to better crystals is still not conclusively answered [2, 3], which can be attributed to the complexity of the system and the corresponding shortage of both fundamental knowledge and experimental evidence of what actually happens during crystal growth under reduced gravity.

A promising alternative for space based experiments, is the use of gradient magnetic fields [4-6], with which it is possible to create an effective microgravity environment for crystal growth, much more accessible and reproducible than by experiments in space. It offers the opportunity to investigate the effect of reduced gravity on crystal growth in great detail [7]. In order to understand the effect of reduced gravity on crystal growth from solution, the complex interplay of crystallization kinetics, fluid flows and mass and/or heat transport has to be studied. Experimentally, this can be quite complicated, and therefore a number of computer simulations have been carried out to give insight into the hydrodynamics during crystal growth [1]. Unfortunately, these simulations are often restricted to a specific set of growth conditions, and typically only consider gravitational accelerations of  $1g$  and  $0g$ . As a consequence, these results do not offer general insight into low gravity crystal growth, but only to specific, limiting cases. Analytical descriptions, on the other hand, can only be obtained for highly simplified cases. Ostrach offers analytical expressions for flow velocities at low gravity levels [8] from which it follows that, in order to obtain diffusion dominated mass transport, the gravitational acceleration should be  $0g$ . His analysis, however, was performed for crystal growth in an infinitely large container, in which no interaction between the flowing solution and container walls exists. That this interaction plays an important role was shown by Ramachandran *et al* [9]. They showed by

simulations of crystal growth in an enclosure the existence of a critical value of the effective gravitational acceleration, higher than  $0g$ , below which mass transport is determined by diffusion rather than convection. The value of the effective gravity where this occurs was found to depend on the size ratio of the crystal and growth container. Understanding the nature of this critical behavior could offer a means to optimize growth conditions for (protein) crystals in situations where the gravitational acceleration cannot be suppressed completely, like in space, or in inhomogeneous environments, like in gradient magnetic fields.

## 6.2 The critical Rayleigh number

Crystal growth in a closed container shows resemblance with the classical Rayleigh-Benard problem [10] where fluid is enclosed between a horizontal hot bottom plate and a cooled top plate. A temperature and density gradient will form, but buoyancy driven convection only sets in if the viscous forces are overcome. If not, heat will be transported by conduction. Although in the case of crystal growth from solution there are concentration gradients instead of thermal gradients, a large similarity exists concerning the hydrodynamics, so we can make use of existing models and theory describing heat transport in enclosures.

To describe mass transport in enclosures, the relevant parameters can be captured in two dimensionless numbers, namely the Rayleigh number  $Ra$ , and the Sherwood number  $Sh$ , given by [11]

$$Ra \equiv \frac{g_{eff} L^3}{\nu D} \frac{\rho_b - \rho_e}{\rho_b}, \quad (6.1)$$

and

$$Sh \equiv \frac{\partial c}{\partial \mathbf{n}} \frac{L}{\Delta c}, \quad (6.2)$$

with  $g_{eff}$  the effective gravitational acceleration,  $\rho_b$  and  $\rho_e$  the density of solution with bulk and equilibrium concentration respectively,  $L$  a characteristic length,  $\nu$  the kinematic viscosity,  $D$  the diffusion coefficient, and  $\frac{\partial c}{\partial \mathbf{n}}$  and  $\Delta c$  the concentration gradient and difference within the enclosure. The Rayleigh number is a measure of the ratio between convective and diffusive mass transport, whereas the Sherwood number reflects the dimensionless concentration gradient in the container, which, in the case of crystal growth, is a measure of the growth rate [12]. Below a critical value of the Rayleigh number, mass is transported only by diffusion and the Sherwood number

has a constant value, but above this critical value, viscous forces are overcome and convection sets in, where the Sherwood number increases with increasing Rayleigh number. So, the critical Rayleigh number for a given geometry can be determined by measuring the Sherwood number as function of the Rayleigh number, which can be changed by varying any of the parameters of Eqn. 6.1. In this chapter, we focus on changing the gravitational acceleration, either by going to space or by application of gradient magnetic fields. A dimensionless effective gravity,  $G_{eff}$ , can be defined as

$$G_{eff} \equiv g_{eff}/g, \quad (6.3)$$

with  $g$  the gravitational acceleration on earth, being  $9.8m/s^2$ .

To understand the effect of reducing gravity, and thus reducing Rayleigh numbers, on convection and mass transport during crystal growth, and to investigate whether the concept of critical Rayleigh numbers also applies to crystal growth from solution, the relation between the Sherwood and Rayleigh number has to be studied. Although well established for simple geometries such as the Rayleigh-Benard problem, finding analytical models for the relation between  $Sh$  and  $Ra$  can be extremely complex for more realistic geometries. Recently, Teertstra *et al.* [13] published a model that gives an accurate description of this relation for the case of heated bodies in concentric enclosures. This model can be adapted to describe crystal growth in enclosures for various values of the Rayleigh number.

### 6.3 The 3-term model

The model developed and thoroughly tested by Teertstra *et al.* [13] divides the hydrodynamics in three domains: a convective one for high Rayleigh numbers, a diffusive domain for low Rayleigh numbers and a transition regime for intermediate Rayleigh numbers (Fig. 6.1). The relation between the Sherwood number and the Rayleigh number can be written as

$$Sh = S + \left( \frac{A}{Ra^2} + \frac{B}{\sqrt{Ra}} \right)^{-1/2}, \quad (6.4)$$

with  $S$ ,  $A$  and  $B$  constants that are determined by the geometry and sizes of the crystal and container. The Sherwood number in the diffusion dominated regime, so for Rayleigh numbers below the critical value, is given by  $S$ . The exact expressions for  $S$ ,  $A$  and  $B$  for various geometries can be found in Teertstra *et al* [14]. Eqn. 6.4



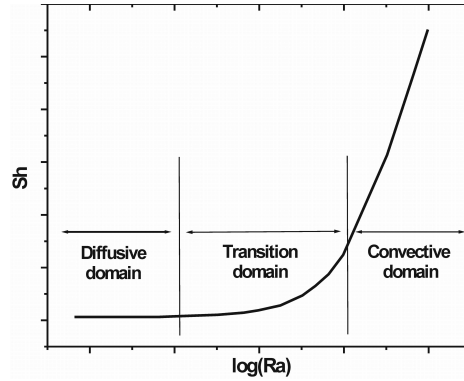


Figure 6.1:  $Sh$  vs.  $\log(Ra)$ . The three domains shown are described by the 3-term model.

can be seen as an extension to low Rayleigh numbers for the generally used relation between  $Sh$  and  $Ra$  for free convection [7, 11]

$$Sh \propto Ra^{1/4}, \quad (6.5)$$

which is reflected in the last term of Eqn. 6.4.

## 6.4 Finite element simulations

The 3-term model is a 3-dimensional, steady-state model for a uniform effective gravitational field, whereas crystal growth is a non-steady-state process and the effective gravity is not necessarily uniform [7]. To test whether the 3-term model can be applied to determine the critical Rayleigh number for crystal growth from solution in an enclosure, the model is compared with the results from 2-dimensional finite element simulations. First, we will test the validity to compare the 2D simulations with the 3D model and determine the critical Rayleigh number for the steady-state case. Second, we will compare this result with simulations having non-steady-state boundary conditions. Third, we will investigate the effects of an inhomogeneous effective gravity, and finally, we will explore possibilities to optimize growth conditions with respect to an inhomogeneous effective gravity.

The finite element simulations are performed with FlexPDE 5 from PDE solutions Inc [15]. The geometry used in the 2-dimensional simulations comprises a square crystal centered in a concentric square enclosure, of which the sizes can be varied. It is assumed that the crystal growth rate is small enough to safely ignore moving boundaries. The simulations are performed in steady-state mode and a non-steady-state mode, depending on the applied boundary conditions. As a model system, we consider the growth of nickel sulfate hexahydrate crystals from a supersaturated aqueous solution. The solutal settings are given in table 6.1 and correspond to an earlier experiment [5]. For not too large concentration variations, the density of the solution is assumed to vary with concentration according to  $\rho = \alpha c + \rho_0$ , with  $\alpha$  a proportionality constant and  $\rho_0$  an offset value.

We used the Vorticity-Streamfunction formulation for the Navier-Stokes, the continuity and mass transport equations in a Boussinesq approximation, given by

$$\text{Navier-Stokes: } \frac{\partial \omega}{\partial t} + \frac{\partial \Psi}{\partial y} \frac{\partial \omega}{\partial x} - \frac{\partial \Psi}{\partial x} \frac{\partial \omega}{\partial y} = \nu \nabla^2 \omega + \frac{-\alpha g}{\rho_0} \frac{\partial c}{\partial x}, \quad (6.6)$$

$$\text{Continuity: } \nabla^2 \Psi - \omega = 0, \quad (6.7)$$

$$\text{Mass transport: } \frac{\partial c}{\partial t} + \frac{\partial \Psi}{\partial y} \frac{\partial c}{\partial x} - \frac{\partial \Psi}{\partial x} \frac{\partial c}{\partial y} = D \left( \frac{\partial^2 c}{\partial x^2} + \frac{\partial^2 c}{\partial y^2} \right). \quad (6.8)$$

The vorticity  $\omega$  is defined as the curl of the velocity, and the streamfunction  $\Psi$  is defined in such a way that the  $x$  and  $y$  components of the flow velocity  $\mathbf{V}$  can be expressed as  $V_x = \frac{\partial \Psi}{\partial y}$  and  $V_y = -\frac{\partial \Psi}{\partial x}$ . For the simulations, a dynamic adaptive mesh refinement was used to automatically enhance resolution where the greatest changes are taking place. The non-slip condition at the crystal interface and container walls was implemented using the penalty method [16].

## 6.5 Results

### 6.5.1 Uniform effective gravity and steady state

The three-term model is a 3D model, while the simulations are 2D. To investigate whether the simulations can be compared with the model, a  $1 \times 1 \text{ mm}^2$  crystal centered in a  $7 \times 7 \text{ mm}^2$  growth container was modeled in the steady-state mode, with the concentration at the container wall and crystal interface fixed at the bulk and

Table 6.1: Values used for the simulations.

Parameter	Value
$c_b$	$1.16 \text{ g/cm}^3$
$c_e$	$1.07 \text{ g/cm}^3$
$\nu$	$0.05 \text{ cm}^2/\text{s}$
$D$	$5 \times 10^{-6} \text{ cm}^2/\text{s}$
$k$	$5 \times 10^{-4} \text{ cm}^{-1}$
$g$	$981 \text{ cm/s}^2$
$\alpha$	0.223
$\rho_0$	$1.1565 \text{ g/cm}^3$

equilibrium concentration, respectively. Figure 6.2a shows a typical example of such a simulation, where the convection plume and depletion zone are clearly visible. In Fig. 6.2b, the streamlines show the flow profile of the solution where two vortices can be seen next to the crystal. For different values of the Rayleigh number, i.e. different values of  $G_{eff}$ , the Sherwood number was computed. The results are fitted using Eqn. 6.4, with  $S$ ,  $A$  and  $B$  as fit parameters (Fig. 6.3 and table 6.2). For this given geometry, the Sherwood number is constant below a Rayleigh number of 100. Here, mass transport is completely diffusion dominated, resulting in a spherically symmetric depletion zone around the crystal. Lowering  $G_{eff}$  further will have no significant effect on this. This is the critical Rayleigh number, corresponding to a  $G_{eff}$  of  $\sim 10^{-4}$ . So to achieve diffusion dominated mass transport, a complete absence of is not required.

Next,  $S$ ,  $A$  and  $B$  were calculated according to Teertstra *et al.* [14] for the 3D analogue of the simulation, using a  $1 \times 1 \times 1 \text{ mm}^3$  crystal centered in a  $7 \times 7 \times 7 \text{ mm}^3$  container (table 6.2). Both the 2D simulation results and 3D calculation were normalized by dividing the outcomes by  $S$ . The results are given in Fig. 6.4. Although the values of  $S$ ,  $A$  and  $B$  for the fit to the 2D simulation and the 3-term model differ, the normalized plots completely overlap, giving the same value for the critical Rayleigh number. Therefore, it is safe to compare the 2D simulations with the 3D model for determining the critical Rayleigh number.

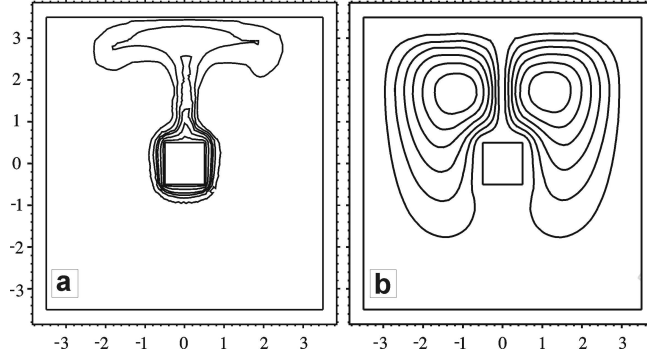


Figure 6.2: a and b: Typical iso-concentration lines and streamlines around a 1x1 mm crystal (white square) centered in a 7x7 mm container, obtained from finite elements simulation. The depletion zone and convection plume can clearly be seen.

Table 6.2:  $S$ ,  $A$  and  $B$  determined from the fit and the 3-term model

Parameter	Fit to 2D-simulation	3-term model
$S$	1.66	4.06
$A$	$1.03 \times 10^6$	$6.11 \times 10^5$
$B$	14.8	2.7

### 6.5.2 Non-steady-state

In reality, crystal growth is not a steady-state process. There is only a limited amount of solute available and the uptake of solute at the interface is governed by the local supersaturation. The concentration, and thus the corresponding density, at the interface will typically not have the equilibrium value, and will change in time. So the definition of the Rayleigh and Sherwood number (Eqns. 6.1 and 6.2) has to be corrected by replacing  $c_{\min}$  and  $\rho_{\min}$  with the actual concentration and density at the crystal interface,  $c_i$  and  $\rho_i$ . When a crystal is introduced in a supersaturated solution, the solution depletes, and as the difference between the bulk and interface concentration increases, the Rayleigh and Sherwood number will show a transient behavior. But as long as during growth the Rayleigh number does not exceed the critical value,

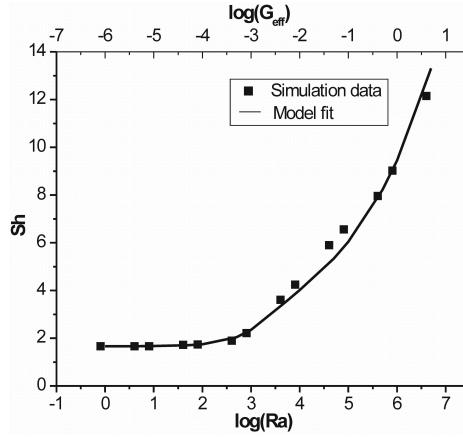


Figure 6.3: Data points from the simulations, represented by the squares, and the 3-term model fit, represented by the line.

the Sherwood number behavior will resemble the case if  $G_{eff} = 0$ .

To incorporate this in the simulations, the mass flux at the container wall is set to zero and at the interface, linear kinetics are assumed. As the mass flux is defined as  $\mathbf{j} = -D \frac{\partial c}{\partial \mathbf{n}}$ , the boundary conditions become

$$\frac{\partial c}{\partial \mathbf{n}_c} = 0, \quad (6.9)$$

and

$$\frac{\partial c}{\partial \mathbf{n}_i} = h(c - c_e), \quad (6.10)$$

with  $\frac{\partial c}{\partial \mathbf{n}_c}$  the flux normal to the container wall,  $\frac{\partial c}{\partial \mathbf{n}_i}$  the concentration gradient normal to the crystal interface,  $h$  the kinetic coefficient  $k$  divided by the diffusion coefficient  $D$  and  $c_e$  the equilibrium concentration. Changing  $h$  or the type of interface kinetics in the simulations only changes the time scale and not the end result, so  $h$  was set at a typical value of  $5 \times 10^{-4} \text{ cm}^{-1}$ . In the non-steady-state case, the Sherwood number will not reach a constant value, but keeps decreasing until the growth container is fully depleted. During the simulation, the Sherwood number was monitored for a period of  $10^4$  seconds for different values of the effective gravity, as can

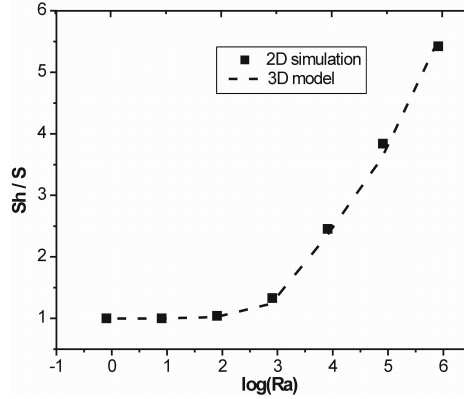


Figure 6.4: 2D simulations (squares) vs. 3D model (dashed line)

be seen in Fig. 6.5. For all values of  $G_{eff}$ , the Sherwood number decreases over time as the depletion zone grows. The plots for below  $10^{-4}$  completely overlap with the one for  $G_{eff} = 0$ , whereas for higher values the separate plots can be distinguished. This reflects that below  $G_{eff} = 10^{-4}$  the Rayleigh number does not exceed the critical value, so mass transport is fully diffusion determined and cannot be distinguished from the case where  $G_{eff} = 0$ . For which  $G_{eff}$  the Rayleigh number exceeds its critical value depends on the nature of the interfacial kinetics, and the exact value cannot be determined by the 3-term model. However, the excellent agreement between the critical value of determined from both the steady-state model and non-steady-state simulations shows that the 3-term model gives a good estimate of the value of the critical Rayleigh number, since variations in interface concentration are not likely to deviate significantly from the steady state situation, especially for low  $G_{eff}$ .

### 6.5.3 Inhomogeneous effective gravity

In refs. [5] and [7], convection was suppressed during growth of nickel sulfate crystals from solution by using gradient magnetic fields. An analysis of the field profile showed that the effective gravity was not homogeneous, but varied parabolically in the growth container, being zero at the crystal and around  $10^{-3}$  further away from the crystal. Nevertheless, convection was suppressed and a widely developed depletion zone was

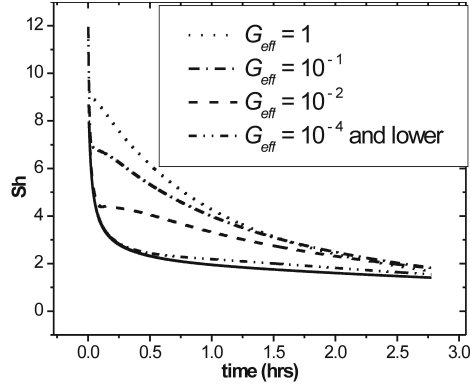


Figure 6.5: The Sherwood number vs. time for the non-steady-state simulations

observed. Our simulations can be extended to describe this situation as well. To get clear results, an exaggerated parabolic variation was introduced in the simulation, with  $G_{eff} = 0$  at the center of the growth container and maxima of  $G_{eff} = 10^{-2}$  at the top and bottom of the growth container (Fig. 6.6). From the previous results we expect some convection to be present in this case. The simulations were performed in a non-steady-state mode with linear interface kinetics. Fig. 6.7 shows the results for a period of 2.75 hours. The decrease of the Sherwood number in time differs from the case when  $G_{eff} = 0$ , and resembles the case of the homogeneous  $G_{eff} = 10^{-3}$ , which is above the critical value. Figs. 6.8a and b shows iso-concentration lines and streamlines after 1200 seconds. The depletion zone has lost its circular symmetry, being extended above the crystal and fattened below. As can be seen in Fig. 6.8b, there are two vortices above and two below the crystal, whereas for a homogeneous  $G_{eff}$  there are only two above the crystal. These additional vortices are formed because depleted solution below the crystal feels an upward force that decreases when the solution rises, due to the inhomogeneity of  $G_{eff}$ . Near the crystal, the upward force is very small and the fluid's momentum causes part of the solution flow sideways and downwards again, forming the vortices.

If a parabolic gravity field like this is present, the effect of the inhomogeneity is enhanced, because the rising depleted solution above the crystal protrudes into regions with a higher  $G_{eff}$ , increasing the driving force for fluid flow. One can, however, tune

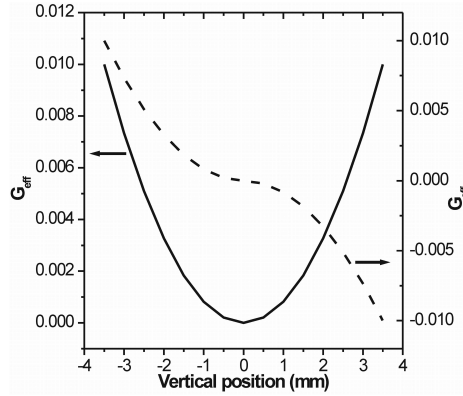


Figure 6.6: The parabolic (full line) and 3rd order polynomial (dashed line) inhomogeneous  $G_{eff}$ , used in the simulations.

the inhomogeneity in such a way that the negative effects are minimized. A possible way is to introduce an inhomogeneous field of which  $G_{eff}$  has negative values above the crystal, and positive below. Then, depleted solution above the crystal will not rise, but actually flows towards the crystal, in the same manner as the depleted solution from below the crystal does. In this way, the depleted solution is effectively trapped in a region of low  $G_{eff}$ . Gradient magnetic fields offer this possibility. To see the effects on the hydrodynamics, a 3rd order polynomial effective gravity field was used in the simulation, keeping the other settings the same as for the parabolic profile. Now  $G_{eff}$  is negative above the crystal and positive below, as can be seen in Fig. 6.6. Fig. 6.7 again shows the results for a period of 2.75 hours. The data points fall between the plots for the homogeneous  $G_{eff} = 0$  and the parabolic profile. Fig. 6.8c and d show the concentration and streamlines after 1200 seconds, and reveal how the depleted solution is "trapped" near the crystal. Thus, by tuning the effective gravity field in such a way that it is negative above the crystal and positive below, reduces the negative effect of the inhomogeneity, as if reducing  $G_{eff}$  towards its critical value.



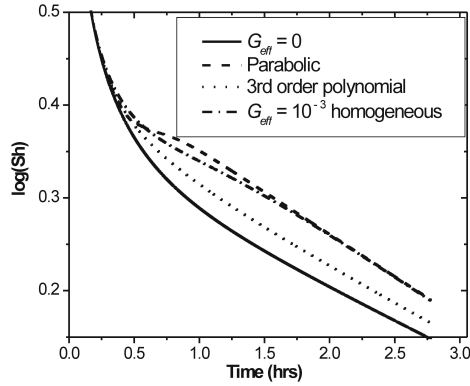


Figure 6.7: The Sherwood number vs. time, compared for homogeneous and inhomogeneous effective gravities.

#### 6.5.4 Optimizing growth conditions for inhomogeneous $G_{eff}$

From the 3-term model, we can predict the critical Rayleigh number for different container sizes below which mass transport is diffusion dominated. If the inhomogeneity of  $G_{eff}$  is known, we can use this to optimize the container size to make sure that mass transport is determined by diffusion during growth. An approximate criterion for this is

$$\overline{G_{eff}}(s_o) < G_{effc}(s_o), \quad (6.11)$$

which says that  $\overline{G_{eff}}(s_o)$ , the mean effective gravity in the growth container as function of the container size  $s_o$ , should be smaller than  $G_{effc}(s_o)$ , the critical effective gravity as function of  $s_o$ . The first term can be determined from the field profile and the second using the 3-term model. Fig. 6.9 shows the critical  $G_{eff}$  as well as the mean effective gravity as function of container size, for a  $1 \times 1 \text{ mm}^2$  crystal in the parabolic effective gravity profile of Fig. 6.7. Eqn. 6.11 is satisfied left from the intersection point of the two graphs, so for container sizes less than  $4 \times 4 \text{ mm}^2$ . To test whether mass transport is really diffusion dominated for this container size, a simulation was performed for this specific situation. The behavior of the Sherwood number was found to be indistinguishable from the case of  $G_{eff} = 0$ , so the critical

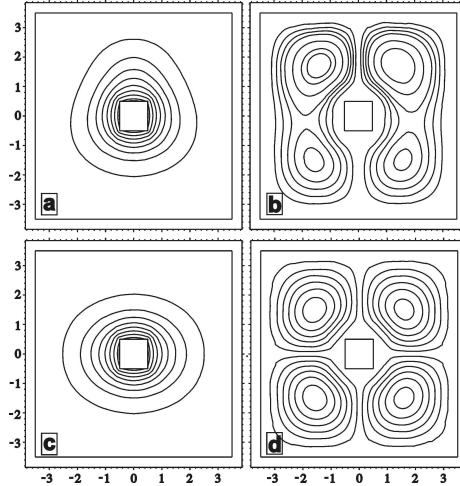


Figure 6.8: a and b: Iso-concentration lines and streamlines obtained from the parabolic  $G_{eff}$  profile. c and d: Iso-concentration lines and streamlines obtained from the 3rd order polynomial  $G_{eff}$  profile.

Rayleigh number was not exceeded, showing that Eqn. 6.11 can be used as a valid optimization criterion. From the simulations however, it was observed that for this specific geometry and inhomogeneity, applying Eqn. 6.11 leads to an underestimate of 10-15% for the maximum allowable container size, especially when using effective gravity fields like the 3rd order polynomial shown in Fig. 6.6. A less strict criterion can be chosen, but nevertheless, the possibility to optimize both container size and effective gravity field by using the 3-term model offers prospects to reach optimum growth conditions.

## 6.6 Discussion

In the simulations, a crystal of constant size was used while in real growth experiments, the crystal starts out as a nucleus. As the critical Rayleigh number depends on the ratio between crystal size and container size, a value found from the 3-term model for the final size of the crystal will not be valid for when the crystal is still small.

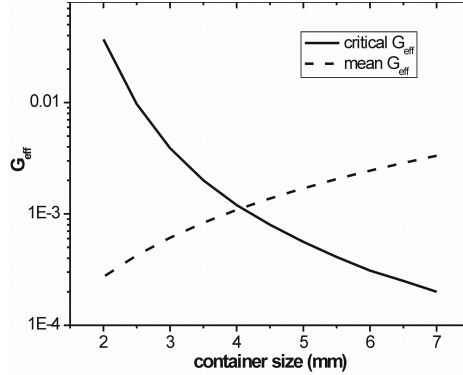


Figure 6.9: The critical  $G_{eff}$  and mean  $G_{eff}$  as function of container size.

However, when the crystal is still small and the depletion zone is still developing, the concentration and density variations will be small. So, convection only begins to play a significant role when the crystal is large. Nevertheless, to get a complete and more accurate image of crystal growth in an enclosure, 3-dimensional simulations including moving boundaries have to be performed. It is questionable however, whether significant new information is obtained compared to the increase of complexity of the simulations.

For non-concentric geometries, like cubic crystals in elongated, rectangular containers, the expressions for the  $S$ ,  $A$ , and  $B$  terms in Eqn. 6.4 are not given by Teertstra *et al.* [14], although our simulations show that the 3-term model is still valid. An approximation can be made by taking the average distances between the crystal and container walls beside and above the crystal, because these influence the value of the critical Rayleigh number most strongly. This average value can be used for calculating  $S$ ,  $A$  and  $B$ .

## 6.7 Conclusion

In this chapter we have shown by combining theory and finite element simulations, that for crystal growth from solution in a closed growth container, there is a critical Rayleigh number below which convection is suppressed and mass transfer is diffusion

dominated. In that case, viscous forces and friction with the container walls cannot be overcome by the buoyant driving force for convection. In practice, this means that it is not necessary to reduce the gravitational acceleration completely to suppress convection, if growth takes place in a container. We have shown that the value of this critical Rayleigh number, and the corresponding critical can be predicted by using the 3-term model of Teertstra *et al* [13]. Albeit a steady state model developed for heat transfer, we have shown that it can also be applied to crystal growth in low gravity, offering the opportunity to optimize the container size for different inhomogeneous effective gravity fields, like when using gradient magnetic fields to reduce to suppress convection.

# Bibliography

- [1] E.H. Snell, J.R. Helliwell, Reports on Progress in Physics **68** (2005) 799
- [2] C.E. Kundrot, R.A. Judge, M.L. Pusey, E. Snell, Crystal Growth & Design **1** (2001) 87
- [3] T. Reichardt, Nature **404** (2000) 114
- [4] N.I. Wakayama, Crystal Growth & Design **3** (2003) 17.
- [5] P.W.G. Poodt, M.C.R. Heijna, P.C.M. Christianen, W.J.P. van Enckevort, W.J. de Grip, K. Tsukamoto, J.C. Maan, E. Vlieg, Applied Physics Letters **87** (2005) 214105
- [6] M.C.R. Heijna, P.W.G. Poodt, J.L.A. Hendrix, K. Tsukamoto, P.C.M. Christianen, W.J.P. van Enckevort, W.J. de Grip, J.C. Maan, E. Vlieg, Applied Physics Letters **90** (2007) 264105
- [7] P.W.G. Poodt, M.C.R. Heijna, P.C.M. Christianen, W.J.P. van Enckevort, W.J. de Grip, K. Tsukamoto, J.C. Maan, E. Vlieg, Crystal Growth & Design **6** (2006) 2275
- [8] S. Ostrach, Annual Review of Fluid Mechanics **14** (1982) 313
- [9] N. Ramachandran, C.R. Baugher, R.J. Naumann, Microgravity Science & Technology **8** (1995) 170
- [10] P.K. Kundu, I.M. Cohen, *Fluid Mechanics 2nd ed.* (Academic Press, San Diego, 2002)
- [11] V.G. Levich, *Physicochemical Hydrodynamics* (Prentice-Hall, Englewood Cliffs, 1962)
- [12] Coulson, J.M.; Richardson, J.F. Chemical engineering; Pergamon Press: Oxford, 1964.
- [13] P. Teertstra, M.M. Yovanovich, J.R. Culham, Thermophysics and Heat Transfer **20** (2006) 297

- 
- [14] P. Teertstra, M.M. Yovanovich, J.R. Culham, *HT-FED04-56633*, ASME Heat Transfer/Fluids Engineering Summer Conference (2004)
  - [15] [www.pdesolutions.com](http://www.pdesolutions.com)
  - [16] F.C.G. DeMarco, C.R. DeAndrade, E.L. Zapparoli, International Communications in Heat and Mass Transfer **30** (2003) 495

## Chapter 7

# A comparison between simulations and experiments for microgravity crystal growth in gradient magnetic fields

Experiments on microgravity crystal growth in gradient magnetic fields for nickel sulfate and lysozyme are compared with finite element simulations. These simulations include the inhomogeneous effective gravity that accompanied the magnet experiments. An excellent agreement between the simulations and the experiments was found. Methods to reduce the adverse effects of the inhomogeneous effective gravity and to optimize the growth conditions are discussed\*.

---

\*Adapted from: P.W.G. Poodt, M.C.R. Heijna, P.C.M. Christianen, W.J.P. van Enckevort, J.C. Maan, E. Vlieg, *submitted to Crystal Growth & Design*

## 7.1 Introduction

Microgravity protein crystal growth is expected to lead to an improvement of protein crystal quality, compared to crystals grown under normal gravity, due to the suppression of buoyancy driven convection [1]. This is highly relevant, because for protein structure determination by X-ray diffraction, protein crystallization is often the quality limiting step. A considerable number of growth experiments have been performed in space, where gravity levels as low as  $10^{-6}g$  can be attained, but the question whether this indeed leads to better crystals is still not conclusively answered [2, 3]. The use of gradient magnetic fields is a promising alternative for space based experiments [4], which we recently have shown by growing both para- and diamagnetic crystals in a microgravity condition [5, 6]. Under experimentally much more controllable conditions than in space, this offers the possibility to study in detail the effect of reduced gravity on the fluid dynamics, mass transport and growth rate [7]. One important aspect about the magnet experiments, however, was that the gravitational acceleration was not homogeneously suppressed throughout the growth cell. The effective gravity varied parabolically, being zero near the crystal but having a higher value further away [7]. That inhomogeneous effective gravities have an effect on the hydrodynamics during growth, was shown in our previous work [8]. In this chapter, we include an inhomogeneous effective gravity in finite element simulations and compare these with our previous magnet experiments, to get a better understanding of the experimental observations. In the first part, the nickel sulfate hexahydrate experiments from ref. [7], and in the second part, experiments with lysozyme described in ref. [6] will be discussed.

## 7.2 Finite element simulations

The finite element simulations were performed using the FlexPDE 5 software from PDE solutions Inc [9]. It is assumed that the crystal growth rate is small enough to safely ignore the moving boundaries. For not too large concentration variations, the density of the solution  $\rho$  is assumed to vary with concentration  $c$  according to  $\rho = \alpha c + \rho_0$ , with a  $\alpha$  proportionality constant and  $\rho_0$  an offset value. We used the Vorticity-Streamfunction formulation for the Navier-Stokes, continuity and mass transport equation in a Boussinesq approximation, given by



$$\text{Navier-Stokes: } \frac{\partial \boldsymbol{\omega}}{\partial t} + \frac{\partial \Psi}{\partial y} \frac{\partial \boldsymbol{\omega}}{\partial x} - \frac{\partial \Psi}{\partial x} \frac{\partial \boldsymbol{\omega}}{\partial y} = \nu \nabla^2 \boldsymbol{\omega} + \frac{-\alpha g}{\rho_0} \frac{\partial c}{\partial x}, \quad (7.1)$$

$$\text{Continuity: } \nabla^2 \Psi - \omega = 0, \quad (7.2)$$

$$\text{Mass transport: } \frac{\partial c}{\partial t} + \frac{\partial \Psi}{\partial y} \frac{\partial c}{\partial x} - \frac{\partial \Psi}{\partial x} \frac{\partial c}{\partial y} = D \left( \frac{\partial^2 c}{\partial x^2} + \frac{\partial^2 c}{\partial y^2} \right). \quad (7.3)$$

with  $\omega$  the vorticity and  $\Psi$  the streamfunction [8]. A dynamic adaptive mesh refinement was used to automatically enhance resolution where the greatest changes are taking place, while the non-slip condition at the crystal interface and container walls was implemented using the penalty method [10]. The mass flux at the container wall is set to zero and linear growth kinetics are assumed at the crystal-solution interface. As the mass flux is defined as  $\mathbf{j} = -D \frac{\partial c}{\partial \mathbf{n}}$ , the boundary conditions become

$$\frac{\partial c}{\partial \mathbf{n}_c} = 0, \quad (7.4)$$

and

$$\frac{\partial c}{\partial \mathbf{n}_i} = h(c - c_e), \quad (7.5)$$

with  $\frac{\partial c}{\partial \mathbf{n}_c}$  the concentration gradient normal to the container wall,  $\frac{\partial c}{\partial \mathbf{n}_i}$  the concentration gradient normal to the crystal interface,  $h$  the kinetic coefficient divided by the diffusion coefficient and  $c_e$  the equilibrium concentration

During the simulations, the dimensionless Sherwood number  $Sh$  can be computed. The Sherwood number is defined as

$$Sh \equiv \frac{\partial c}{\partial \mathbf{n}} \frac{L}{\Delta c}, \quad (7.6)$$

with  $\frac{\partial c}{\partial \mathbf{n}}$  the concentration gradient at the crystal interface,  $L$  a characteristic length and  $\Delta c$  the difference between the bulk and equilibrium concentration. It reflects the dimensionless concentration gradient at the crystal interface, and is a measure for the amount of mass transported to the crystal, which is directly related to the crystal growth rate [12]. Finally, a dimensionless effective gravity is defined as

$$G_{eff} \equiv g_{eff}/g, \quad (7.7)$$

with  $g$  the gravitational acceleration on earth, being  $9.8m/s^2$ .

## 7.3 Nickel sulfate hexahydrate experiments

### 7.3.1 Results

In refs. [5] and [7], a  $1 \times 2 \times 2 \text{ mm}^3$  nickel sulfate hexahydrate crystal was submerged in a  $7 \times 7 \times 13 \text{ mm}^3$  growth container filled with supersaturated solution. A gradient magnetic field was applied to suppress convection and in-situ schlieren microscopy was used to monitor fluid flow, mass transport and growth rate. The effective gravity was, however, not uniform, and in order to find out how this affected the fluid dynamics, we compare finite element simulation including an inhomogeneous effective gravitational field with the experimental observations.

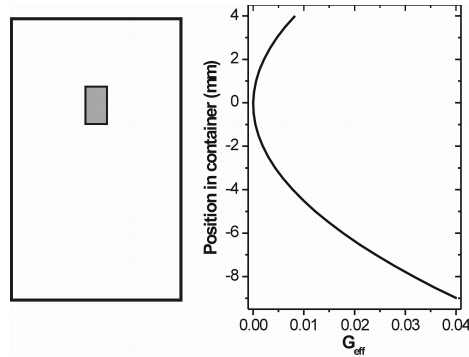


Figure 7.1: The geometry (left) and effective gravity profile (right) used in the simulations for growth of a nickel sulfate crystal. The  $1 \times 2 \text{ mm}^2$  crystal (gray) is placed in a  $7 \times 13 \text{ mm}^2$  container.

In the simulations, a  $1 \times 2 \text{ mm}^2$  crystal in a  $7 \times 13 \text{ mm}^2$  growth container was used (Fig. 7.1), which reflects the geometry of the experiments. The parameters used for the simulations are given in table 7.1. From the field profile of the magnet, a parabolic effective gravity profile was calculated, and included in the simulations, as shown in Fig. 7.1.

Figs. 7.2a and b show the streamlines and iso-concentration lines around the crystal after a simulation corresponding to 1500 seconds. The depletion zone has significantly expanded, but shows a pear shaped profile that is extended above the crystal and fattened below. There are two vortices above and two below the crystal,

Table 7.1: Values used for the simulations for nickel sulfate crystal growth

Parameter	Value
$c_b$	$1.16 \text{ g/cm}^3$
$c_e$	$1.07 \text{ g/cm}^3$
$\nu$	$0.05 \text{ cm}^2/\text{s}$
$D$	$5 \times 10^{-6} \text{ cm}^2/\text{s}$
$h$	$5 \times 10^{-4} \text{ cm}^{-1}$
$g$	$981 \text{ cm/s}^2$
$\alpha$	0.223
$\rho_0$	$1.1565 \text{ g/cm}^3$

shaping the depletion zone, whereas for a homogeneous  $G_{eff}$  we found only two above the crystal [8]. The additional vortices are formed because depleted solution below the crystal feels an upward force that decreases when the solution rises due to the inhomogeneity of  $G_{eff}$ . Near the crystal, the upward force is very small and the fluid's momentum causes part of the solution to flow sideways and downwards again, forming the vortices. Fig. 7.2c shows a schlieren microscopy image of the left side of a growing nickel sulfate crystal in a gradient magnetic field [7]. With schlieren microscopy, the concentration gradient was visualized in the horizontal direction. Although in the vertical direction, no information about the concentration gradient is available, it is still clearly visible that the depletion zone has extended widely, to approximately 12 times of its original width at  $G_{eff} = 1$ , showing a similar pear shaped profile as in Fig. 7.2b.

Fig. 7.3 shows a vector plot of the flow velocity in the growth container, obtained from the simulation, where the vortices from the streamline plot can be recognized. Near the crystal side faces, where the opposite rotating vortices meet, the vector plot shows an erratic behavior with parts of the fluid flowing upward and others downward, next to each other. This is in accordance with the experimental observations, where small particles present in the growth solution followed the solution flow during growth and showing the same erratic behavior [7]. Some particles moved up, others down, though very slow, with no single source identifiable. However, from the simulation it follows that this behavior originates from the interacting vortices above and below the crystal. Additionally, the flow velocity obtained from the simulation and experiments have the same order of magnitude of  $10^{-3} \text{ mm/s}$ , which is less than 1% of the flow

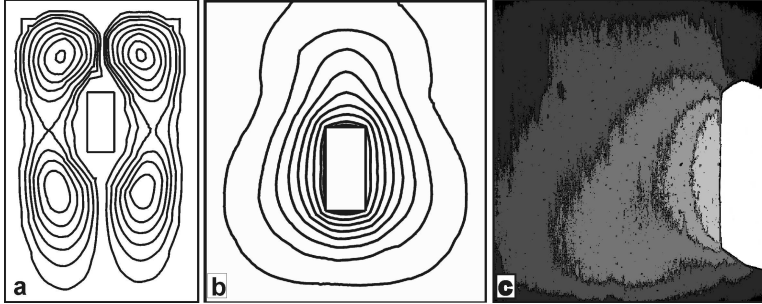


Figure 7.2: (a) and (b) Streamlines and iso-concentration lines around a growing nickel sulfate crystal after simulations corresponding to 1500 s (different scales). c. Schlieren image of the left side of a growing nickel sulfate crystal (white), taken from chapter 3.

velocity at  $G_{eff} = 1$ .

In ref. [7], the growth rate of the crystal was measured over time. It decreased rapidly during the first 15 minutes of the experiment, after which it reached a constant value. This is not expected if mass transport is completely diffusion dominated, because then the growth rate should keep decreasing until the entire growth container becomes depleted. Possibly, due to the inhomogeneity of  $G_{eff}$ , enough convection remains for the growth rate to reach a constant value. However, during the simulations with the inhomogeneous effective gravity, the Sherwood number never reached a constant value, which is likely caused by the 2-dimensionality of the simulations. This can only be confirmed by doing full 3D simulations.

### 7.3.2 Optimization

The presence of the additional vortices, the resulting shape of the depletion zone, the erratic behavior of the solution near the crystal and possibly the constant growth rate, are all direct and unwanted consequences of the inhomogeneity of the effective gravity. In ref. [8], we proposed two methods to reduce these effects, first by tuning the magnetic field profile, and second, by optimizing the container size with respect to the inhomogeneity of  $G_{eff}$ . As the first method can be quite difficult, we apply here the second approach. For this, the concept of the critical effective gravity is

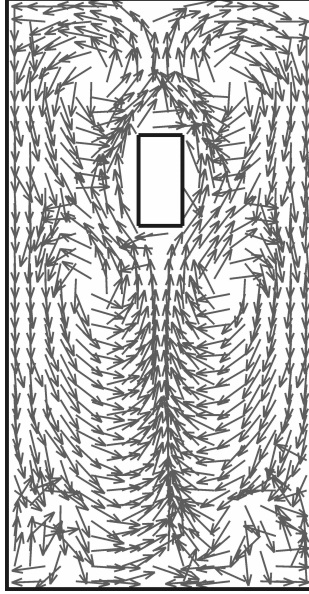


Figure 7.3: Vector plot of the flow velocity around a growing nickel sulfate crystal after a simulation corresponding to 1500 s.

used. Below a critical value of the effective gravity, buoyancy driven convection will be suppressed because the driving force for convection cannot overcome the viscous and frictional forces. Then, although the gravitational acceleration is not zero, mass transport is completely determined by diffusion. The critical effective gravity can be calculated using the 3-term model described in refs. [8] and [12].

In ref. [8] we proposed a criterion for the critical effective gravity:

$$\overline{G_{eff}}(s_o) < G_{effc}(s_o), \quad (7.8)$$

which means that  $\overline{G_{eff}}(s_o)$ , the mean effective gravity in the growth container as function of the container size  $s_o$ , should be smaller than  $G_{effc}(s_o)$ , the critical effective gravity as function of the container size  $s_o$ . Although using Eqn. 7.8 gives an underestimate of the maximum allowable container size of 10-15% [8], it can be

used as a rule of thumb. If a cubic crystal centered in a concentric growth container is assumed, the critical effective gravity can be calculated using the 3-term model, as described in ref. [8], while the mean effective gravity can be determined from the field profile. Fig. 7.4 shows both the critical and the mean effective gravity as function of

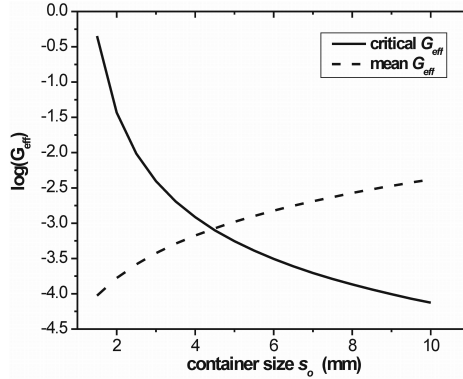


Figure 7.4: The mean and critical effective gravity as function of the container size for the growth of nickel sulfate crystals.

container size, for a  $1 \times 1 \text{ mm}^2$  nickel sulfate crystal in the parabolic effective gravity profile of Fig. 7.1. Eqn. 7.8 is satisfied left from the intersection point of the two graphs, so below a container size of  $4.5 \times 4.5 \text{ mm}^2$ . For this optimized geometry, mass transport is completely diffusion determined, and the effects of the inhomogeneity are negligible.

An extreme example of the effect of an inhomogeneous  $G_{eff}$  was given in ref. [7], where the field profile was chosen such that it varied linearly over the growth container. Here  $G_{eff}$  had a positive value above the crystal, and was negative below (Fig. 7.5). If the field profile is included in the simulation, it results in two convection plumes, one oriented upwards and one downwards, as can be seen in Fig. 7.5b. The result from the simulation agrees very well with the experimental schlieren image of Fig. 4.8.

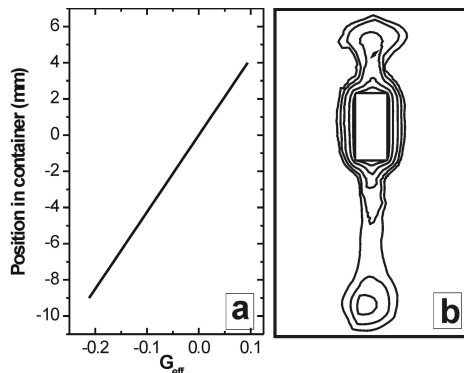


Figure 7.5: (a) The effective gravity profile used in the simulation. (b) Iso-concentration lines depicting the depletion zone around the crystal from the simulation. Two convection plumes are visible, one going up and one down.

## 7.4 Lysozyme experiments

In the experiments in ref. [6], a lysozyme crystal was seeded onto the wall of a  $4 \times 8 \times 18 \text{ mm}^3$  growth container filled with supersaturated solutions, placed in a gradient magnetic field and observed by shadowgraphy. For the simulations, the container and crystal dimensions are translated to a  $0.5 \times 0.5 \text{ mm}^2$  crystal attached to a  $4 \times 18 \text{ mm}^2$  container, as shown in Fig. 7.6a. In the experiment, a different magnet was used than for the nickel sulfate experiments, and a new effective gravity profile was determined from the field profile (Fig. 7.6b). The parameters used in the simulation are given in table 7.2. From all the components in the protein crystallization solution, only the lysozyme concentration was allowed to vary during the simulation.

Fig. 7.6c shows the concentration distribution after a simulation corresponding to 3000 seconds. The depletion zone has extended to approximately the size of the crystal, but a plume is still present, albeit weak. In the shadowgraphy images taken during the experiment described in ref. [6] however, no plume was visible anymore. Probably, the gradients in refractive index in the plume became smaller than the detection limit of the shadowgraphy microscope. Also for this case, an optimization was performed according to Eqn. 7.8. Fig. 7.7 shows both the critical and the mean effective gravity as function of container size, for a  $0.5 \times 0.5 \text{ mm}^2$  crystal in the

Table 7.2: Values used for the simulations of lysozyme crystal growth

Parameter	Value
$c_b$	$3 \times 10^{-2} \text{ g/cm}^3$
$c_e$	$3 \times 10^{-3} \text{ g/cm}^3$
$\nu$	$0.01 \text{ cm}^2/\text{s}$
$D$	$1 \times 10^{-6} \text{ cm}^2/\text{s}$
$h$	$1 \text{ cm}^{-1}$
$g$	$981 \text{ cm/s}^2$
$\alpha$	0.3032
$\rho_0$	$1.0049 \text{ g/cm}^3$

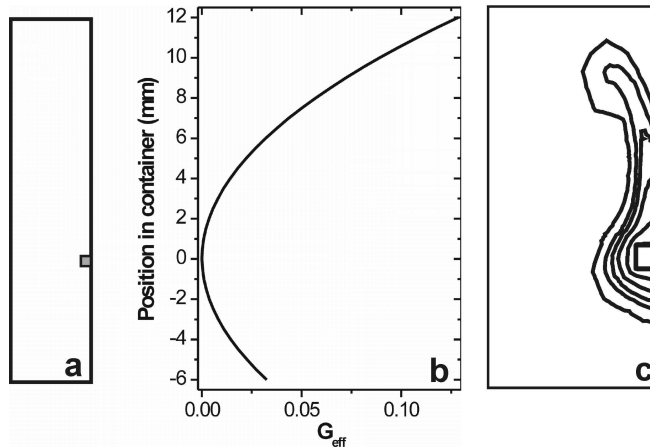


Figure 7.6: The geometry (a) and effective gravity profile (b) used in the simulations for the growth of lysozyme. The  $0.5 \times 0.5 \text{ mm}^2$  crystal (gray) is placed on the wall of a  $4 \times 18 \text{ mm}^2$  container. (c) Simulated iso-concentration lines around a growing lysozyme crystal after 3000 s of growth.



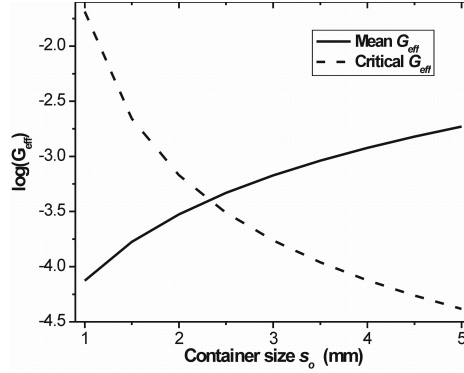


Figure 7.7: The mean and critical effective gravity as function of container size, for lysozyme.

parabolic effective gravity profile. Eqn. 7.8 is satisfied left of the intersection point of the two graphs, so below a container size of  $\sim 2.3 \times 2.3 \text{ mm}^2$ . This is almost half the size found for the nickel sulfate optimization, and a lot smaller than the container used in the experiment. Nevertheless, the large reduction of the growth rate from  $30$  to  $2 \mu\text{m/hr}$ , observed in the experiment shows that convection was largely suppressed. The fact that the crystal was seeded on the container wall helped considerably, because the wall is a significant source of friction, slowing down the flowing solution near the crystal.

## 7.5 Discussion and conclusions

Although the simulations were 2-dimensional and simplified, the comparison between simulations and experiments shows a remarkable agreement for many observations. Especially in the case of the nickel sulfate experiments, the simulations offer explanations for the shape of the depletion zone and erratic flows near the crystal, which could not be easily obtained through experiments. We showed that for crystal growth in gradient magnetic fields, the effects of an inhomogeneous effective gravity field cannot be ignored, and care should be taken to minimize the negative effects, by optimizing growth container dimensions, by minimizing the inhomogeneity of the effective

gravity or by a combination of both. Combining experiments and simulations offers a powerful tool to study crystal growth from solution in microgravity, and can help to determine the optimum conditions for (protein) crystal growth in gradient magnetic fields.

# Bibliography

- [1] E.H. Snell, J.R. Helliwell, Reports on Progress in Physics **68** (2005) 799
- [2] C.E. Kundrot, R.A. Judge, M.L. Pusey, E. Snell, Crystal Growth & Design **1** (2001) 87
- [3] T. Reichardt, Nature **404** (2000) 114
- [4] N.I. Wakayama, Crystal Growth & Design **3** (2003) 17.
- [5] P.W.G. Poodt, M.C.R. Heijna, P.C.M. Christianen, W.J.P. van Enkevort, W.J. de Grip, K. Tsukamoto, J.C. Maan, E. Vlieg, Applied Physics Letters **87** (2005) 214105
- [6] M.C.R. Heijna, P.W.G. Poodt, J.L.A. Hendrix, K. Tsukamoto, P.C.M. Christianen, W.J.P. van Enkevort, W.J. de Grip, J.C. Maan, E. Vlieg, Applied Physics Letters **90** (2007) 264105
- [7] P.W.G. Poodt, M.C.R. Heijna, P.C.M. Christianen, W.J.P. van Enkevort, W.J. de Grip, K. Tsukamoto, J.C. Maan, E. Vlieg, Crystal Growth & Design **6** (2006) 2275
- [8] P.W.G. Poodt, P.C.M. Christianen, W.J.P. van Enkevort, J.C. Maan, E. Vlieg, *to be published*
- [9] [www.pdesolutions.com](http://www.pdesolutions.com)
- [10] F.C.G. DeMarco, C.R. DeAndrade, E.L. Zapparoli, International Communications in Heat and Mass Transfer **30** (2003) 495.
- [11] J.M. Coulson, J.F. Richardson, *Chemical engineering* (Pergamon Press, Oxford, 1964)
- [12] P. Teertstra, M.M. Yovanovich, J.R. Culham, Thermophysics and Heat Transfer **20** (2006) 297



## **Part II**

# **The BAD method**



## Chapter 8

# **Buoyancy assisted diffusion limited crystal growth: harnessing gravity to suppress convection**

A new upside-down geometry is proposed to achieve all the beneficial effects of microgravity crystal growth, by making use of buoyant forces instead of compensating for them. We show by finite element simulations and growth experiments on sodium chlorate that crystal growth in an upside-down geometry leads to the formation of a buoyancy assisted depletion zone. The effects on growth rate and morphology that are observed are all indicative of diffusion limited growth, just as would happen in the absence of gravity. The simplicity of this growth method offers the possibility to perform large scale protein crystal growth experiments under microgravity-like conditions, without the requirement of compensating for gravity.

## 8.1 Introduction

Microgravity protein crystal growth is believed to lead to an improvement of protein crystal quality, compared to crystals grown under normal gravity [1]. This is highly relevant, because for protein structure determination by X-ray diffraction, protein crystallization is often the quality limiting step. There are three major reasons why crystal growth in the absence of gravity would result in higher quality crystals [1]. First, in the absence of buoyancy driven convection, diffusion will become the sole means of mass transport, accompanied by the formation of an extended depletion zone. The interface supersaturation, and thus the growth rate will continuously decrease, so fewer defects will be formed. Second, large impurities like dimers will diffuse even slower, decreasing their incorporation rate, known as diffusional purification [2]. Third, merging due to sedimentation of microcrystals will not occur.

Until recently, the only way to significantly reduce the gravitational acceleration for prolonged times was to go to space, where gravity is reduced to  $\sim 10^{-6}g$  [1]. Many protein crystal growth experiments have been performed on board Space Shuttles or stations. However, the costs, low accessibility, and residual accelerations ( $g$ -jittering) make this approach less practical. An alternative for space are gradient magnetic fields, in which a magnetic force compensates the gravitational force [3]. In chapter 5 it is shown that this technique can be used to suppress convection during growth of lysozyme crystals, at a fraction of the cost and effort of space based experiments. In this chapter we describe another method to achieve the same benefits of crystal growth in space or magnetic fields, not by compensating for the gravitational force, but by making use of it in an upside down geometry.

Consider a setup like in Fig. 8.1, where a growing crystal is located at the top of a closed growth cell filled with supersaturated solution. During growth of the crystal, the solution near the crystal becomes depleted of solute. As the density of the depleted solution decreases, it feels an upward buoyant force. For a freely suspended crystal buoyancy driven convection would set in, but for the upside down geometry there is no room for a convective flow to develop. The depleted solution is forced to accumulate at the top of the cell and fresh material has to be supplied from below the crystal. Under the influence of buoyant forces, the depleted solution forms a horizontally stratified depletion zone, expanding downwards, while convective flows cannot form. We will call this a Buoyancy Assisted Depletion (BAD) zone. During the BAD zone formation, mass transport towards the crystal becomes increasingly more difficult, and the growth of the crystal becomes diffusion limited. On top of



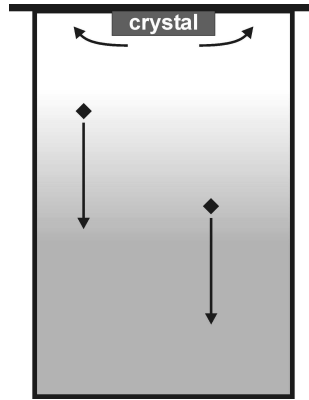


Figure 8.1: Crystal growth in the upside-down geometry. A growing crystal is attached to the top of a growth cell. Depleted solution is forced to accumulate at the top because of buoyancy, leading to diffusion limited growth. Also, sedimenting microcrystals will not be incorporated into the growing crystal.

that, due to diffusional purification, impurity incorporation rates are reduced and, for obvious reasons, sedimenting microcrystals will not be incorporated. Whereas conventionally it requires suppression of gravity to achieve these conditions, using the upside down geometry it is possible to harness gravity to achieve the same.

Although appearing similar, the method we propose is very different from that of the hanging drop method, because in the latter method no depletion zone is formed owing to the location of crystals at the air-solution interface and the effects of Marangoni convection. Our use of a completely filled container overcomes this problem. Other growth geometries with the crystal on top have proposed before. Moreno *et al.* [6] proposed the upside-down geometry as a method to slow down the diffusion of precipitant during protein crystal growth in gels, where convection is already suppressed. Wakayama [7] proposed to use magnetic fields to force growing crystals to float at the solution-air interface. This would, however, lead to Marangoni convection because of the surface tension gradients at the solution-air interface that accompany the concentration gradients in the BAD zone [8].

## 8.2 Theory

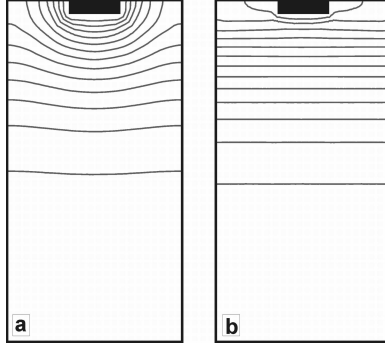


Figure 8.2: Iso-concentration lines indicating the depletion zone around a growing sodium chlorate crystal at  $0g$  (a) and  $1g$  (b), for a simulation corresponding to 1 hour. Between the lines  $\Delta c = 10^{-3} g/cm^{-3}$ .

To investigate how the BAD zone formation affects interface supersaturation and growth rate, we used a simplified model and analytically solved the diffusion equation to obtain the time and position dependent concentration. Assume a geometry like in Fig. 8.1, where the  $z$ -coordinate is chosen parallel to the gravitational acceleration, with the origin at the bottom facet of the crystal. To find an expression for the time- and position dependent concentration  $c(r, t)$  in the growth cell, Fick's second law,

$$\frac{\partial c(r, t)}{\partial t} = \nabla(D(r, t)\nabla c(r, t)), \quad (8.1)$$

with  $D$  the diffusion coefficient, has to be solved. If the height of the growth cell is much larger than the size of the crystal, the cell can be approximated as being semi-infinite. Assuming that the concentration is uniform in the lateral plane and the diffusion coefficient is constant, Eqn. 8.1 reduces to

$$\frac{\partial c(z, t)}{\partial t} = D \frac{\partial^2 c(z, t)}{\partial z^2}. \quad (8.2)$$

Growth rates will be small, so moving boundaries are ignored. Furthermore, the interfacial flux, and thus the growth rate, is determined by a balance between mass

transport towards the interface and interface kinetics. In the case of linear kinetics, it is given by

$$D \left. \frac{\partial c(z, t)}{\partial z} \right|_{z=0} = \beta (c(z, t)|_{z=0} - c_e), \quad (8.3)$$

with  $\beta$  the kinetic coefficient and  $c_e$  the equilibrium concentration. Taking Eqn. 8.3 as boundary condition, and  $c(z, t)|_{t=0} = c_b$ , with  $c_b$  the bulk concentration, as initial condition, the solution of Eqn. 8.2 can be determined via the Laplace transform method [9] (appendix A) and is given by [10]

$$c(z, t) = (c_e - c_b) \left[ \operatorname{erfc} \left\{ \frac{z}{2\sqrt{Dt}} \right\} - \exp [hz + h^2 Dt] \operatorname{erfc} \left\{ \frac{z}{2\sqrt{Dt}} + h\sqrt{Dt} \right\} \right] + c_b, \quad (8.4)$$

with  $h = \frac{\beta}{D}$ . The interface concentration  $c_i$  can be found by evaluating Eqn. 8.4 for  $z = 0$ :

$$c_i(t) = c(z, t)|_{z=0} = (c_e - c_b) \left( 1 - \exp [h^2 Dt] \operatorname{erfc} \left\{ h\sqrt{Dt} \right\} \right) + c_b. \quad (8.5)$$

The growth rate  $v_g$  is given by the interfacial flux, multiplied by the volume of the diffusing unit  $\Omega$  (e.g. molecular volume):

$$v_g(t) = D \left. \frac{\partial c(z, t)}{\partial z} \right|_{z=0} \Omega = -Dh (c_e - c_b) \exp [h^2 Dt] \operatorname{erfc} \left\{ h\sqrt{Dt} \right\} \Omega. \quad (8.6)$$

In the case where crystal growth mechanisms give rise to non-linear kinetics, like spiral growth, this derivation is not valid, and finding analytical expressions is more challenging.

If during the BAD zone formation, the growth process of the crystal becomes limited by mass transport rather than by interface kinetics, the interface concentration quickly reaches the equilibrium value and Eqns. 8.4 and 8.6 reduce to [10]

$$c(z, t) = (c_b - c_e) \operatorname{erf} \left\{ \frac{z}{2\sqrt{Dt}} \right\} + c_e, \quad (8.7)$$

$$v_g(t) = \frac{D\Omega(c_b - c_e)}{\sqrt{\pi Dt}}. \quad (8.8)$$

So for a large enough value of  $h\sqrt{Dt}$ , the growth rate shows a behavior like

$$v_g(t) \propto \frac{1}{\sqrt{t}}. \quad (8.9)$$

A more precise description of the formation of a BAD zone is possible using finite element simulations. For this we used FlexPDE 5 from PDE solutions Inc [11]. The 2D simulations are performed according to a procedure described in chapter 6, using a 2 x 0.5 mm<sup>2</sup> crystal attached to the top of a 7 x 13 mm<sup>2</sup> growth container. As a model, we have used sodium chlorate crystal growth, for which Bennema [13] observed a linear relationship between growth rate and supersaturation for low supersaturations, and linear interface kinetics are assumed in the simulations. The parameters used for the simulation are given in table 8.1 and are taken from Wang and Hu [14], with  $\nu$  the kinematic viscosity,  $\alpha$  the slope of the density as function of concentration and  $\rho_0$  the density of the bulk solution. Figure 8.2a shows the depletion zone after a simulation corresponding to 1 hour, in the absence of gravity ( $g = 0$ ), where the depletion zone has a hemispherical-like shape. Next, the same setup was simulated, but now with a gravitational acceleration of  $1g$ . Normally, this would result in buoyancy driven convection and a thin boundary layer, leading to a steady state growth rate. However, this does not occur in the upside down geometry, as can be seen in Fig. 8.2b. In this case, depleted solution accumulates at the top of the growth container and, although the gravitational acceleration is not zero, a wide BAD zone develops. Near the crystal, the iso-concentration lines show a slight curvature around the crystal, while further away, the buoyancy induced stratification of the depleted solution is clearly visible. Fig. 8.3 shows the concentration gradient at the crystal interface as function of time, which can be used as a measure for the growth rate. It shows a fast decrease in the beginning, after which it shows an asymptotic behavior towards zero, not reaching a constant value. The curve can be fitted with a power law with an exponent of -0.5, in agreement with Eqn. 8.9, indicating a fully diffusion determined growth rate.

### 8.3 Experimental

In line with the simulations, sodium chlorate crystals were used to test the proposed method. Crystals of 2.5 x 2.5 x 1 mm<sup>3</sup> were glued onto a glass cover slide using silicone glue. The rim of a 7 x 7 x 13 mm<sup>3</sup> glass container with an open top was

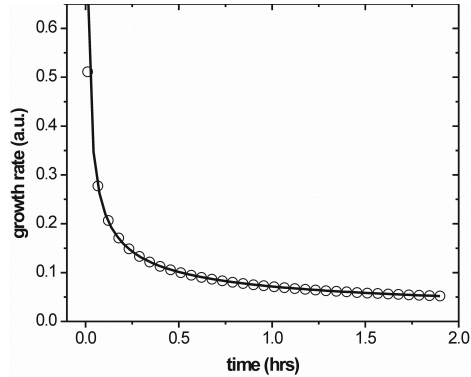


Figure 8.3: The growth rate as function of time of a sodium chlorate crystal grown in the upside-down geometry, obtained from simulations. The power law fit has an exponent of -0.5.

slightly coated with grease. Then, the container was filled with a solution containing  $0.745 \text{ g/cm}^3$  sodium chlorate, and kept at a temperature of  $20 \pm 1^\circ\text{C}$ , corresponding to a supersaturation of 3.3%. The cover slide with crystal is placed on the container, where the grease acts as a seal to prevent evaporation. The growing crystal was observed by schlieren microscopy in order to follow the development of the depletion zone and growth rate. With schlieren microscopy, gradients in refractive index, for instance caused by gradients in temperature or concentration, can be visualized [15]. The method is described in chapter 2.

## 8.4 Results

Fig. 8.4 shows schlieren images of the development of the BAD zone directly after immersion of the crystal (a), after 4 minutes (b), after 14 minutes (c) and after 56 minutes (d). The crystal is indicated by the white area, while the black parts next to the crystal are a projection of the sealing grease. White indicates a high and dark gray a low concentration gradient. It can be clearly seen that the solution that is depleted at the crystal interface spreads along the top of the growth container,

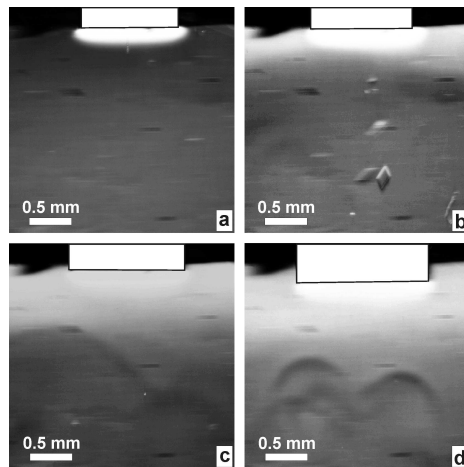


Figure 8.4: Schlieren images of the development of a BAD zone around a growing sodium chlorate crystal directly after immersion (a), after 4 minutes (b), after 14 minutes (c) and after 56 minutes (d). The crystal is indicated by the white area. The black parts next to the crystal are a projection of the sealing grease. In (d) convection plumes are visible that arise from from crystals nucleated at the bottom of the container.

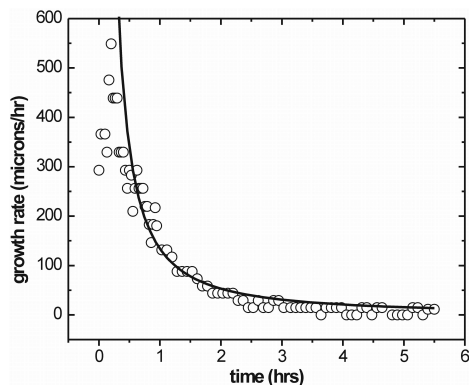


Figure 8.5: The growth rate as a function of time of a sodium chlorate crystal grown in the upside down geometry. The power law fit has an exponent of -1.3.

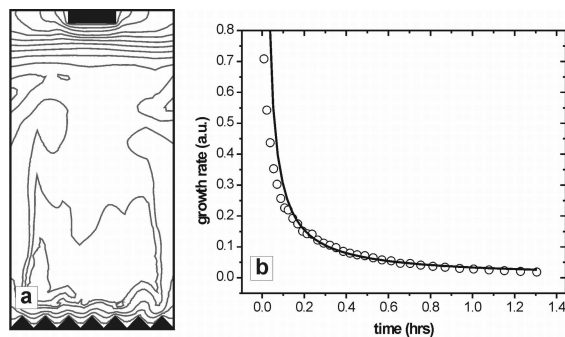


Figure 8.6: Iso-concentration lines of a simulation corresponding to 1 hour (a) and growth rate as a function of time (b) obtained from a simulation where crystals are also growing on the bottom of the growth cell. The black shapes represent growing crystals. The power law fit has an exponent of -0.95.

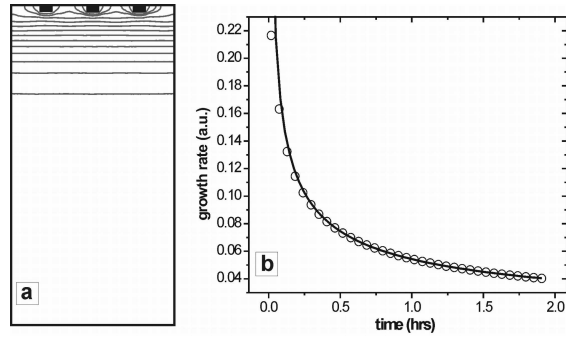


Figure 8.7: Iso-concentration lines of a simulation corresponding to 1000 seconds (a) and growth rate (b) obtained from a simulation for three crystals in the upside down geometry, where the black shapes represent growing crystals. The power law fit has an exponent of  $-0.5$ .

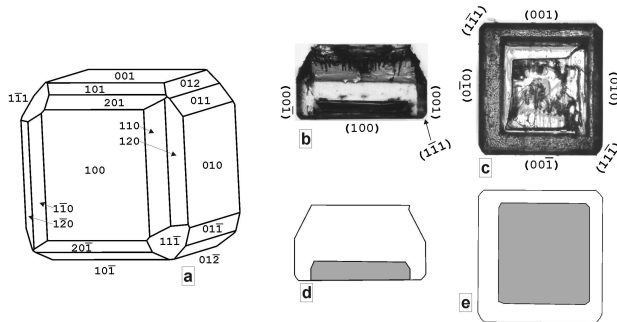


Figure 8.8: (a) The morphology of sodium chlorate crystals grown at low supersaturation. (b) Side and (c) bottom view of a sodium chlorate crystal grown in the upside down geometry. (d) and (e) show the contours of the crystal, where the depression is highlighted.



Table 8.1: Values used for the simulations

<b>Parameter</b>	<b>Value</b>
$c_b$	$0.714 \text{ g/cm}^3$
$c_e$	$0.7 \text{ g/cm}^3$
$\nu$	$1.3 \times 10^{-2} \text{ cm}^2/\text{s}$
$D$	$1.5 \times 10^{-5} \text{ cm}^2/\text{s}$
$h$	$200 \text{ cm}^{-1}$
$\alpha$	0.55
$\rho_0$	$1.043 \text{ g/cm}^3$

forming a stratified BAD zone slowly expanding downwards, as was already indicated by the simulations. The growth rate of the crystal was measured by recording the displacement of the crystal's bottom (100) face during growth (Fig. 8.5). It shows a continuously decreasing behavior, never reaching a constant value, as is expected for diffusion determined mass transport. From Eqn. 8.9 and the simulations, for large  $t$  a power law behavior is expected, with an exponent of -0.5. However, if the experimental results are fitted with a power law, the exponent has a value of -1.3. The growth rate decreases faster than as expected from Eqns. 8.6 and 8.8. One reason for this is the nucleation and growth of crystals on the bottom of the growth container. Despite filtering of the solution, formation of these crystals was not prevented. While these crystals are growing on the bottom of the container, they deplete solution that rises toward the top of the container, where it merges with the BAD zone. The convection plumes associated with this process are clearly visible in figure 8.4d. In this way the depletion zone expands faster and the concentration gradient decreases faster than would be expected, slowing down the growth rate more.

To model this, a new simulation was performed, with growing crystals on the bottom of the growth container, represented by triangles to describe their irregular orientation on the bottom (Fig. 8.6a). The concentration gradient at the crystal interface was again taken as a measure for the growth rate, where a power law fit showed an exponent of -0.95 (Fig. 8.6b). Although much lower than -0.5, the exponent is not as low as found experimentally. The discrepancy between the exponent derived from the simulation and experiment may be caused by the fact that the simulations are 2D, while the experiment is 3D. Furthermore, the exponent depends on the rate of depletion of the solution by the bottom crystals, and thus on their surface area. In

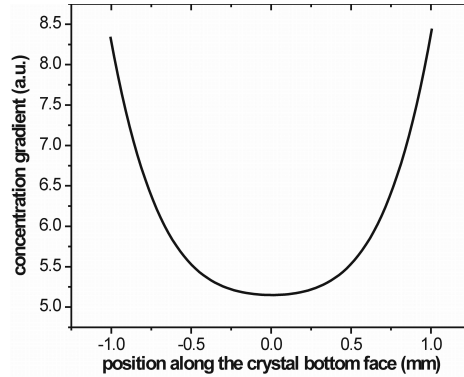


Figure 8.9: The concentration gradient along the bottom face of a sodium chlorate crystal, growing in the upside-down geometry, after a simulation corresponding to 1 hour.

principle, the supply of depleted solution from below makes the effects of the upside down growth geometry more pronounced, and thus more effective. However, the fluid flow induced by the rising solution can disturb the BAD zone, degrading its beneficial effects.

In the experiment described above, one single seed crystal was used. If a growth experiment includes a nucleation phase, it is likely that there will be more than one small crystal to start with. How this influences the formation of a BAD zone was investigated by simulations. Fig. 8.7a shows the BAD zone around 3 small crystals in the upside down geometry. In the early stages of growth, a hemispherical depletion zone is formed around the individual crystals. However, soon these depletion zones spread and merge to form the typical BAD zone. A fit to the concentration gradient at the interface of the crystals again shows a power law behavior with an exponent of  $-0.5$  (Fig. 8.7b).

The growth of sodium chlorate crystals in the upside down geometry has a profound effect on the morphology of the crystals. Under normal conditions, sodium chlorate crystals have a cubic morphology bounded by six  $\{100\}$  planes, but often with a flattened shape [16]. When supersaturations at the crystal interface are low, additional faces appear; four polar  $\{111\}$  type faces and twelve  $\{110\}$  and  $\{120\}$  type faces [16], as shown in Fig. 8.8a. These additional faces are indeed observed on crys-

tals grown in the upside down geometry, indicating the pronounced effect of the BAD zone on the interface supersaturation. Fig. 8.8b and c show a side and a bottom image respectively, of a sodium chlorate crystal grown for two days in the upside-down geometry, where some of the faces are indicated. At the top of the crystal, where it was glued to the cover slide, the faces show an irregular shape. In this part the crystal contains a lot of inclusions and irregularities, caused by the presence of the glue and the cover slide. At the bottom (100) face of the crystal, a large square depression is visible centered on the face, approximately a quarter of the crystal thickness deep. For clarity, this depression is highlighted in the contour of the images, as can be seen in Fig. 8.8d and e. This is an effect of the BAD zone. If during crystal growth mass transport is completely diffusion determined, like in the upside-down geometry, morphologically instable or hopper growth can occur [17]. Fig. 8.9 shows the concentration gradient along the bottom face of a growing sodium chlorate crystal, obtained from the simulations. Near the edges of the crystal, the concentration gradient, and thus the growth rate, is higher than at the middle of the crystal face. The flat shape of the crystal face becomes unstable, turns concave and, if growth continues, a hole forms in the crystal face.

## 8.5 Discussion and conclusion

In this chapter we have demonstrated a method to achieve all the beneficial effects of microgravity crystal growth, not by compensating gravity, but by making use of it. We have shown by simulations and experiments that by growing sodium chlorate crystals in an upside-down geometry, a buoyancy assisted depletion zone is formed. The corresponding reduction of the interfacial supersaturation leads to a significant decrease of the growth rate and has profound effects on the morphology of the grown crystals. All these effects are typical for diffusion limited crystal growth, showing that upside-down crystal growth can be used as an alternative for microgravity, without the experimental complexities. The simplicity of the upside-down method allows for a combination with techniques widely used in protein crystallization, like batch crystallization and screening of crystallization conditions, with the possible beneficial effects of microgravity, in the laboratory. Studying the effects of upside-down crystal growth on protein crystallization, focussing on the crystal quality, is the next step.

## 8.6 Appendix.

Redefining concentration and time as  $\varphi = c(z, \tau) - c_b$ , with  $\tau = Dt$ , Eqns. 8.2 and 8.3 become

$$\frac{\partial \varphi}{\partial \tau} = \frac{\partial^2 \varphi}{\partial z^2}, \quad (\text{A1})$$

$$\left. \frac{\partial \varphi}{\partial z} \right|_{z=0} = h(\varphi|_{z=0} + c_b - c_e), \quad (\text{A2})$$

with  $h = \beta/D$ . The initial condition becomes  $\varphi|_{\tau=0} = 0$ .

Using Eqn. A2 as boundary condition, Eqn. A1 can now be solved by application of the Laplace transform that removes the time variable from Eqn. A1, leaving an ordinary differential equation. The Laplace transform of  $f(t)$  is defined by

$$\mathcal{L}(f(t)) = \int_0^{\infty} f(t) \exp[-pt] dt, \quad (\text{A3})$$

where  $p$  is a number sufficiently large to make the integral converge. Tables of Laplace transforms can be found in, for instance, ref. [9]. The Laplace transform of the left term of Eqn. A1 in terms of  $\tau$  is given, through integration by parts, by

$$\int_0^{\infty} \frac{\partial \varphi}{\partial \tau} \exp[-p\tau] d\tau = \left( [\varphi \exp[-p\tau]]_0^{\infty} + p \int_0^{\infty} \varphi \exp[-p\tau] d\tau \right) = p\bar{\varphi}, \quad (\text{A4})$$

with  $\bar{\varphi}$  the Laplace transform of  $\varphi$ . The term in the square brackets vanishes because of the initial condition. The Laplace transform of the right term in Eqn. A1 is given by

$$\int_0^{\infty} \frac{\partial^2 \varphi}{\partial z^2} \exp[-p\tau] d\tau = \frac{\partial^2}{\partial z^2} \int_0^{\infty} \varphi \exp[-p\tau] d\tau = \frac{\partial^2 \bar{\varphi}}{\partial z^2}. \quad (\text{A5})$$

Eqn. A1 then becomes

$$p\bar{\varphi} = \frac{\partial^2 \bar{\varphi}}{\partial z^2}, \quad (\text{A6})$$

having a solution in the form of

$$\bar{\varphi} = k \exp[-\sqrt{p}z]. \quad (\text{A7})$$

The Laplace transforms of the left and right terms of the boundary condition A3 are given by

$$\int_0^{\infty} \frac{\partial \varphi}{\partial z} \Big|_{z=0} \exp[-p\tau] d\tau = -k\sqrt{p}, \quad (\text{A8})$$

$$\int_0^{\infty} h(\varphi|_{z=0} + c_b - c_e) \exp[-p\tau] d\tau = h \left( k + \frac{c_b}{p} - \frac{c_e}{p} \right). \quad (\text{A9})$$

Because A8=A9,  $k$  can be obtained, with which Eqn. A7 becomes

$$\frac{\bar{\varphi}}{(c_e - c_b)} = \frac{h \exp[-\sqrt{p}z]}{p(\sqrt{p+h})}. \quad (\text{A10})$$

To find an expression for  $\varphi(z, t)$ , the inverse Laplace transform of Eqn. A10 has to be found. From ref. [9], the inverse transform of the right term of Eqn. A10 is given by

$$\mathcal{L}^{-1} \left( \frac{h \exp[-\sqrt{p}z]}{p(\sqrt{p+h})} \right) = \operatorname{erfc} \left\{ \frac{z}{2\sqrt{\tau}} \right\} - \exp[hz + h^2\tau] \operatorname{erfc} \left\{ \frac{z}{2\sqrt{\tau}} + h\sqrt{\tau} \right\}. \quad (\text{A11})$$

Knowing that  $\varphi = c(z, \tau) - c_b$  and  $\tau = Dt$ , the expression for the concentration becomes

$$c(z, t) = (c_e - c_b) \left[ \operatorname{erfc} \left\{ \frac{z}{2\sqrt{Dt}} \right\} - \exp[hz + h^2Dt] \operatorname{erfc} \left\{ \frac{z}{2\sqrt{Dt}} + h\sqrt{Dt} \right\} \right] + c_b. \quad (\text{A12})$$



# Bibliography

- [1] E. H. Snell, J. R. Helliwell, *Reports on Progress in Physics* **68**, 799-853 (2005)
- [2] C.P. Lee, A.A. Chernov, *Journal of Crystal Growth* **3-4**, 531 (2002)
- [3] N. I. Wakayama, *Crystal Growth & Design* **3**, 17 (2003)
- [4] P.W.G. Poodt, M.C.R. Heijna, P.C.M. Christianen, W.J.P. van Enckevort, W.J. de Grip, K. Tsukamoto, J.C. Maan, E. Vlieg, *Applied Physics Letters* **87** (2005) 214105
- [5] M.C.R. Heijna, P.W.G. Poodt, J.L.A. Hendrix, K. Tsukamoto, P.C.M. Christianen, W.J.P. van Enckevort, W.J. de Grip, J.C. Maan, E. Vlieg, *Applied Physics Letters* **90** (2007) 264105
- [6] A. Moreno, E. Saridakis, N.E. Chayen, *Applied Crystallography* **35**, 40 (2002)
- [7] N.I. Wakayamama, *Japanese Journal of Applied Physics Part 2* **45**, L235 (2006)
- [8] H.U. Walter, *Fluid sciences and materials science in space* (Springer, Berlin, 1987)
- [9] R.V. Churchill, *Operational mathematics* (McGraw-Hill, New York, 1958)
- [10] J. Crank, *The mathematics of diffusion 2n ed* (Clarendon Press, Oxford 1979)
- [11] [www.pdesolutions.com](http://www.pdesolutions.com)
- [12] P.W.G. Poodt, P.C.M. Christianen, W.J.P. van Enckevort, J.C. Maan, E. Vlieg, *to be published*
- [13] P. Bennema, *Journal of Crystal Growth* **1**, 287 (1967)
- [14] W. Wang, W.R. Hu, *Journal of Crystal Growth* **3-4**, 398 (1996)
- [15] G.S. Settles, *Schlieren and shadowgraph techniques* (Springer, Berlin, 2001)
- [16] J. Szurgot, M. Szurgot, *Crystal Research and Technology* **30**, 71 (1995)
- [17] A.A. Chernov, *Journal of Crystal Growth* **24**, 11 (1974)





## Chapter 9

# Buoyancy assisted diffusion limited growth of lysozyme crystals

The upside-down crystal growth method is applied to the growth of tetragonal hen egg-white lysozyme using silanized mica nucleation substrates. In this way, elongated and optically perfect crystals were obtained, demonstrating growth at low supersaturation caused by a buoyancy assisted depletion zone. The crystal quality was verified by X-ray diffraction measurements. For small crystals, the quality of the diffraction data sets was limited by crystal size, while for larger crystals it was limited by the detector size. No effects of the growth method on X-ray crystal quality could be observed, indicating that the lysozyme crystals, even the ones with lower quality, are already of such perfection that improvement could not be detected.

## 9.1 Introduction

In the previous chapter, the upside-down crystal growth method was introduced. It was shown that this growth geometry, not to be confused with the hanging drop method [1], leads to the formation of a Buoyancy Assisted Depletion (BAD) zone and a corresponding growth rate behavior that is typical for diffusion limited growth. As a result from our observations, we stated that this technique can possibly be added to the list of alternatives for microgravity protein crystal growth in space, next to gel growth [2, 3], microfluidics [4] and gradient magnetic fields (chapter 5). In this chapter, methods to achieve crystal growth on a crystallization substrate, necessary for the formation of a BAD zone, are discussed. An example is given for lysozyme crystal growth, for which the effect of the BAD method on crystal quality was investigated using X-ray diffraction.

## 9.2 The nucleation substrate

For an ideal growth experiment in the BAD geometry, the protein crystals should only nucleate and grow on the top cover of the growth container and not in the bulk solution or on the other walls of the container. This can be realized by using a solutal composition that is positioned in the metastable zone of the phase diagram [1], and by taking care that the solution is free of potential sources for heterogeneous nucleation, like dust particles. In general, the barrier for nucleation on the container walls will be smaller than in the solution and contact nucleation will take place [6]. If, however, as top cover of the growth container a substrate is used that has an even lower nucleation barrier, nucleation will take place preferentially on this substrate. The height of the nucleation barrier depends on the roughness of the substrate, the interactions between the substrate surface and protein molecules, and, in case of crystalline substrates, the lattice mismatch between the protein crystal and substrate.

It is possible to choose or engineer a substrate to achieve preferential nucleation by influencing one or a combination of these factors. Attempts to do so can be classified in three categories. First, by chemical modification of substrates, like silanizing glass or mica to change the hydrophobicity of the surface [7, 8], or treating surfaces with poly-L-lysine [9], poly-L-aspartate [10], lipids [11] and fatty acids [12], which facilitate nucleation by electrostatic interactions with the protein molecules. Second, by using physically modified substrates, like porous glass, silicon or polycarbonate [13, 14] to lower the nucleation barrier by reduction of the surface free energy. Finally, mineral

substrates can be used because possible epitaxial relationships between protein crystals and the mineral may exist [15]. Up to now, no universal nucleation substrate has been found, and different techniques have to be applied for individual proteins. Thus to determine which method works best for which protein is still a question of trial and error. However, finding the proper nucleation substrate can be part of the screening process for optimal crystallization conditions, next to, for example pH, supersaturation and precipitants.

To test whether protein crystal growth in the BAD geometry really leads to improvement of protein crystal quality, tetragonal hen Egg-White Lysozyme (HEWL) crystals were grown in both the BAD and the normal geometry. As a nucleation substrate, silanized mica was used, according to the recipe described by Tang *et al.* [8]. This particular substrate gives nicely separated HEWL crystals, which can be easily removed from the substrate for further handling. Crystal removal can be a problem for untreated glass substrates, because the crystals adhere strongly and are easily damaged while trying to remove them.

### 9.3 Substrate preparation and crystal growth

A mica sheet (muscovite) was cleaved and submerged in a 1% (v/v) 3-aminopropyl triethoxysilane solution in water. After 5 minutes, the sheets were washed using demineralized water and heated in a stove at 110°C for 2 hours. The sheets are cut in 1.5 by 1.5 cm<sup>2</sup> pieces and stored in a desiccator. The lid of a 0.5 ml eppendorf tube is cut off, the rim slightly greased with vacuum grease and the tube filled up to the top with a solution containing 10 mg/ml lysozyme hen egg-white lysozyme (Sigma, lot 094K1454) and 4 wt% sodium chloride in a pH 4.5 acetate buffer. Next, the silanized mica sheet is placed with the cleaved side on the rim of the eppendorf tube and gently pressed, so that the grease acts as a seal to prevent evaporation. Finally, the tubes are stored at a constant temperature of 16.5°C until crystals of the required size are obtained.

For faster results, a nucleation step can be included. To do so, a 2.62 mm thick, 6.02 mm inner diameter rubber quad-ring (Eriks, Alkmaar, the Netherlands) is placed on a glass cover slide, and filled with the lysozyme solution. The cleaved side of the silanized mica is placed on top of the rubber ring and pressed to close the cell, where the capillary force of the solution holds the parts together. After this, the growth cell is placed in a refrigerator for 5-10 minutes, until tiny microcrystals can be seen on

the mica surface under a microscope. The mica sheets are then lightly flushed with buffer solution and placed on top of the filled eppendorf tube.

## 9.4 Results

Despite the specially prepared mica sheet, tetragonal HEWL crystals nucleated on all the walls of the eppendorf tube. The density of crystals on the mica substrate was actually lower than on the walls of the eppendorf tube, leading to nicely separated, individual crystals. Of all the HEWL crystals we grew, the ones that grew on the mica substrate in the BAD geometry showed the highest optical perfection and were completely transparent. The faces were smooth and well defined, showing no cracks. The majority of the lysozyme crystals on the mica surface grew with their  $c$ -axis parallel to the substrate or with a small angle with respect to this. All these crystals were elongated or even needle-like along the  $c$ -axis. Fig. 9.1 shows examples of a crystal grown in a conventional way (a) and of a crystal grown in the BAD geometry (b). Durbin and Feher [16] and Grimbergen *et al.* [17] found that the morphology of tetragonal lysozyme changes with supersaturation, where crystals become elongated along the  $c$ -axis for lower supersaturations, because of the different growth rate behavior of the  $\{110\}$  and  $\{101\}$  faces of the crystals (Fig. 9.2). As the bulk supersaturation used would normally give rise to short crystals, the elongated crystals on the substrate indicate that these crystals grew at a low local supersaturation, as expected by the presence of a BAD zone.

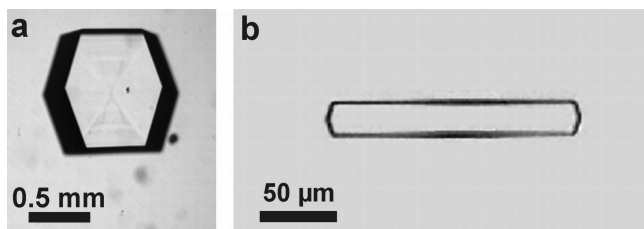


Figure 9.1: HEWL crystals grown in the normal growth geometry (a) and in the upside-down geometry (b), with the  $c$ -axis oriented horizontally.

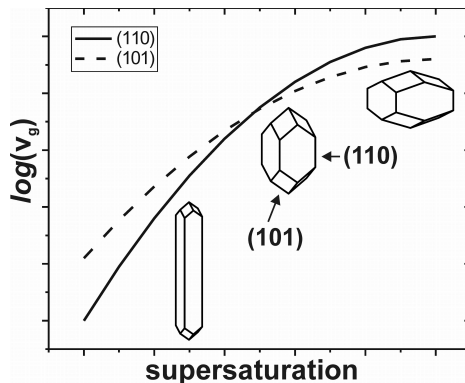


Figure 9.2: The growth rate of the (101) and (110) faces of tetragonal HEWL crystals as function of supersaturation, and its effect on the morphology [16, 17].

For protein crystallographers, however, it is the X-ray diffraction quality that is of interest, while the optical quality is hardly relevant. To get an indication whether HEWL crystal growth in the BAD geometry leads to an improvement of the X-ray diffraction quality of the crystals, complete data sets were measured of four upside-down grown and three normally grown crystals. The crystals were all grown according to the above protocol, where for the normally grown crystals the eppendorf tubes were stored with the mica substrate down. The selected crystals were soaked in a 20%(v/v) glycerol solution and cooled in a 100K nitrogen stream during the measurements. The data sets were collected on a 345 mm MAR research image plate (MarResearch, Hamburg, Germany). The rotation range per image was  $1^\circ$  and the detector was set at a distance of 100 mm from the crystal. Each image was exposed for 10 minutes using a Cu- $K_\alpha$  rotating anode X-ray source (FR591, Bruker Nonius, Delft, the Netherlands). The maximum resolution at the edge of the detector was 1.55 Å. The data was analyzed with MOSFLM v. 6.2.5 and SCALA v. 3.2.21 [18]. The results are shown in Table 9.1 and Figs. 9.3 and 9.4. No unique figure of merit exists for characterizing the X-ray quality of crystals and thus we list several [19].  $R_{merge}$  is a measure of agreement among multiple measurements of the same reflections between different measurements being in different frames of data or different data sets [20].  $R_{merge}$  is calculated as

Table 9.1: The results of X-ray diffraction data analysis

<i>Crystal</i>	1	2	3	4	5	6	7
<i>BAD geometry</i>	X		X	X			X
<i>Volume (<math>10^3 \mu\text{m}^3</math>)</i>	432	640	700	1792	3200	4000	5376
<i>Resolution (<math>\text{\AA}</math>)</i>	1.9	1.7	1.7	1.55	1.55	1.55	1.55
<i><math>R_{merge}</math> (cutoff at <math>1.9\text{\AA}</math>)</i>	12.1	6.6	7.0	4.1	3.9	3.7	3.8
<i>1.9\text{\AA} resolution shell:</i>							
<i><math>R_{merge}</math></i>	48.9	21.1	24.5	9.0	6.8	7.0	6.7
<i><math>R_{r.i.m.}</math></i>	52.6	22.7	26.5	9.7	7.4	7.5	7.2
<i><math>R_{p.i.m.}</math></i>	19.1	8.4	10.0	3.6	2.7	2.7	2.6
<i><math>I/\sigma</math></i>	4.4	9.2	7.4	16.6	24.5	24.9	26.1
<i>Mosaicity (degrees)</i>	0.40	0.38		0.34	0.44	0.47	0.48
<i><math>\mathbf{a} = \mathbf{b}</math> (<math>\text{\AA}</math>)</i>	78.883	78.818	78.957	78.870	78.871	78.811	78.881
<i><math>\mathbf{c}</math> (<math>\text{\AA}</math>)</i>	36.978	36.986	37.031	37.012	36.982	36.982	37.004

$$R_{merge} = \frac{\sum_{hkl} \sum_i \left| I_i(hkl) - \overline{I(hkl)} \right|}{\sum_{hkl} \sum_i I_i(hkl)}, \quad (9.1)$$

with  $I_i(hkl)$  the the intensity of the  $i^{th}$  ( $hkl$ ) reflection and  $\overline{I(hkl)}$  the average intensity of multiple observations. The lower  $R_{merge}$ , the better the quality of the X-ray data set. It can be determined for the entire data set as well as for a single resolution shell.  $R_{merge}$  does not only depend on the quality of the crystal, but also on the redundancy of the data, which is the number of measured reflections divided by the number of unique reflections. This can be corrected for by using the Redundancy Independent Merging  $R$  factor,  $R_{r.i.m.}$ , sometimes also called  $R_{meas}$ , given by [19]

$$R_{r.i.m.} = \frac{\sum_{hkl} \left[ N/(N-1)^{1/2} \right] \sum_i \left| I_i(hkl) - \overline{I(hkl)} \right|}{\sum_{hkl} \sum_i I_i(hkl)}, \quad (9.2)$$

with  $N$  the redundancy. Another indicator that can be calculated is the Precision Indicating Merging  $R$  factor,  $R_{p.i.m.}$ , describing the precision of the averaged mea-

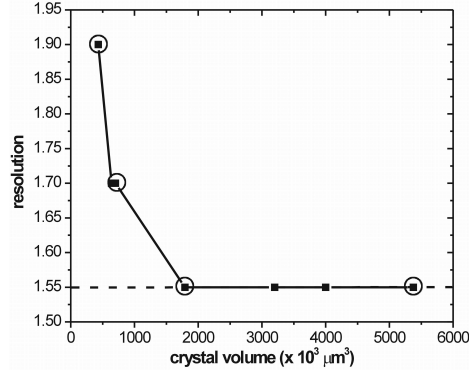


Figure 9.3: The resolution as function of crystal volume. The encircled points represent the crystals grown in the upside-down geometry.

surement and is given by [19]

$$R_{p.i.m.} = \frac{\sum_{hkl} \left[ 1/(N-1)^{1/2} \right] \sum_i |I_i(hkl) - \overline{I(hkl)}|}{\sum_{hkl} \sum_i I_i(hkl)}. \quad (9.3)$$

Other indicators measured are the resolution, the signal-to-noise ratio  $I/\sigma$  and the mosaic spread.

In table 9.1, the data set resolution is given for each crystal. If the resolution is plotted versus the crystal volume (Fig. 9.3), there is a clear size dependency below  $\sim 1500 \times 10^3 \mu\text{m}^3$ , while for larger volumes, the resolution is limited by the detector. The actual resolution for the larger crystals is probably higher. However, no effect of the growth method is visible in the resolution. The lowest resolution measured was 1.9 Å for crystal 1. To make a fair comparison between the crystals,  $R_{merge}$  was determined for all data sets using a cutoff at 1.9 Å (Fig. 9.4). In addition,  $R_{merge}$ , now together with  $R_{r.i.m.}$ ,  $R_{p.i.m.}$  and  $I/\sigma$ , was also determined for the 1.9 Å resolution shell, all showing a similar behavior as in Fig. 9.4, a clear size dependency for small crystals and a more or less constant value for larger crystals. The signal-to-noise ratio shows a size dependency for all crystal sizes. This indicates that the  $R$  values

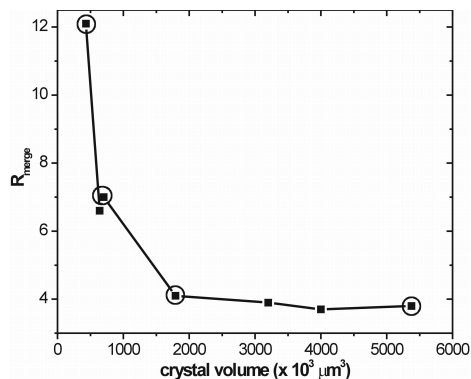


Figure 9.4:  $R_{\text{merge}}$  for the entire dataset with a cutoff at  $1.9\text{\AA}$  as a function of crystal volume. The encircled points represent the crystals grown in the upside-down geometry.

for small crystals are limited by the size of the crystal and for larger crystals by the detector size. However, none of the measurements, including the mosaicity, show any effect of the growth method. The quality of the data set is limited by crystal and detector size, but apparently not by crystal quality.

## 9.5 Discussion and conclusion

The BAD crystal growth method shows great potential as an alternative for microgravity although no quality improvement could be observed in the X-ray diffraction analysis of HEWL crystals grown in the BAD geometry. The quality of the data sets was determined either by the crystal or detector size, and not by crystal quality. In other words, the HEWL crystals grown are all of very good X-ray quality, including the normally grown crystals. Any differences in quality are so subtle that they are insignificant, at least for the parameters determined in this analysis and the laboratory set-up used here, an observation also made by Weiss [19]. So, HEWL is a wrong model system as the crystals are already very good and there is little room for improvement. This, however, does not mean that the method does not work. The elongated mor-



phology of the BAD grown crystals as well as their optical perfection point to growth at a low supersaturation, which can only be explained by the presence of a BAD zone. To prove that the BAD method can improve crystal quality, synchrotron radiation could be used to reach better resolutions, or other protein crystals have to be used that have an intrinsically low quality, so that there really is something to improve.

What makes this technique unique with respect to other alternatives for microgravity crystal growth is its simplicity and compatibility with already well established techniques in the protein crystallography community, like high throughput crystallization and automated screening of crystallization conditions. It offers the possibility to improve the quality of protein crystals and to study the effects of convection free crystal growth, without requiring complicated experimental conditions.



# Bibliography

- [1] A. McPherson, *Crystallization of biological macromolecules* (Cold Spring Harbor Laboratory Press, New York, 1999)
- [2] M. C. Robert, K. Provost, F. Lefaucheu, *Crystallization of nucleic acids and proteins: a practical approach*, edited by A. Ducruix and R. Giegé (IRL, Oxford, 1999)
- [3] J. M. García-Ruiz, J. Drenth, M. Riés-Kautt A. Tardieu, *A World without Gravity: Research in Space for Health and Industrial Processes*, edited by G. Seibert, B. Titton, and B. Battrick (ESA, Noordwijk, The Netherlands, 2001)
- [4] D. C. Carter, P. Rhodes, D. E. McRee, L. W. Tari, D. R. Dougan, G. Snell, E. Abola, R. C. Stevens, *Journal of Applied Crystallography* **38**, 87 (2005)
- [5] M.C.R. Heijna, P.W.G. Poodt, J.L.A. Hendrix, K. Tsukamoto, P.C.M. Christiaenen, W.J.P. van Enkevort, W.J. de Grip, J.C. Maan, E. Vlieg, *Applied Physics Letters* **90** (2007) 264105
- [6] W.J.P. van Enkevort, *Journal of Crystal Growth* **259**, 190 (2003)
- [7] G. Falini, S. Fermani, G. Conforti, A. Ripamonti, *Acta Crystallographica D* **58**, 1649 (2002)
- [8] L. Tang, Y.B. Huang, D.Q. Liu, J.L. Li, K. Mao, L. Liu, Z.K. Cheng, W.M. Gong, J. Hu, J.H. He, *Acta Crystallographica D* **61**, 53 (2005)
- [9] L. Rong, H. Komatsu, S. Yoda, *Journal of Crystal Growth* **235**, 489 (2002)
- [10] S. Fermani, G. Falini, M. Minnucci, A. Ripamonti, *Journal of Crystal Growth* **224**, 327 (2001)
- [11] S.A. Darst, M.A. Edwards, *Current Opinions in Structural Biology* **5**, 640 (1995)
- [12] T. Kubo, H. Hondoh, T. Nakada, *Crystal Growth & Design* **7**, 416 (2007)
- [13] N.E. Chayen, E. Saridakis, R.P. Sear, *Proceedings of the National Academy of Sciences* **103**, 597 (2006)
- [14] D. Dobrev, D. Baur, R. Neumann, *Applied Physics A* **80**, 451 (2005)

- 
- [15] A. McPherson, P. Shlichta, *Science* **239**, 385 (1988)
- [16] S.D. Durbin, G. Feher, *Journal of Crystal Growth* **76**, 583 (1986)
- [17] R.F.P. Grimbergen, E.S. Boek, H. Meekes, P. Bennema, *Journal of Crystal Growth* **207**, 112 (1999)
- [18] <http://smb.slac.stanford.edu/facilities/software/mosfm/>
- [19] M.S. Weiss, *Journal of Applied Crystallography* **34**, 130 (2001)
- [20] J. Drenth, *Principles of protein X-ray crystallography* (Springer-Verlag, New York, 1994)

---

# Summary and outlook

## Introduction

Protein crystal growth in microgravity is believed to yield higher quality crystals than their terrestrial grown counterparts, because of the suppression of buoyancy driven convection, diffusion limited transport of protein molecules and the reduction of the growth rate, impurity incorporation and sedimentation. The quality of a protein crystal is important for determining the molecular structure of the protein by X-ray crystallography, because the better the crystal quality the higher the accuracy of the determined molecular structure. Because good quality protein crystals can be very difficult to grow, the crystal quality is often the limiting factor in the structure determination process. That is why a considerable effort has been put in growth of protein crystals in microgravity in space. The high costs, complexity and low accessibility can make this approach less practical however. On top of that, although space growth experiments have a history of over 25 years, the answer whether microgravity crystal growth really leads to an improvement of protein crystal quality is still not conclusively answered.

This thesis describes research performed on two alternative methods for improving protein crystal quality without having to go to space; by gradient magnetic fields and by an upside-down geometry.

## Part 1

With gradient magnetic fields, a magnetic force can be applied on an object that compensates the gravitational force to let it appear weightless. Demonstrations of levitation by gradient magnetic fields raised the question whether this technique could also be used for creating a microgravity-like environment for protein crystal growth. If so, it would offer an alternative for experiments in space. The levitation of diamagnetic materials is possible with commercially available superconducting magnets. However, experiments with growing crystals levitating in gradient magnetic fields showed that levitation is not the proper condition. Instead, the variation of the magnetic and gravitational force with concentration has to be taken in account, resulting in a factor 3 higher product of magnetic field and gradient for suppression of convection than for levitation of diamagnetic protein solutions, and a factor 3 smaller for paramagnetic solutions. This brings creating a microgravity like condition for diamagnetic protein crystal growth beyond the reach of most magnet facilities. The High Field Magnet Laboratory at the Radboud University Nijmegen, however, possesses

magnets that can reach these conditions, offering the unique possibility to study the effects of suppression of convection on crystal growth in great detail.

The possibility to suppress convection with gradient magnetic fields was investigated with nickel sulfate hexahydrate and hen egg-white lysozyme crystal growth. Although nickel sulfate is not a protein, it is much easier to handle than proteins and acts as a model system to study the effects of the magnetic field on the fluid dynamics, mass transport and crystal growth. It is also paramagnetic, requiring a much lower gradient magnetic field than for diamagnetic materials to suppress convection. Special microscopes were constructed that fit in the bore of the magnet and that can not only visualize the growing crystal but also concentration gradients and convective flows, as described in chapter 2.

Chapter 3 shows the first experimental example of suppression of convection during crystal growth by gradient magnetic fields. A nickel sulfate crystal growing in a gradient magnetic field was observed by schlieren microscopy to visualize the disappearance of the convection plume and the formation of a wide depletion zone, just as would happen in microgravity. The use of magnetic fields, however, offers the unique possibility to tune the effective gravitational acceleration, and thus the amount of convection, even including negative gravity.

The tunability of the amount of convection is explored in depth in chapter 4, where the width of the depletion zone was measured as a function of the effective gravity by varying the gradient magnetic field, showing a behavior as expected from fluid dynamics theory. The growth rate shows a significant decrease when convection is suppressed. An analysis of the field profile of the magnet used shows the importance of choosing the proper position within the magnet to minimize the inhomogeneity of the effective gravity. Nevertheless it is shown that in the vicinity of the crystal, effective gravitational accelerations in the milligravity range were still sufficient to suppress convection.

The next step was to suppress convection for crystal growth of a diamagnetic protein. Although technically challenging due to the high gradient magnetic fields required, in chapter 5 it is shown that for protein solutions, convection can also be suppressed during crystal growth. Using shadowgraphy, the disappearance of the convection plume during lysozyme crystal growth was visualized, showing that gradient magnetic fields can be used as an alternative for microgravity. However, the very high gradient magnetic field required to do this for diamagnetic proteins ( $\sim 4500 \text{ T}^2/\text{m}$ ) imposes a restriction on the growth experiments, because these high magnetic fields can only be sustained for a few hours, much too short to perform a full growth

experiment. So unfortunately, checking whether growth under these conditions leads to an improvement of crystal quality could not be done.

In most crystal growth experiments, the drag on the flowing solution during convection that is caused by the walls of the growth container cannot be ignored. If crystal growth from solution takes place in a closed container, a critical gravitational acceleration can be defined, below which buoyancy driven convection is suppressed and mass transport is completely determined by diffusion at gravitational accelerations higher than  $0g$ . In chapter 6, using finite element simulations and an analytical model, we show that it is possible to predict this critical value. This result can be used to optimize growth conditions for microgravity protein crystal growth, if the gravitational acceleration cannot be cancelled completely, like in space, or is cancelled inhomogeneously, like in gradient magnetic fields.

In chapter 7, the finite element simulations are extended to compare them to the experiments on crystal growth in gradient magnetic fields for nickel sulfate and lysozyme. These simulations include the inhomogeneous effective gravity that accompanied the magnet experiments, giving further insight into the observations described in chapters 3 to 5.

## Part 2

Part 2 of this thesis discusses another method to suppress convection for the improvement of protein crystal quality. In chapter 8, a new method is proposed to achieve all the beneficial effects of microgravity crystal growth, by making use of buoyant forces instead of compensating for them, by using an upside-down geometry. We show by finite element simulations and growth experiments on sodium chlorate that crystal growth in an upside-down geometry leads to the formation of a buoyancy assisted depletion zone. The effects on growth rate and morphology that are observed are all indicative of diffusion limited growth, just as would happen in the absence of gravity. The simplicity of this growth method offers the possibility to perform large scale protein crystal growth experiments under microgravity-like conditions, without the requirement of compensating for gravity.

In chapter 9, the upside-down crystal growth method is applied to the growth of tetragonal hen egg-white lysozyme using silanized mica nucleation substrates. The morphology of the grown crystals indicates growth at low supersaturation caused by a buoyancy assisted depletion zone. The crystal quality was verified by X-ray diffraction measurements. No effects of the growth method on X-ray crystal quality could be observed, indicating that the lysozyme crystals, even the ones with lower quality, are

already of such perfection that improvement could not be detected.

## Conclusion and outlook

The question whether crystal growth in gradient magnetic fields really helps to increase crystal quality could not be answered because the required conditions could not be sustained long enough for a complete growth experiment. To overcome this, a custom magnet has to be constructed that can sustain high gradient magnetic fields for a long period of time with a considerable homogeneity. Another option is to focus on paramagnetic proteins which require much lower gradient magnetic fields, so that the current equipment can be used. Either way, the use of gradient magnetic fields is a very promising technique for the improvement of protein crystal quality. Although no proof was obtained that supports this, all the boundary conditions that are held responsible for crystal quality improvement in microgravity, like suppression of convection, diffusion limited mass transport and a reduced growth rate, are shown to be present. In fact, this brings this technique more or less in the same position as crystal growth in space! An added benefit is the ability to control the amount of convection by tuning the magnetic field. This can also be of interest for other fields of research in fluid dynamics, heat/mass transport, cavitation, or any other system where gradients in magnetic susceptibility are present. With gradient magnetic fields, the amount of convection becomes a newly accessible variable.

The upside-down crystal growth method shows great potential as an alternative for microgravity crystal growth, because of its simplicity and compatibility with well established crystallization methods. However, more research is required, for instance on the nucleation substrate and the influence of the shape and size of the growth container on the formation of the buoyancy assisted depletion zone. Nevertheless, this technique finally offers the possibility to answer the question whether suppression of convection and all its related phenomena really can improve the quality of protein crystals.

The research that lead to this thesis is the results of a cooperation between physicists, chemists, crystallographers and biologists, combining theoretical and experimental knowledge in crystal growth, magnet technology, optics, fluid dynamics, crystallography and biochemistry. It is my opinion that such a cooperation is vital in succeeding to find ways to improve the quality of protein crystals (and of course for many other scientific subjects). For the future, the questions to be answered are: what is it that we actually want to improve, how do we define quality and how do we measure it, and which experimental techniques, diagnostical methods and theoretical



insights can be used? These are questions a single chemist, physicist or biologist cannot answer. The only way to do it, independent of which technique will be used, is by learning from each other.

# Samenvatting

## Inleiding

Proteïnen, in de volksmond ook wel eiwitten genoemd, is een verzamelnaam voor een grote groep moleculen die een zeer belangrijke rol in het leven spelen. Proteïnen dienen onder andere als bouw materiaal, transporteurs en regelaars in alle levende organismen. Voor biologen, medici en farmaceuten is het zeer interessant om te weten hoe de verschillende proteïne moleculen functioneren. Enerzijds omdat het een fundamenteel inzicht kan bieden over hoe het “leven” werkt, maar ook omdat het dan wellicht mogelijk is gericht medicijnen te ontwikkelen die de functie van een proteïne molecuul beïnvloeden om ziekten te genezen. Hiervoor is het noodzakelijk om de vaak ingewikkelde moleculaire structuur van het betreffende proteïne te kennen. Wetenschappers hebben de afgelopen decennia methoden ontwikkeld waarmee ze zeer nauwkeurig de structuur van moleculen kunnen bepalen, door ze te bestralen met röntgenstraling en te meten hoe deze straling wordt verstrooid. Dit lukt echter alleen als er heel veel van dezelfde moleculen heel dicht en netjes geordend op elkaar gepakt zijn in een kristal.

Het groeien van een kristal van proteïne moleculen gebeurt vanuit een oplossing en is niet wezenlijk anders dan het groeien van bijvoorbeeld een suikerkristal, het gaat alleen een stuk lastiger. Het resultaat van de vaak langdurige proteïne kristalgroei experimenten zijn meestal kleine en kwalitatief slechte kristallen. Dit is een probleem, want hoe slechter het kristal, hoe onnauwkeuriger de moleculaire structuurbevestiging met röntgenstraling. Er wordt dus flink gezocht naar methoden om betere kwaliteit proteïne kristallen te verkrijgen, en hiervoor worden letterlijk kosten noch moeite bespaard. Bijvoorbeeld door de kristallen in de ruimte te groeien.

In de ruimte is het kristal en zijn oplossing gewichtloos. Het groeien van proteïnekristallen in gewichtloosheid zou kristallen van betere kwaliteit moeten opleveren dan onder normale, aardse omstandigheden. Dit heeft te maken met de invloed van de zwaartekracht op de oplossing van waaruit het kristal groeit. Kleine dichtheidsverschillen die in de oplossing ontstaan doordat proteïne moleculen vanuit de oplossing in het kristal verdwijnen, leiden onder invloed van zwaartekracht tot vloeistofstromingen in de oplossing; een proces dat convectie wordt genoemd. Deze stromingen transporteren onzuiverheden naar het kristal die in het ingebouwd kunnen worden en nieuwe proteïne moleculen waardoor het kristal relatief snel kan blijven groeien. Daarnaast kunnen andere kleine kristallen in de oplossing naar beneden zakken, op elkaar

---

vallen en ingebouwd worden, wat sedimentatie wordt genoemd. Al deze processen kunnen leiden tot kristallen van slechte kwaliteit.

In gewichtloosheid zal convectie niet kunnen ontstaan. Nieuwe proteïne moleculen moeten nu door diffusie naar het groeiende kristal getransporteerd worden, wat veel langzamer gaat dan door convectie. Hierdoor zal de groeisnelheid afnemen waardoor de proteïne moleculen rustig de tijd hebben om netjes in het kristal te worden ingebouwd. Ook zullen veel minder onzuiverheden ingebouwd worden en zal sedimentatie niet plaats vinden. De verwachting is dat dit tot een verbetering van de kristalkwaliteit leidt. Om deze reden zijn er veel pogingen gedaan om goede proteïne kristallen te groeien in de ruimte. De hoge kosten, de complexiteit en geringe toegankelijkheid maken deze aanpak echter minder praktisch. Bovendien is, ondanks een historie van meer dan 25 jaar, de vraag of kristalgroei in gewichtloosheid echt betere kristallen oplevert nog steeds niet compleet beantwoord.

Dit proefschrift beschrijft onderzoek naar twee alternatieve methoden voor het uitschakelen van convectie tijdens de groei van proteïne kristallen om zo betere kristallen te verkrijgen, zonder naar de ruimte te gaan. Dit kan door kristalgroei in hoge magneetvelden (deel 1) en door middel van de BAD methode (deel 2).

## Deel 1

Met een gradiënt magnetisch veld kan een magnetische kracht worden uitgeoefend op een object. Dit kan gebruikt worden om de zwaartekracht te compenseren, zodat het object gewichtloos lijkt. De magnetische kracht wordt hierbij bepaald door het product van de magnetische veldsterkte en de gradiënt van de magnetische veldsterkte. Experimenten met magnetische levitatie hebben de deur geopend voor proteïne kristalgroei in gewichtloosheid in hoge magneetvelden. Als dat mogelijk zou zijn, dan zou het als een alternatief kunnen dienen voor kristalgroei in de ruimte. Magnetische levitatie van objecten is mogelijk met commercieel verkrijgbare magneten, maar experimenten met kristalgroei tijdens magnetische levitatie hebben duidelijk gemaakt dat dit niet de juiste conditie is om convectie te verminderen. De juiste conditie kan berekend worden door te bepalen hoe de dichtheid en de magnetische susceptibiliteit van de oplossing variëren met concentratie. Het resultaat voor diamagnetische proteïne oplossingen is een drie maal hoger product van magnetische veldsterkte en gradiënt om convectie te verminderen dan nodig is voor levitatie. Voor paramagnetische oplossingen is een drie maal kleiner product nodig. De benodigde hoge velden brengen het creëren van een gewichtloosheidachtige omstandigheid voor het groeien van proteïne kristallen buiten het bereik van de meeste magneten

laboratoria. Het laboratorium voor hoge magneetvelden van de Radboud Universiteit Nijmegen is echter in het bezit van magneten die deze condities kunnen halen. Dit biedt de unieke mogelijkheid om de kristalgroei in gewichtloosheid uitvoerig en nauwkeurig te bestuderen.

De mogelijkheid om magnetische velden te gebruiken om convectie tijdens proteïnekristalgroei te onderzoeken is gedaan met nikkelsulfaat hexahydraat en het proteïne lysozym. Nikkelsulfaat is geen proteïne, maar het is veel makkelijker te kristalliseren dan proteïnen en dient als een modelsysteem om de effecten van magnetische velden op vloeistofdynamica, massatransport en kristalgroei te bestuderen. Ook is het paramagnetisch, wat betekent dat er geen extreem hoge magneetvelden nodig zijn om convectie uit te schakelen. Er zijn speciale microscopen gebouwd die in de magneet passen, waarmee zowel een groeiend kristal als vloeistofstromingen en concentratie gradiënten gevisualiseerd kunnen worden. Deze microscopen staan beschreven in hoofdstuk 2.

In hoofdstuk 3 worden het eerste experimentele voorbeeld getoond van het dempen van convectie tijdens kristalgroei in magnetische velden. Een nikkelsulfaat kristal is gegroeid in een magneet terwijl met een speciale schlieren microscoop het verdwijnen van de convectie is waargenomen, net zoals in de ruimte zou gebeuren. Het gebruik van magnetische velden biedt echter iets wat kristalgroei in de ruimte niet biedt: de unieke mogelijkheid om de mate van zwaartekracht aan te passen, en daarmee de mate van convectie, waardoor zelfs een omgekeerde zwaartekracht mogelijk wordt.

De instelbaarheid van de mate van convectie is verder uitgediept in hoofdstuk 4, waar de breedte van de depletie zone (een maat voor in hoeverre convectie is verminderd) is gemeten als functie van de effectieve zwaartekracht, door de magnetische veldsterkte te variëren. Het resultaat komt volledig overeen met wat verwacht wordt vanuit de theorie. De groeisnelheid van het kristal toont daarbij een zeer duidelijke afname als convectie is verminderd. Een analyse van het veldprofiel van de gebruikte magneet toont het belang van het kiezen van de juiste positie in de magneet om inhomogeniteiten in de effectieve zwaartekracht te minimaliseren, maar dat het niet nodig is de zwaartekracht geheel uit te schakelen. Een vermindering van een zwaartekracht in de buurt van het kristal met een factor duizend is voldoende om convectie grotendeels te dempen.

De volgende stap was het dempen van convectie tijdens de groei van een kristal van een diamagnetisch proteïne. Hoewel een uitdaging vanuit een technisch oogpunt vanwege de hoge magnetische velden die nodig zijn, wordt in hoofdstuk 5 beschreven dat het mogelijk is om ook convectie te uit te schakelen voor diamagnetische proteï-

nen. Met een schaduwgrafie-microscop is het verdwijnen van de convectie zichtbaar gemaakt tijdens het groeien van een lysozym kristal. Echter, het zeer hoge product van magnetische veldsterkte en gradiënt benodigd voor het creëren van een toestand van gewichtloosheid beperkt de mogelijkheden voor het groeien van proteïnekristallen in een magneet, omdat deze hoge velden slecht enkele uren volgehouden kunnen worden; veel te kort voor een volledig groei experiment. Helaas bleek het dus niet mogelijk te bepalen of het groeien van een proteïne kristal terwijl convectie is uitgeschakeld door magnetische velden, leidt tot verbetering van de kristal kwaliteit.

Als kristalgroei plaatsvindt in een afgesloten bakje, dan kan het effect van de wrijving die de wanden van het bakje op de stromende oplossing tijdens convectie uitoefent niet worden verwaarloosd. In dat geval kan er een kritische effectieve zwaartekracht worden gedefinieerd waar beneden convectie is gedempt en massatransport geheel gelimiteerd is door diffusie, terwijl de zwaartekracht niet helemaal is uitgeschakeld. In hoofdstuk 6 wordt getoond, door middel van eindige elementen simulaties en een analytisch model, dat de waarde van deze kritische effectieve zwaartekracht voorspeld kan worden. Dit resultaat kan gebruikt worden om groeiomstandigheden te optimaliseren indien gewichtloosheid niet volledig bereikt wordt, zoals in de ruimte, of niet homogeen, zoals in hoge magneetvelden.

In hoofdstuk 7 worden de eindige elementen simulaties uitgebreid om ze te vergelijken met de experimenten beschreven in hoofdstukken 3 tot en met 5. Deze simulaties bevatten de inhomogene effectieve zwaartekracht die aanwezig was tijdens de magneet experimenten, waardoor een beter inzicht is verkregen in de resultaten van de experimenten.

## Deel 2

Deel 2 van dit proefschrift beschrijft een andere methode om convectie tijdens kristalgroei te dempen om zo de kristalkwaliteit te verbeteren. In hoofdstuk 8 wordt een nieuwe methode voorgesteld om alle voordelen van gewichtloosheid voor kristalgroei te verkrijgen, door gebruik te maken van zwaartekracht in plaats hiervoor te compenseren. Dit kan door het bakje waarin het kristal groeit om te keren zodat het kristal aan de bovenkant van het bakje groeit in plaats van op de bodem. Op die manier kan convectie niet ontstaan. We laten door middel van eindige elementen simulaties en kristalgroei experimenten met natrium chloraat zien, dat kristalgroei in deze geometrie leidt tot de formatie van wat we een “Buoyancy Assisted Depletion (BAD) zone” noemen. De waargenomen effecten hiervan op de groeisnelheid en morfologie wijzen allemaal op diffusie gelimiteerde groei, net als in gewichtloosheid. De eenvoud

van deze groeimethode, die we de BAD methode noemen, biedt de mogelijkheid om op grote schaal proteïnekristallisatie te verrichten onder omstandigheden die overeen komen met gewichtloosheid, zonder voor de zwaartekracht te hoeven compenseren.

In hoofdstuk 9 wordt deze methode toegepast op de groei van tetragonale kippe-eiwit lysozym kristallen op gesilaniseerde mica nucleatiesubstraten. De morfologie van de gegroeide kristallen wijzen op groei bij lage oververzadigingen veroorzaakt door de afwezigheid van convectie. De kristalkwaliteit is gecontroleerd door röntgen diffractie. Er is geen effect van de methode op kristalkwaliteit waargenomen, omdat de kwaliteit van de kristallen, zelfs van de normaal gegroeide, al dusdanig goed is dat enige verbetering niet detecteerbaar is.

## Conclusie en vooruitzichten

De vraag of kristalgroei in terwijl convectie is gedempt met magnetische velden echt leidt tot kwaliteitsverbetering van de kristallen, kon niet worden beantwoord omdat de benodigde condities niet lang genoeg vol gehouden konden worden voor een volledig groei-experiment. Een oplossing hiervoor is het ontwerpen van een magneet die hoge gradiënt velden aankan voor een langere tijd met voldoende homogeniteit. Een andere optie is het concentreren op paramagnetische proteïnen, waarvoor veel lagere velden nodig zijn en bestaande apparatuur gebruikt kan worden. Hoe dan ook, het gebruik van magnetische gradiënt velden is een veelbelovende techniek voor het verbeteren van de kwaliteit van proteïnekristallen. Hoewel hier geen bewijs is aangetoond, zijn alle randvoorwaarden aanwezig die verantwoordelijk gehouden worden voor de verbetering van de kristalkwaliteit, zoals het dempen van convectie, diffusie gelimiteerd massatransport en een afname van de groeisnelheid. Om precies te zijn, brengt dit deze techniek op dezelfde hoogte als kristal groei in de ruimte! Van grote toegevoegde waarde is de mogelijkheid om de mate van convectie te variëren door het magnetisch veld te veranderen. Dit kan ook interessant zijn voor andere onderzoeksgebieden in vloeistofdynamica, massa/warmte transport, cavitatie, of ieder ander systeem waar gradiënten in magnetische susceptibiliteit aanwezig zijn. Via magnetische gradiënt velden is de mate van convectie een nieuw toegankelijke variabele.

Kristalgroei volgens de BAD methode toont veel potentie als alternatief voor kristalgroei in gewichtloosheid, vanwege zijn eenvoud en compatibiliteit met wijd gebruikte kristallisatie technieken. Echter, meer onderzoek is nodig, bijvoorbeeld naar een geschikt nucleatiesubstraat en de invloed van de vorm en grootte van de groeicontainer op de vorming van de BAD zone. Desalniettemin biedt deze techniek de mogelijkheid om de vraag of het dempen van convectie en alle daar aan gerelateerde

effecten echt de kwaliteit van proteïnekristallen kan verbeteren.

Het onderzoek dat is beschreven in dit proefschrift is het resultaat van een samenwerking tussen fysici, chemici, kristallografen en biologen, waarbij theoretische en experimentele kennis van kristalgroei, magneet technologie, optica, vloeistofdynamica, kristallografie en biochemie is toegepast en ontwikkeld. Het is mijn persoonlijke mening dat zulk een samenwerking van groot belang is voor het vinden van methoden om de kwaliteit van proteïnekristallen te verbeteren (en natuurlijk vele andere wetenschappelijke vraagstukken). Om dit voor elkaar te krijgen moet eerst worden afgevraagd wat we precies willen verbeteren, hoe we kristalkwaliteit moeten definiëren en welke experimentele technieken, diagnostische methoden en theoretische inzichten kunnen worden toegepast. Dit zijn vragen die een enkele chemicus, fysicus of bioloog niet kan beantwoorden. De enige manier om dit te laten slagen, onafhankelijk van welke techniek uiteindelijk zal worden gebruikt, is door verder samen te werken over de grenzen van de afzonderlijke disciplines heen.

# List of publications

M.F. Reedijk, J. Arsic, D. Kaminski, P. Poodt, J.W.M. van Kessel, W.J. Szweryn, H. Knops, E. Vlieg, *New ( $\sqrt{3} \times \sqrt{3}$ )  $R30^\circ$  phase of Pb on Ge(111) and its consequence for the melting transition*, Physical Review Letters **90** (2003) 056104

M.F. Reedijk, J. Arsic, D. Kaminski, P. Poodt, H. Knops, P. Serrano, G.R. Castro, E. Vlieg, *Melting behavior of the  $\beta$  - Pb/Ge(111) structure*, Physical Review B **67** (2003) 165423

J. Arsic, D.M. Kaminski, N. Radenovic, P. Poodt, W.S. Graswinckel, H.M. Cuppen, E. Vlieg, *Thickness-dependent ordering of water layers at the NaCl(100) surface*, Journal of chemical physics **120** (2004) 9720

J. Arsic, D. Kaminski, P. Poodt, E. Vlieg, *Liquid ordering at the Brushite - {010} - water interface*, Physical review B **69** (2004) 245406

D. Kaminski, P. Poodt, E. Aret, N. Radenovic, E. Vlieg, *Surface alloys, overlayer and incommensurate structures of Bi on Cu(111)*, Surface Science **575** (2005) 233

P.W.G. Poodt, M.C.R. Heijna, P.C.M. Christianen, W.J.P. van Enkevort, W.J. de Grip, K. Tsukamoto, J.C. Maan, E. Vlieg, *Suppression of convection using gradient magnetic fields during crystal growth of  $NiSO_4 \cdot 6H_2O$* , Applied Physics Letters **87** (2005) 214105

D. Kaminski, P. Poodt, E. Aret, N. Radenovic, E. Vlieg, *Observation of a liquid phase with an orthorhombic orientational order*, Physical Review Letters **96** (2006) 056102

P. W. G. Poodt, M. C. R. Heijna, K. Tsukamoto, W. J. de Grip, P. C. M. Christianen, J. C. Maan, W. J. P. van Enkevort, E. Vlieg, *Using gradient magnetic fields to suppress convection during crystal growth*, Crystal Growth & Design **6** (2006) 2275

M.C.R. Heijna, P.W.G. Poodt, J.L.A. Hendrix, K. Tsukamoto, P.C.M. Christianen, W.J.P. van Enkevort, W.J. de Grip, J.C. Maan, E. Vlieg, *Magnetically controlled gravity for protein crystal growth*, Applied Physics Letters **90** (2007) 264105



P.W.G. Poodt, P.C.M. Christianen, W.J.P. van Enkevort, J.C. Maan, E. Vlieg, *The critical Rayleigh number in low gravity crystal growth from solution*, Submitted for publication to Crystal Growth & Design

P.W.G. Poodt, M.C.R. Heijna, P.C.M. Christianen, W.J.P. van Enkevort, J.C. Maan, E. Vlieg, *A comparison between simulations and experiments for microgravity crystal growth in gradient magnetic fields*, Submitted for publication to Crystal Growth & Design

P.W.G. Poodt, M.C.R. Heijna, A. Schouten, W.J.P. van Enkevort, E. Vlieg, *Buoyancy assisted diffusion limited crystal growth: harnessing gravity to suppress convection*, Submitted for publication

# Curriculum Vitae

Naam: Paul Poodt

Geboren: 17 November 1979 te Zevenaar

Opleiding:

1992 - 1998 VWO, Candea College Zevenaar

1998 - 2003 Scheikunde, Radboud Universiteit Nijmegen (Cum Laude)  
*Hoofdrichting:* Vaste Stof Chemie (Prof. Dr. E. Vlieg)  
*Stage onderwerp:* Structure determination of interfaces  
by interface x-ray diffraction  
*Nevenrichting:* Toegepaste Fysica (Prof. Dr. H. ter Meulen)  
*Stage onderwerp:* Oxyacetylene flame chemical vapour  
deposition of diamond

2003 - 2007 Promotie onderzoek bij de afdeling Vaste Stof Chemie en  
het High Field Magnet Laboratory  
Radboud Universiteit Nijmegen  
*Onderwerp:* Suppression of convection during protein  
crystal growth  
*Promotores:* Prof. Dr. E. Vlieg en Prof. Dr. ir. J.C. Maan

Per 1 mei 2007 werkzaam bij Vision Dynamics te Eindhoven. Gedetacheerd bij  
TNO en de Technische Universiteit Eindhoven.











